A Thesis

entitled

AN ULTRASONIC INVESTIGATION OF ELASTIC ANISOTROPY IN SOLIDS

submitted for the

Degree of Doctor of Philosophy

in the

University of London

by

Robert Taylor Smith, M.Sc., A.R.C.S.

February, 1965

ABSTRACT

Anisotropy in the elastic properties of solids due to statically applied, finite, directional stresses has been investigated by means of ultrasonic interferometric techniques. The small stress-induced changes in the velocity of propagation of ultrasonic waves are related to third-order elastic moduli using a recent theory of Thurston and Brugger. Details of the electronic measuring equipment and interference conditions are described, and results are presented for both longitudinal and shear waves in strained polycrystalline metal specimens, including several different steels, a magnesium alloy and pure tungsten and molybdenum. The third-order elastic moduli are calculated and compared with alternative non-linear elasticity data. Finally, the general theory of Thurston and Brugger is specialised for single crystals of trigonal symmetry, and a sufficient number of experimental configurations are analysed such that all 14 independent third-order moduli may be evaluated from experiments similar to those described for polycrystalline metals.

ACKNOWLEDGEMENTS

The author wishes to express his sincere thanks to Dr. R.W.B. Stephens of the Acoustics Group, Imperial College, for constant guidance and encouragement throughout this project, and is grateful to Professor P.M.S. Blackett and Professor C.C. Butler for laboratory facilities. He wishes to thank Mr. A. Davis, Mr. W. Shand and the technical staff of the Physics Department for help in the design and construction of the mechanical parts of the apparatus, and Mr. E.R. Sparks for much of the photographic work. He is grateful to the United Kingdom Atomic Energy Authority, Harwell, for the provision of a research bursary and also for the loan of some electronic equipment. Finally, he wishes to thank his wife, Doreen, for encouragement and support at all times, and especially during the final preparation of this thesis.

CONTENTS

		Page No.
	Abstract	2
	Acknowledgments	3
	List of contents	4
	List of principal symbols	5
Chapter		
1	Review of previous work	9
2	Measuring equipment and experimental techniques	53
3	Experimental measurements on polycrystalline metals	95
4	Discussion of experimental results for polycrystalline metals	124
5	Theory of small-amplitude elastic wave propagation in strained crystals of trigonal symmetry	136
	Suggestions for further work	162
Appendix		
1	Electronic equipment	164
2	Calibration of variable delay line	169
3	Method of determining the vibration direction of shear wave transducers	170
4	Relationship between the stress derivatives $(\rho_o W^2)'_o$ and $(\rho_o V^2)'_o$ for isotropic solids	173
	References	174

LIST OF PRINCIPAL SYMBOLS

Symbol	Equation (or table) where first used	Meaning
a_i	1	Lagrangian particle coordinates
a	83	linear coefficient in Bridgman definition of isothermal compressibility
A	97	numerical constant
A,B,C	Table 2	third-order stiffnesses for isotropic solid (Gol'dberg)
A^S_{jkpm}	24	effective second-order stiffnesses
b	83	non-linear coefficient in Bridgman definition of isothermal compressibility
B	84	isothermal bulk modulus
$c^S_{jkpqrs....}$	13	adiabatic n^{th}-order stiffnesses - tensor and reduced coefficients, respectively (Brugger)
$c^S_{JPR..}$	14	
$c_{jkpqrs....}$	36	'mixed n^{th}-order stiffnesses - tensor and reduced coefficients, respectively (Brugger)
$c_{JPR..}$	36	
d	48	time delay per scale division of delay line
D	48	delay line divisions
e_{11}	Table 11	piezoelectric constant
E	76	Young's modulus
f	44	frequency
f_o	63	resonant frequency of transducer
f_n	64	frequency at interference 'null'

Symbol	Equation (or table) where first used	Meaning
F	97	linear combination of second-order compliances
G	97	linear combination of second-order stiffnesses and compliances and third-order stiffnesses
H	7	enthalpy per unit mass
k	42	propagation constant
K	63	ratio of mechanical impedances of transducer and specimen
l,m,n	Table 2	third-order stiffnesses for isotropic solid (Murnaghan)
L, L_o	28	specimen thickness (strained and unstrained, respectively)
m	42	pulse-echo number
$\underline{M}$	38	unit vector along direction of uniaxial compressive stress
n	46	arbitrary integer
$\underline{n}$	3	unit vector along actual propagation direction
$\underline{N}$	27	unit vector along propagation direction ('material' coordinates)
p,q	94	direction cosines
P	33	applied stress; hydrostatic pressure
Q	70	slope of curve of D versus ΔP
R	75	numerical constant

Symbol	Equation (or table) where first used	Meaning
$s^S_{jkpq....}$	15	adiabatic n^{th}-order compliances - tensor and reduced coefficients, respectively (Brugger)
$s^S_{JP..}$	16	
S	7	entropy per unit mass
S	49	slope of curve of D versus $\Delta W/W_o$
t	3	time
t_{jk}, t_J	7, 11	thermodynamic tensions - tensor and reduced notation, respectively
T	7	temperature
u_i	1	components of particle displacement
U_k	30	components of particle displacement (material coordinates)
U	7	internal energy per unit mass
U_1, U_2	42, 43	instantaneous amplitude of rf signal
v	83	volume
V	3	phase velocity
w	35	eigenvalue of equation 31
w_{jk}	31	tensor describing propagation conditions (elastic stiffness)
W	27	'natural' phase velocity
x_i	1	strained particle coordinates
X_i	22	strained particle coordinates (initial state)
X,Y,Z	Table 11	crystallographic axes, cartesian axes
Z	63	specific mechanical impedance

Symbol	Equation (or table) where first used	Meaning
β	84	isothermal compressibility
β_{ijkm}	23	'effective' second-order stiffnesses (tensor notation)
γ	42	reflection phase shift
δ_{ik}	4	Kronecker delta
ε_{11}	Table 11	zero-strain permittivity
η_{jk}	7, 26	Lagrangian strains (tensor notation)
η_J	11	Lagrangian strains (reduced notation)
λ,	76	Lamé stiffness constants
ν_1, ν_2, ν_3	Table 2	third-order stiffnesses for isotropic solid (Toupin and Bernstein)
ϕ	42	arbitrary phase angle
ρ	1	density
σ	77	Poisson's ratio
τ	64	pulse transit time
Γ_{ik}	6	Christoffel stiffnesses
ω	3	angular frequency

CHAPTER 1

REVIEW OF PREVIOUS WORK

1.1 PROPAGATION OF SMALL-AMPLITUDE ELASTIC WAVES IN UNSTRAINED AEOLOTROPIC SOLIDS

The theory used to describe the propagation of small-amplitude elastic waves in unstrained aeolotropic solids has its origins in the early nineteenth century work of Hamilton [1], Cauchy [2] and Green [3]. An analysis was developed to explain the propagation of transverse vibrations in the elastic solid which was supposed at that time to represent the luminiferous aether. Somewhat later Christoffel [4] published a long memoir on elastic wave propagation in aeolotropic solids and the problem was developed further by Lord Kelvin [5] in his Baltimore lectures at the turn of the century.

It is convenient at this stage to define an aeolotropic solid as a homogeneous solid whose physical properties vary with direction. In this respect such a solid might well be described as anisotropic, though it should be noted that the latter description does not automatically imply homogeneity. For example, the physical properties of single crystals are evidently aeolotropic, whereas those of a polycrystalline metal possessing microstructural inhomogeneities, such as

preferential grain alignment, are better described as anisotropic.

In the general case of plane wave propagation in aeolotropic solids, the phase velocity varies markedly depending on the propagation direction. Further, the energy flow is not in general coaxial with the normal to the planes of constant phase, nor is the displacement vector normal or parallel to the wavefront. An analysis for calculating the velocities and displacements for non-dispersive materials was outlined by Lord Kelvin in his Baltimore lectures [5] and general expressions for the direction of energy flow were derived by Love [6]. Although the basic principles were established long ago, progress lapsed until comparatively recently, when a revival of interest in the problems of plane wave propagation was stimulated by the development of suitable means of generating and detecting elastic waves at ultrasonic frequencies. At these high frequencies (upwards of a few megacycles per second), elastic energy propagates in fairly well defined beams and the plane wave approach becomes applicable, provided certain restrictions on the wavelength are observed. In order that a crystal lattice should be regarded as a continuum, the lattice spacing must be very much smaller than the elastic wavelength. On the other hand, the wavelength itself must be very much smaller than the specimen dimensions to avoid undue complications from boundary effects and guided wave modes of propagation.

Within the last decade or so, numerous theoretical and experimental investigations have been made on the detailed characteristics of plane wave propagation in crystalline materials of particular symmetries. For example, wave propagation in cubic and hexagonal crystals was extensively analysed by Musgrave [7] and Miller and Musgrave [8], and the more complicated case of trigonal symmetry by Farnell [9]. Of the several reviews available, noteworthy examples are those of Huntington [10], Musgrave [11] and Hearmon [12].

The standard theory of plane wave propagation in crystalline materials of arbitrary symmetry is summarised below in the convenient and compact notation of tensor analysis. It is important to note that the following theory is applicable only to the case of small-amplitude waves in unstrained materials, when the usual assumptions of small displacements and displacement gradients are made.

It is shown in standard textbooks [13] that the linearised equations of small-amplitude particle motion, neglecting the effect of body forces, may be written:

$$\rho_o \ddot{u}_i = c_{ijkm} \frac{\partial^2 u_k}{\partial a_j \partial a_m} \qquad (1)$$

$$i,j,k,m = 1,2,3$$

Unless specifically stated otherwise, it will be assumed from this point that the usual dummy suffix convention applies, i.e. any term which contains a repeated or 'dummy' suffix is summed over the values 1,2,3. In equation (1), ρ_o is the unstrained density, and u_i are the components of particle displacement, defined by:

$$u_i = x_i - a_i \tag{2}$$

where x_i, a_i denote the particle coordinates in the strained and unstrained states with respect to some fixed Cartesian reference frame. Moreover, the a_i terms serve to identify the particle or 'material point' and are referred to as Lagrangian or material coordinates, whereas the x_i terms merely specify a point in space and are known as Eulerian or spatial coordinates [13].

At ultrasonic frequencies, the particles are assumed to vibrate under adiabatic conditions and the c_{ijkm} of equation (1) are therefore the adiabatic or 'isentropic' second-order elastic coefficients. The formal definition and significance of these elastic coefficients and the label 'second-order' will be discussed more fully in subsequent sections of this chapter.

A solution of equation (1) for a plane progressive wave may be written:

$$u_i = U_i \exp\left[j\omega\left(t - \frac{n_p a_p}{V}\right)\right] \tag{3}$$

where the U_i are constants depending on the generation conditions, ω is the angular frequency, t the time, n_i are the components of a unit vector along the propagation direction, and V is the phase velocity of the wave. Substitution into the equation of motion gives the following relation for the components of the displacement, u_k.

$$\left(c_{ijkm}\, n_j\, n_m - \rho_o V^2 \delta_{ik} \right) u_k = 0 \tag{4}$$

in which δ_{ik} is the familiar Kronecker delta, defined by:

$$\delta_{ik} = \begin{cases} 0 , & i \neq k \\ 1 , & i = k \end{cases}$$

For non-trivial solutions, the determinant of the coefficients of u_k in equation (4) must vanish identically.

Thus $$\left| \Gamma_{ik} - \rho_o V^2 \delta_{ik} \right| \equiv 0 \tag{5}$$

where $$\Gamma_{ik} = c_{ijkm}\, n_j\, n_m \tag{6}$$

is a second-rank symmetric tensor whose components may be identified with the Christoffel stiffnesses [6]. The secular equation (5) determines the phase velocity as a function of direction, and since it is cubic in $\rho_o V^2$, there are in general three velocities associated with each

propagation direction. Classical arguments show that the three distinct eigenvalues, $\rho_o v^2$, are all positive real and also that their associated displacement eigenvectors, $\underline{u}$, form an orthogonal triad provided Γ_{ik} is positive definite. Thus for any general direction, $\underline{n}$, three waves may be propagated having mutually perpendicular displacement vectors but different phase velocities. However, it is only when $\underline{n}$ is itself an eigenvector of Γ_{ik} that the displacement vectors are either exactly longitudinal or exactly transverse.

The components of the displacement vector for a particular velocity eigenvalue may be found by substituting the appropriate root of equation (5) back into equation (4). It is found that the displacement vector corresponding to the largest root, $\rho_o v^2$, is more or less in the direction of the normal to the wavefront and thus represents a quasi-longitudinal or compressional wave, whereas the two remaining displacement vectors are quasi-transverse. Farnell [9] gives a general expression for the direction of energy flow for these quasi-waves.

Borgnis [14] has discussed the problem of finding so-called 'specific' directions, for which the displacement vectors are exactly longitudinal or transverse, and has called the corresponding waves 'pure'. However Farnell, for his definition of 'pure' waves requires not only that the displacement vectors be exactly longitudinal or

transverse, but also that the direction of energy flow should lie along the propagation direction. The former condition does not necessarily imply the latter. For example, in the case of propagation along the trigonal (z) axis in α-quartz, the displacement vectors for the three waves are either exactly longitudinal or transverse. However, although the energy flow for the longitudinal wave is along the z-axis, the energy for the two degenerate (equal velocity) shear waves flows at an angle of about 16° to the z-axis.

Further details on special peculiarities of wave propagation in crystals and other anisotropic solids may be found in references cited above [7-12, 14] and in the author's M.Sc. dissertation [15].

1.2 NON-LINEAR ELASTIC THEORY

There is considerable experimental evidence to show that the velocity of an ultrasonic wave in a solid is influenced by the action of macroscopic stresses. Moreover, the velocity-stress dependence cannot be fully explained solely on the basis of the linear elastic theory of the preceding section. The difficulty is removed, however, by regarding a small amplitude wave in a stressed solid as an infinitesimal perturbation on an initial finite deformation. It is then possible to develop equations of motion from standard non-linear elastic theory. At this

stage it is convenient to outline the salient features of non-linear elastic theory and defer the discussion of wave propagation in stressed solids until the next section.

The formidable problems associated with finite deformations and non-linear elasticity may be expressed advantageously in tensor notation, a device used extensively by Brillouin in his early and subsequent work [16, 17]. Murnaghan [18], however, has made considerable progress with a matrix formulation. According to Murnaghan, not even an initially isotropic material can remain elastically isotropic under the action of any stress system other than simple hydrostatic pressure or tension. This statement gives some idea of the complexity to be encountered in any discussion of wave propagation in strained aeolotropic solids.

The concept of a so-called 'strain-energy function' is basic to most non-linear elastic theories and it is usual to define the stored elastic energy, Φ, as a polynomial expansion in the components of finite strain, η_{ij}, as shown, for example, in the following expression:

$$\Phi(\eta) = \frac{1}{2} c_{ijkm} \eta_{ij} \eta_{km} + \frac{1}{6} c_{ijkmpq} \eta_{ij} \eta_{km} \eta_{pq} + \frac{1}{n!} c_{ijkmpq} \cdots \eta_{ij} \eta_{km} \eta_{pq} \cdots + \cdots$$

However, Truesdell's analysis of wave propagation in deformed isotropic materials [19] is a notable exception in that the theory was developed from generalised non-linear stress-strain relations. Truesdell showed that postulation of a strain-energy function imposes restrictions on the general theory and leads to an interesting test for the validity of the strain-energy itself. The results were presented as a simple identity between the speeds of one longitudinal and one transverse wave and a design experiment for testing this identity has been described by Smith [20].

In the typical polynomial expansion for the stored-energy function shown above, the coefficients of strain products of degree n are known as n^{th}-order elastic constants. Several versions of the polynomial expansion occur in the literature [18, 21-23], but on comparison, their differences are found to be trivial; for example, inclusion or omission of strain-product terms of zero and first-order, and sometimes simple numerical factors. The terms of zero- and first-order may be identified with an intrinsic energy and an initial hydrostatic strain, respectively. If the body is referred to an initial unstrained state, the first-order term vanishes. Further, since the equations of motion are based on derivatives of the strain-energy function, the zero-order term is of no consequence in a discussion of elastic wave propagation. However, the magnitudes of the elastic constants themselves are necessarily modified

by the inclusion or omission of the numerical factors in the stored-energy function. The possible existence of such factors should be recognised when comparing higher-order elastic constants from different sources of reference.

An alternative definition of higher-order elastic coefficients based on thermodynamic potentials has been proposed recently by Brugger [24]. The new definitions will be adopted here since they have the following advantages over several systems based on strain-energy functions:

(a) They follow naturally from accepted definitions for the second-order coefficients.

(b) Conventional relations are retained between the tensor and abbreviated Voigt [25] notations for stresses and strains.

(c) Thermodynamic relations involving the elastic coefficients are readily transcribed from the tensor to the abbreviated notation and vice-versa.

(d) The elastic coefficients defined thermodynamically are identical with those encountered in anharmonic lattice theory, as described for example by Ziman [26].

The required thermodynamic potentials per unit mass are the internal energy, U, and the enthalpy, H, which may be defined in terms of the conjugate variables S and T, and t_{jk} and η_{jk}/ρ_o.

Thus $$dU = TdS + \frac{1}{\rho_o} t_{jk}\, d\eta_{jk}$$

$$dH = TdS - \frac{1}{\rho_o} \eta_{jk}\, dt_{jk} \qquad (7)$$

where T is the temperature, S the entropy, t_{jk} are the 'thermodynamic tensions' [13] and η_{jk} the Lagrangian strains. The 'thermodynamic tensions' have the same physical character as ordinary stresses, and are related to them via the nine deformation gradients, $\frac{\partial x_i}{\partial a_p}$ [13].

From equations (7), $$t_{jk} = \rho_o \left(\frac{\partial U}{\partial \eta_{jk}}\right)_S$$

$$\text{and} \quad \eta_{jk} = -\rho_o \left(\frac{\partial H}{\partial t_{jk}}\right)_S \qquad (8)$$

Since the Lagrangian strains (defined in equation (26)) and the thermodynamic tensions are symmetric, i.e. $\eta_{jk} = \eta_{kj}$ and $t_{jk} = t_{kj}$, only six of the nine possible tensor components are independent and it is possible to introduce an abbreviated notation [25]. The conversion scheme for the subscripts is as follows: $11 \longrightarrow 1$, $22 \longrightarrow 2$, $33 \longrightarrow 3$, $23 = 32 \longrightarrow 4$, $13 = 31 \longrightarrow 5$, $12 = 21 \longrightarrow 6$.

Considering the thermodynamic potentials as functions of the single subscript variables, equations (7) and (8) become:

$$dU = TdS + \frac{1}{\rho_o} t_J d\eta_J \qquad (9)$$

$$dH = TdS - \frac{1}{\rho_o} \eta_J dt_J$$

with $$t_J = \rho_o \left(\frac{\partial U}{\partial \eta_J}\right)_S \qquad (10)$$

and $$\eta_J = -\rho_o \left(\frac{\partial H}{\partial t_J}\right)_S$$

Between the thermodynamic tensions and strains in the full and abbreviated notations, the following relationships are defined according to convention [27]:

$$t_{ab} \equiv t_A \qquad (11)$$

$$\eta_{ab} \equiv \frac{1}{2}(1 + \delta_{ab})\,\eta_A$$

where the capital subscripts run from 1 to 6. Note that the so-called 'engineering shear strains' (A = 4, 5 or 6) are twice the corresponding full tensor components ($a \neq b$), whereas the tensions are the same in both notations. Further relations between certain partial derivatives in the two systems follow from equations (8), (10) and (11).

Thus

$$\rho_o\left(\frac{\partial U}{\partial \eta_{jk}}\right)_S = t_{jk} \equiv t_J = \rho_o\left(\frac{\partial H}{\partial t_j}\right)_S$$

Hence

$$\frac{\partial}{\partial \eta_{jk}} \equiv \frac{\partial}{\partial \eta_J} \tag{12a}$$

Similarly

$$-\rho_o\left(\frac{\partial H}{\partial t_{jk}}\right)_S = \eta_{jk} \equiv \frac{1}{2}(1+\delta_{jk})\eta_J = -\frac{1}{2}(1+\delta_{jk})\rho_o\left(\frac{\partial H}{\partial t_J}\right)_S$$

Hence

$$\frac{\partial}{\partial t_{jk}} \equiv \frac{1}{2}(1+\delta_{jk})\frac{\partial}{\partial t_J} \tag{12b}$$

It is now possible to introduce Brugger's concept of higher-order elastic coefficients in both full and abbreviated notations. The isentropic n^{th}-order elastic constants are defined as the n^{th} partial derivatives of the internal energy U with respect to the Lagrangian strains, for $n \geq 2$.

Thus
$$c^S_{jkpq....} = \rho_o\left(\frac{\partial^n U}{\partial \eta_{jk}\partial \eta_{pq....}}\right)_S \tag{13}$$

$$\text{and} \quad c^{S}_{JP\ldots} = \rho_o \left(\frac{\partial^{n} U}{\partial \eta_J \, \partial \eta_{P\ldots}} \right)_S \tag{14}$$

Similarly the isentropic n^{th}-order elastic compliances are defined as the n^{th} partial derivatives of the enthalpy H with respect to the thermodynamic tensions.

$$\text{i.e.} \quad s^{S}_{jkpq\ldots} = - \rho_o \left(\frac{\partial^{n} H}{\partial t_{jk} \, \partial t_{pq\ldots}} \right)_S \tag{15}$$

$$\text{and} \quad s^{S}_{JP\ldots} = - \rho_o \left(\frac{\partial^{n} H}{\partial t_J \, \partial t_{P\ldots}} \right)_S \tag{16}$$

Comparison of equations (13) and (14), making use of the identity (12a), gives:

$$c^{S}_{jkpq\ldots} = c^{S}_{JP\ldots} \tag{17}$$

while from equations (15), (16) and (12b), it follows that:

$$s^{S}_{jkpq\ldots} = \frac{1}{2}(1 + \delta_{jk}) \; \frac{1}{2}(1 + \delta_{pq}) \ldots s^{S}_{JP\ldots} \tag{18}$$

Brugger has shown that, starting from the thermodynamic free energy F and Gibbs function G, a completely analogous set of relations can be derived for the <u>isothermal</u> higher-order elastic constants and compliances, but these, will not be required here.

Consider the internal energy as a Maclaurin series expansion in the components of finite strain under isentropic conditions. Then:

$$\rho_o U(\eta) = \rho_o U'(0,S)\,\eta_{jk} + \frac{1}{2!}\rho_o U''(0,S)\eta_{jk}\eta_{pq} + \frac{1}{3!}\rho_o U'''(0,S)\,\eta_{jk}\eta_{pq}\eta_{rt} + \ldots + \ldots \qquad (19)$$

where

$$\rho_o U(\eta) = \rho_o U(\eta,S) - \rho_o U(0,S)$$

and the dashes indicate partial derivatives with respect to the Langrangian strains. Except for the first, these partial derivatives are simply the n^{th}-order elastic coefficients evaluated at zero strain. (The first derivative is a thermodynamic tension which vanishes at zero strain). The quantity $\rho_o U(\eta)$ may now be re-written:

$$\rho_o U(\eta) = \frac{1}{2}\,c^S_{jkpq}\,\eta_{jk}\,\eta_{pq} + \frac{1}{6}\,c^S_{jkpqrt}\,\eta_{jk}\,\eta_{pq}\,\eta_{rt} + \ldots. \qquad (20)$$

and can be identified as a stored-energy function, in which the zero-strain elastic coefficients are functions of the entropy (or temperature). In the reduced notation:

$$\rho_o U(\eta) = \frac{1}{2}\,c^S_{JP}\,\eta_J\,\eta_P + \frac{1}{6}\,c^S_{JPR}\,\eta_J\,\eta_P\,\eta_R + \ldots. \qquad (21)$$

Brugger presents general conversion relations between the reduced notation elastic coefficients appearing in equation (21) and others current in the literature.

The number of independent n^{th}-order elastic constants required to

describe non-linear behaviour in an aeolotropic solid of lowest symmetry is $\frac{(5+n)!}{5!n!}$ i.e. 21 second-order, 56 third-order, 126 fourth-order constants, and so on for a triclinic crystal. For each of the 32 crystal classes [28], the number of independent third order constants is well-known [15, 22]. Recently the schemes have been extended to the fourth order by Krishnamurty [29] and Ghate [30], and the results for all crystal classes are summarised in Table 1. The numerical entries in Table 1 refer only to the number of independent non-zero n^{th}-order elastic constants. However there are, in all cases, additional non-zero constants which are either simple multiples or combinations of the independent constants. Detailed schemes showing the essential symmetries of all the non-zero second- [31] and third-order [22, 32, 33] constants have been prepared for each crystal class.

It has been emphasised that the magnitude of the elastic constants depends on the particular definition of the strain-energy function. For isotropic symmetry, several schemes for the three third-order constants are in use, principally those of Murnaghan [18], Toupin and Bernstein [23], and Gol'dberg [34]. The conversion relations among the three sets have been summarised by the author [20] and are shown in Table 2.

To conclude this section, attention is drawn to a recent

System	Crystal Class - Schoenflies Symbols	Number of Independent Elastic Constants		
		2nd-order	3rd-order	4th-order
Triclinic	C_1, S_2	21	56	126
Monoclinic	C_2, C_s, C_{2h}	13	32	70
Orthorhombic	D_2, C_{2v}, D_{2h}	9	20	42
Tetragonal	C_4, S_4, C_{4h}	7	16	36
	$C_{4v}, D_{2d}, D_4, D_{4h}$	6	12	25
Trigonal	C_3, S_6	7	20	42
	C_{3v}, D_3, D_{3d}	6	14	28
Hexagonal	C_6, C_{3h}, C_{6h}	5	12	24
	$C_{6v}, D_{3h}, D_6, D_{6h}$	5	10	19
Cubic	T, T_h	3	8	14
	T_d, O, O_h	3	6	11
Isotropic		2	3	4

TABLE 1 NUMBER OF INDEPENDENT n^{th}-ORDER ELASTIC COEFFICIENTS FOR THE VARIOUS CRYSTAL CLASSES

Murnaghan; Hughes and Kelly	*Toupin and Bernstein*	*Gol'dberg; Jones and Kobett*
l	$\frac{1}{2}\nu_1 + \nu_2$	$B + C$
m	$\nu_2 + 2\nu_3$	$\frac{1}{2}A + B$
n	$4\nu_3$	A
$2l - 2m + n$	ν_1	$2C$
$m - \frac{1}{2}n$	ν_2	B
$\frac{1}{4}n$	ν_3	$\frac{1}{4}A$
n .	$4\nu_3$	A
$m - \frac{1}{2}n$	ν_2	B
$l - m + \frac{1}{2}n$	$\frac{1}{2}\nu_1$	C

TABLE 2 CONVERSION RELATIONS BETWEEN THIRD-ORDER ELASTIC CONSTANTS FOR ISOTROPIC SOLIDS

observation by Thurston [35], that elastic constants can be defined in at least three contexts: (i) as derivatives of a stored-energy function, (ii) as coefficients in a generalised stress-strain relation, or (iii) as coefficients in an equation of motion. In the infinitesimal theory, all three sets of second-order coefficients are equivalent, but under conditions of finite strain, the corresponding 'effective' second-order elastic constants are not generally equivalent except for the special case of hydrostatic strain.

1.3 THEORIES OF SMALL-AMPLITUDE WAVE PROPAGATION IN STRAINED AEOLOTROPIC SOLIDS

A small-amplitude elastic wave in a strained aeolotropic solid may be regarded as an infinitesimal dynamic perturbation superimposed on an initial finite deformation. To proceed further, it is essential to distinguish three sets of coordinates, namely: the 'natural' or unstressed material coordinates, a_i; the 'initial' coordinates in the homogenously deformed body, $X_i(a)$; finally, the coordinates $x_i(a)$, which describe the perturbed state. The components of particle displacement from the initial state due to the wave may now be defined as:

$$u_i = x_i - X_i \tag{22}$$

This definition of displacement is similar to the corresponding relation in the infinitesimal theory (equation (2)).

It is tempting to transfer the linearised equations of small-amplitude motion from the infinitesimal theory to the case of finite initial strain. Thus:

$$\rho \ddot{u}_i = \beta_{ijkm} \frac{\partial^2 u_k}{\partial X_j \partial X_m} \tag{23}$$

where the β_{ijkm} are 'effective' second-order elastic coefficients for the particular initial state, and ρ is the density of the initially strained material. Although this idea is attractive, its usefulness is somewhat limited, since Thurston [35] has shown that the 'effective' elastic constants do not enjoy the full symmetry of the conventional second-order constants c_{ijkm}, except for the case of initial finite hydrostatic strain. Moreover, in many experimental observations, the ultrasonic wave velocity has been determined as a function of uniaxial stress, and it is more convenient to interpret these results in terms of higher-order elastic coefficients, which obey all the usual symmetry operations [24].

During the past twenty years, the theory of small-amplitude wave propagation in strained aeolotropic solids has been developed extensively. Most of the work is based on Murnaghan's finite strain formulation [18]

and associated stored-energy functions, but there are several exceptions [19, 36, 37] as noted in the previous section. For a material of given symmetry, attempts to solve the equations of motion may be divided into two types. In the more usual approach, the equations of motion are derived from a restricted strain-energy function in which only those terms relevant to the particular symmetry are retained. After linearising the equations, plane wave solutions are sought for particular propagation directions and simple stress configurations. This procedure can become excessively tedious, especially for materials of low symmetry. The alternative method consists of setting up completely general linearised equations of motion for arbitrary stress systems and solving for plane waves. Particular characteristics such as crystal symmetry, wave-type, propagation direction and stress system are then substituted into the general solution. Although at first sight the second technique might appear the more intractable of the two, in fact this is not the case. Once the general solution is available, the algebraic manipulation required is much reduced compared with the first method.

In all experimental investigations reported up to the present time, the velocities of ultrasonic waves have shown a linear dependence on externally applied stresses, whether hydrostatic or uniaxial, provided the specimens were not plastically deformed. Consistent with this

fact, it is usual to terminate polynomial expansions for stored-energy functions after third-degree strain products. That this approximation should be sufficient is a special consequence of the relative magnitudes of the higher- and second-order elastic coefficients. Thus, the third-order constants, which are unusually large (about an order of magnitude greater than the second-order constants) have an appreciable effect on the elastic properties of a solid when the strains are finite. On the other hand, the fourth-order constants are relatively insignificant even under conditions of finite deformation [38]. All the wave propagation theories reviewed below are based on derivatives of stored-energy functions expanded only to third-degree strain products.

The velocity-stress dependence of elastic waves in isotropic materials has been analysed by Hughes and Kelly [38], Toupin and Bernstein [23], and Thurston and Brugger [40]. Their theories show several important differences. Hughes and Kelly base their analysis on a strain-energy function restricted to isotropic symmetry, whereas the others derive general solutions and then specialise for the isotropic case. In addition, Hughes and Kelly give explicit relationships for the wave velocity as a function of stress, but the others present expressions for the velocity derivatives evaluated at zero stress. Further, in contrast to Toupin and Bernstein, Thurston and Brugger define their velocity derivatives so as to incorporate changes

in specimen dimensions caused by the deformation. However, although different sets of third-order constants are used (Table 2), the three theories are fully consistent.

An examination of Table 1 shows that several of the crystal 'systems' are divided into two sub-groups of higher and lower symmetry. For example, the cubic sub-group consisting of the crystal classes O, O_h and T_d requires six independent third-order constants, whereas the other cubic sub-group, T and T_h, requires eight. The characteristics of elastic wave propagation in strained crystals belonging to the sub-group O, O_h and T_d, have received considerable attention since this sub-group is the simplest after isotropic symmetry. Once again, two methods of analysis should be distinguished. On the one hand, Seeger and Buck [41] and later, Mason et al. [42] derived explicit relations for the velocity-stress dependence, from a strain-energy function restricted to cubic symmetry. On the other hand, Thurston [13] and Thurston and Brugger [40] specialised a general solution for the cubic case and obtained a complete set of expressions for the velocity derivatives evaluated at zero stress.

The problem of wave propagation in strained aeolotropic solids becomes increasingly more complex for decreasing crystalline symmetry. It is not surprising, then, that such information for other than isotropic or simple cubic symmetries is relatively scarce. Recently, however,

Einspruch and Manning [43] have applied the more usual analytical method based on restricted strain-energy functions to the following crystal classes: cubic sub-group of lower symmetry (T, T_h); hexagonal sub-group of higher symmetry (C_{6v}, D_{3h}, D_6, D_{6h}); tetragonal sub-group of higher symmetry (C_{4v}, D_{2d}, D_4, D_{4h}); and the orthorhombic system (D_2, C_{2v}, D_{2h}). In the case of the cubic, hexagonal and tetragonal sub-groups listed, a sufficient number of combinations of wavetype, propagation direction, and stress system were analysed to allow unique determination for all the relevant third-order constants. For orthorhombic symmetry, only 18 of the 20 independent third-order constants could be included in solutions for 'pure' waves. The case of the trigonal sub-group of higher symmetry (C_{3v}, D_3, D_{3d}), has been solved by the author, and the results are presented in detail in Chapter 5.

The experimental results obtained during the course of the present work will be interpreted in terms of the theory of Thurston and Brugger [40]. Furthermore, the theoretical analysis presented in Chapter 5 is based on their general solution for wave propagation in strained crystals. At this stage, therefore, it seems appropriate to outline the general theory and introduce certain definitions and special relationships which will be required later.

Using Murnaghan's finite strain formulation, Thurston and Brugger [40]

derived a general equation of motion [44] and linearised the latter about an initial state of homogeneous strain. Their resulting equation of motion for the components of particle displacement is:

$$\rho_o \ddot{u}_j = \tilde{A}^S_{jkpm} \frac{\partial^2 u_k}{\partial a_p \partial a_m} \tag{24}$$

where the tensor A^S_{jkpm} is given by:

$$A^S_{jkpm} = \delta_{jk} t_{pm} + \frac{\partial x_j}{\partial a_q} \frac{\partial x_k}{\partial a_n} c^S_{pqmn} \tag{25}$$

A ~ sign over a symbol indicates that the quantity is evaluated at the initial deformed state, where $x \longrightarrow X$; $A^S_{jkpm} \longrightarrow \tilde{A}^S_{jkpm}$; $t_{pm} \longrightarrow \tilde{t}_{pm}$, and $c^S_{pqmn} \longrightarrow \tilde{c}^S_{pqmn}$, etc. The quantities t_{pm} and c^S_{pqmn} were defined in Section 1.2 as derivatives of the thermodynamic internal energy U with respect to the Lagrangian strains, η_{rs}, where:

$$\eta_{rs} = \frac{1}{2} \left(\frac{\partial x_b}{\partial a_r} \frac{\partial x_b}{\partial a_s} - \delta_{rs} \right) \tag{26}$$

A plane wave solution of equation (24) is assumed in the form:

$$u_j = A_j \exp \left[j\omega \left(t - \frac{N_i a_i}{W} \right) \right] \tag{27}$$

In the last equation, the quantity W is the wave speed referred to the material or natural coordinates, and is called the 'natural velocity' for propagation normal to a material plane of natural normal

$\underline{N}$. In a typical ultrasonic pulse-echo experiment where mechanical energy is reflected back and forth between two parallel faces of a specimen, the 'natural velocity' is equal to the unstrained path length, L_o, divided by the transit time in the strained state. This should be compared with the true velocity, V, which is equal to the strained path length, L, divided by the transit time in the strained state. Thus:

$$V = \frac{L}{L_o} W \tag{28}$$

From the experimental point of view, it is a considerable advantage to refer measured changes in transit time to the 'natural' unstrained path length via the 'natural' velocity W, rather than use the true velocity and correct for changes in the actual path length.

The propagation conditions are obtained by substituting the trial solution (27) into the linearised equation of motion (24).

$$\left[\mathring{A}^{S}_{jkpm} N_p N_m - \rho_o W^2 \delta_{jk} \right] u_k = 0 \tag{29}$$

The possible values of $\rho_o W^2$ are eigenvalues of the second-rank symmetric tensor $S_{jk} = \mathring{A}^{S}_{jkpm} N_p N_m$, and the possible particle displacements, $\underline{u}$, are the corresponding eigenvectors (cf. equation (4), the propagation condition for the infinitesimal theory). For a given natural normal, $\underline{N}$,

the eigenvectors, $\underline{u}$, form a real orthogonal set in the deformed initial state provided S_{jk} is positive definite. In general, S_{jk} depends on the rotation as well as the strain, via the definition of $\overset{\leftarrow S}{A}_{jkpm}$ in equation (25). This simply means that the particle displacements must rotate with the material during a general deformation. To obtain a representation independent of rotation, Thurston and Brugger transformed the particle displacement, $\underline{u}$, back to the natural undeformed direction of the material line along it by the transformation:

$$u_j = \frac{\partial X_j}{\partial a_q} U_q \tag{30}$$

The propagation conditions then become:

$$\left[w_{jk} - \rho_o W^2 \delta_{jk} \right] U_k = 0 \tag{31}$$

$$\text{where } w_{jk} = N_r N_s \left[\delta_{jk} \tilde{t}_{rs} + (\delta_{qk} + 2\,\eta_{qk}) \tilde{c}^S_{jrqs} \right] \tag{32}$$

All quantities in equations (31) and (32) are dependent only on the strain and one other thermodynamic variable, which may be either entropy or temperature. The possible values of $\rho_o W^2$ for propagation normal to a 'material' surface, $\underline{N}$, are now the eigenvalues of w_{jk}. It is important to realise that the corresponding material eigenvectors, $\underline{U}$, are not in general orthogonal but are rotated into the orthogonal set of particle displacements, $\underline{u}$, by the initial deformation. In the absence of an

initial strain, the quantities $\tilde{t}_{rs}$ and $\tilde{\eta}_{qk}$ vanish in equation (32), so that $w_{jk} \longrightarrow \Gamma_{jk}$ of the infinitesimal theory.

For a particular temperature, the propagation velocity of an elastic wave in an unstrained material depends only on the second-order elastic moduli and the density, whereas the initial slope of an experimental curve of propagation velocity versus stress involves both second- and third-order moduli. In principle, therefore, it should be possible to determine the third-order moduli from the initial slopes of such curves. Thurston and Brugger [40] have shown that it is sufficient to consider deformed states depending on a single variable, P, which may represent a hydrostatic pressure or a uniaxial load per unit natural undeformed area. They referred the strain components to the natural unstressed state at a particular temperature and developed the finite strain theory outlined above to obtain a general expression for the quantity:

$$(\rho_o W^2)'_{P=0} \equiv \left[\frac{\partial}{\partial P} (\rho_o W^2) \right]_T \tag{33}$$

The full general result, which forms the basis of the analysis presented in Chapter 5, is rather complex. Thus:

$$(\rho_o W^2)'_{P=0} = t'_{ab}(0)\left[N_a N_b + U^o_j U^o_k \left(2ws^T_{jkab} + N_r N_s s^T_{ipab} C_{jrksip}\right)\right] \tag{34}$$

where the elastic coefficients and compliances are all evaluated at P = 0,

and the dashes indicate derivatives with respect to P. The quantity $\underline{U}^{o}$ denotes a limiting eigenvector of the tensor $w_{jk}(P)$ as $P \rightarrow 0$, and w is the corresponding eigenvalue. Hence, from equation (31):

$$w = (\rho_o w^2)_{P=0} = (\rho_o V^2)_{P=0} \tag{35}$$

It should be realised that the C_{jrksip} are neither isentropic nor isothermal third-order elastic coefficients but rather they are 'mixed' coefficients defined by:

$$C_{jrksip} = \left(\frac{\partial c^{S}_{jrks}}{\partial \eta_{ip}} \right)_{T;P=0} \tag{36}$$

Brugger [24] has given a thermodynamic relationship between the 'mixed' coefficients and the isentropic coefficients discussed in Section 1.2, but since the difference between the two sets is unlikely to be significantly greater than experimental uncertainties in the C's, the argument will not be elaborated further. It can be shown that the derivatives, $t'_{ab}(0)$, appearing in equation (34) reduce to very simple forms when the variable, P, represents hydrostatic pressure or uniaxial stress.

For hydrostatic pressure, $$t'_{ab}(0) = -\delta_{ab} \tag{37}$$

while for a uniaxial compression in the direction of a unit vector, $\underline{M}$,

$$t'_{ab}(0) = -M_a M_b \tag{38}$$

A useful relationship between the quantities $(\rho_o W^2)'_{P=0}$ and $(\rho_o V^2)'_{P=0}$ has been derived by Thurston and Brugger [40].

$$\left[(\rho_o V^2)' - (\rho_o W^2)'\right]_{P=0} = 2N_k N_m F^o_{km} w \tag{39}$$

where

$$F^o_{km} = \left(\frac{\partial \eta_{km}}{\partial P}\right)_{T;P=0} = s^T_{kmab} t'_{ab}(0) \tag{40}$$

Table 3 shows the results obtained by Thurston and Brugger for the derivatives $(\rho_o W^2)'_{P=0}$ for various combinations of wave-type, propagation direction and stress system in an isotropic solid. Using equations (39) and (40), it can easily be verified (Appendix 4) that these results are fully consistent with those presented by Toupin and Bernstein [23] for the derivatives $(\rho_o V^2)'_{P=0}$.

1.4 EXPERIMENTAL MEASUREMENT OF ULTRASONIC PROPAGATION VELOCITY IN ELASTICALLY STRAINED SOLIDS

As indicated in the previous section, the third-order elastic coefficients can be evaluated from experimental determinations of the velocity of small-amplitude ultrasonic waves in elastically strained solids. Particular combinations of the zero-strain third-order 'stiffnesses' (elastic constants) can be calculated from the initial slopes of the velocity-stress curves, provided the relevant second-order stiffnesses are already known. For polycrystalline metals, the

Type of stress	Propagation direction N	Mode[a]	Displacement direction U	$w \equiv (\rho_0 V^2)_{p=0}$	$(\rho_0 V^2)'$
Hydrostatic pressure	arbitrary	L	$\parallel$ to N	$c_{11}^S = \lambda^S + 2\mu$	$-1 - \frac{1}{3B}(2w + 3\nu_1 + 10\nu_2 + 8\nu_3)$
Hydrostatic pressure	arbitrary	S	$\perp$ to N	$c_{44} = \mu$	$-1 - \frac{1}{3B}(2w + 3\nu_2 + 4\nu_3)$
Uniaxial compression	$\perp$ to stress	L	$\parallel$ to N	$c_{11}^S = \lambda^S + 2\mu$	$\frac{1}{E}[\sigma(2w + 8\nu_3) + \nu_1(2\sigma - 1) + \nu_2(8\sigma - 2)]$
Uniaxial compression	$\perp$ to stress	S	$\parallel$ to stress	$c_{44} = \mu$	$\frac{1}{E}[-2w + \nu_2(2\sigma - 1) + 2\nu_3(\sigma - 1)]$
Uniaxial compression	$\perp$ to stress	S	$\perp$ to stress	$c_{44} = \mu$	$\frac{1}{E}[\sigma(2w + 4\nu_3) + \nu_2(2\sigma - 1)]$

[a] L = longitudinal, S = shear; $B = \lambda^T + \frac{2}{3}\mu$ = isothermal bulk modulus; $E = 1/s_{11}^T = 3\mu B/(\lambda^T + \mu)$ = isothermal Young's modulus; $\sigma = -s_{12}^T/s_{11}^T = \lambda^T/2(\lambda^T + \mu)$ = isothermal Poisson's ratio.

TABLE 3 SMALL-AMPLITUDE WAVE PROPAGATION IN STRAINED ISOTROPIC SOLIDS (after Thurston and Brugger [40])

measured changes in ultrasonic velocity are typically of the order of a few parts in 10^4 or 10^5 for an applied stress of 100 bars.* Unfortunately, stresses of this order are quite capable of producing plastic deformation in single crystal specimens, and since the foregoing theory of wave propagation is valid only for finite 'elastic' strains, there is an upper limit to the magnitudes of stresses which can usefully be applied to single crystals. In such cases, the changes in ultrasonic velocity are likely to be somewhat smaller than the corresponding values for polycrystalline metals. Consequently, it is most desirable that the experimental techniques should at least be capable of resolving velocity changes of the order of a few parts in 10^6.

It is extremely doubtful whether any absolute measurement of ultrasonic velocity can be made with an accuracy better than one part in 10^4, but this restriction on the precision of measurement certainly does not apply to relative changes in velocity. Very recently, Blume (45) has claimed a resolution of a few parts in 10^8 for velocity changes,

---

* 1 bar = 10^6 dyne cm^{-2}

while precisions of parts in 10^6 or 10^7 are fairly commonplace.[20,46,47] At this stage, it is convenient to review the various methods available for ultrasonic velocity measurement with some indication of their respective limitations. This will be followed by a very brief summary of the experimental measurements on elastically strained solids, since a more comprehensive survey has been presented by the author elsewhere [15, 20].

(i) Experimental techniques.

All the methods of ultrasonic velocity measurement mentioned below are particular variants on the so-called 'pulse-echo' technique, in which short pulses of mechanical energy are reflected back and forth between two parallel faces of a specimen. The mechanical energy is generated from short pulses of electrical (rf) signal using some suitable electromechanical transducer which, for example, may be a piezo-electric crystal. As it propagates, the mechanical energy is gradually attenuated, usually by a combination of several mechanisms. A partial reconversion to electrical energy may occur either at the generating transducer (single-ended operation) or at a similar transducer located on the opposite face of the specimen (double-ended operation). The phase velocity of the ultrasonic wave can be calculated from measurements of the transit time of the mechanical pulse and the path length, provided distortion of the pulse-shape is

not detectable. The calculated velocity may be seriously in error if the latter restriction is disregarded [48, 49], but under favourable conditions Markham [50] has shown that obsolute measurements can be made with an accuracy of about one part in 10^4.

Several variations on this basic pulse-echo technique have been developed by McSkimin. For example, the 'phase-comparison' method [51] is especially suitable for ultrasonic velocity measurements in solid specimens of small dimensions. In this method, the length of the driving pulse is made approximately equal to twice the transit time for a single 'round-trip' in the specimen so that successive pulse-echoes, which are normally time-separated, overlap and produce phase interference effects. Measurements are made by sweeping the carrier frequency of the transmitter pulse and observing those frequencies at which the overlapped echoes are in phase. A similar arrangement has been used by Williams and Lamb [52] with an interesting modification in that the transmitter is pulsed twice in rapid succession, the time between the double pulse action being approximately equal to the 'round-trip' travel time so that the echoes from the two separate driving pulses overlap. Interference effects are observed in the signal which is received by a separate transducer. In particular, the second echo received from the primary driving pulse interferes with the first echo from the second driving pulse. The resolution of the system is

enhanced by observing carrier frequencies for which the overlapped echoes are in antiphase and also by generating the second driving pulse at less than full amplitude to compensate for the extra attenuation incurred by the primary in its first round trip in the specimen.

An alternative technique developed by McSkimin and known as the 'pulse-superposition' method [53] can be seen as a logical extension of the double-pulse system just described. In the pulse-superposition method, the transmitter is pulsed at a high repetition rate controlled by a high-stability cw oscillator of variable frequency. This frequency is adjusted so that the echoes from the time-separated driving pulses overlap and interfere constructively, and the oscillator period is then equal to an integral multiple of the basic ultrasonic round-trip travel time, plus an integral multiple (positive or negative) of the period of the rf carrier signal. McSkimin shows how the basic round-trip travel time can be determined without ambiguity. This method has the advantage that all the echoes are used in building up the required interference pattern, in contrast to the phase-comparison techniques. The absolute accuracy of these methods is limited by the necessity to evaluate the small phase shift occurring at the transducer/specimen interface (or 'buffer-rod'/specimen interface in some arrangements [51]). This can be done provided the thickness and acoustic properties of the coupling medium are known. However, the necessary correction does not present

too much difficulty if the coupling film can be made sufficiently thin and uniform.

There are numerous special interference techniques for measuring velocity changes with typical resolutions of a few parts in 10^6, and these have been described by the author in a review already cited [20]. Moreover, the experimental apparatus developed during the present work incorporates several of these special features, and will be discussed in detail in Chapter 2.

Another method particularly suitable for measuring changes in ultrasonic velocity is known as the 'sing-around' technique. In this system, separate transmitting and receiving transducers are used and a particular echo is 'gated' out of the detected pulse-echo train and made to re-trigger the transmitter. The closed system then 'sings-around' at a repetition rate determined by the total transit time of the selected pulse-echo. Changes in velocity produce corresponding changes in transit time, and are indicated by variations in the 'sing-around' repetition frequency, which can be accurately monitored using digital frequency measuring equipment. The main limitation of the technique is the fact that the transmitter triggering point depends on the amplitude of the received echo, and if this amplitude is not constant, the resulting changes in 'sing-around' frequency may be misinterpreted as velocity changes. In addition, the subsidiary time delays associated with

electrical leads, etc. in the closed loop must be maintained constant throughout an experiment to avoid misleading results. Under controlled conditions, Forgacs [47] has estimated that velocity changes of a few parts in 10^7 can be detected.

In Blume's method [45], the frequency of a continuous high-stability reference oscillator in a coherent pulse-echo apparatus is phase-locked to the spacing, in time, of the acoustic echoes. A change in echo spacing is thereby converted into the same fractional change in oscillator frequency, which is measured continuously. Echo spacing changes of 2 to 3 parts in 10^8 have been resolved at a central reference oscillator frequency of 12 Mc/s. In contrast to the 'sing-around' technique, this method is largely insensitive to changes in echo amplitude so that the final accuracy attainable is set by the temperature stability of the sample.

(ii) Experimental measurements in strained solids

The conventional pulse-echo technique was used with limited accuracy in several early investigations of the effects of hydrostatic pressure on the elastic properties of solids. Lazarus [54] measured ultrasonic velocities in single crystals of cubic symmetry such as alkali halides and pure metals up to a pressure of 10,000 bars. Later, his results were analysed by Hearmon [22], using a theory specially

developed for cubic symmetry by Birch [21] from Murnaghan's finite strain formulation [55, 18]. Hearmon was able to evaluate several combinations of the 6 third-order elastic coefficients for these cubic materials. Although the data was insufficient for a unique determination, the combinations of third-order moduli were all negative and about an order of magnitude larger than those of second-order, in agreement with Birch's prediction [21]. The basic pulse-echo technique has also been used by Hughes and Kelly [39] and several others [56-58] for ultrasonic velocity measurements in polycrystalline solids and single crystals up to high hydrostatic pressures. On the other hand, McSkimin et al. have used the pulse-superposition [59, 60], and phase-comparison [42, 61] methods for similar hydrostatic pressure investigations, mainly on single crystals of germanium and quartz.

In order to evaluate all the third-order moduli for a given material, it is usually necessary to extend the experimental measurements to include simple uniaxial stresses. Hughes and Kelly [39] did this for several isotropic solids, but the precision of measurement obtained with a standard pulse-echo apparatus was not very high, especially in the case of polycrystalline Armco iron where the ultrasonic velocity changes were small. More accurate results for polycrystalline metals have been obtained using special interference techniques [20], by Rollins et al. [62], and Pauthier-Camier [63], and also by Crecraft [64] with a

'sing-around' method. Drabble and Gluyas [65] have applied the latter method to ultrasonic velocity measurements in uniaxially stressed germanium single crystals, and have evaluated all six third-order moduli. Their results are probably better estimates than an alternative set computed for the same material by Bateman et al. [42], who used the phase-comparison technique.

1.5 THIRD-ORDER ELASTIC COEFFICIENTS IN RELATION TO PROBLEMS OF SOLID-STATE PHYSICS

Many problems of solid state physics require a knowledge of the anharmonic character of the interatomic force constants in crystals. On the atomic scale, the anharmonic terms in the potential energy of the lattice represent a necessary exchange mechanism by means of which quantised sound waves (phonons) in different branches of the vibrational spectrum can reach thermal equilibrium. Unfortunately, there is very little reliable information on the interatomic force functions except for ionic and molecular crystals, and a full treatment in terms of anharmonic lattice theory usually becomes prohibitively complicated. Born and Huang [66] have made some advances along these lines, but for several non-linear problems of the solid state Ziman [26] has shown that a simpler and adequate approach can often be made by assuming an

elastic continuum model which includes anharmonic terms. It is reasonable to assume that the first anharmonic term in this macroscopic approximation should dominate the non-linear physical properties. The importance of the third-order elastic coefficients immediately becomes apparent, since it is these which describe the primary elastic anharmonicity.

It is sometimes convenient to consider the thermal vibrations of a crystal lattice as acoustic waves of very short wavelength, and Ziman [26] has shown how these waves may reach equilibrium by scattering one another via the anharmonic terms in the lattice energy. The macroscopic third-order elastic constants used by Ziman in the theory of 'phonon-phonon' interactions are identical with Brugger's thermodynamic coefficients [24]. Phonon-phonon interactions also play a central part in many current theories proposed to explain the observed attenuation of high frequency ultrasonic waves in crystals [67-70]. In these theories it is assumed that energy is scattered from a macroscopic travelling sound wave by interactions with the thermal phonons of the lattice. Several stringent conditions must be satisfied in order that such a concept should be valid and these are discussed by Ziman. Very recently, Mason and Bateman [71] have correlated ultrasonic attenuation measurements in pure germanium and silicon with the third-order elastic coefficients calculated for these materials from stress-induced

ultrasonic velocity changes [42, 60, 61, 65]. The observed attenuations were in good agreement with calculations based on a phonon-phonon loss mechanism first proposed by Akhiezer [72] and extended by Mason [71].

In addition to interacting with thermal phonons in the lattice, there is the possibility that ultrasonic waves can interact with each other. The latter phenomenon has recently received considerable attention, both theoretical and experimental. For isotropic media, Rollins et al. [62], and Jones and Kobett [73] have derived resonance conditions and selection rules for acoustic wave interactions from non-linear equations of motion [34]. Similar selection rules can be derived from a quantum mechanical approach [74]. Direct confirmation of elastic wave interaction in polycrystalline magnesium and aluminium has been obtained by Rollins [75, 76] from ultrasonic experiments in the lower megacycle range. Under resonant conditions, interaction between two ultrasonic beams can lead to generation of a third collimated beam with frequency, $\omega_3 = \omega_1 \pm \omega_2$, and wave-vector, $\underline{k}_3 = \underline{k}_1 \pm \underline{k}_2$. Both longitudinal and transverse waves were generated and detected, and the experimental results agreed well with the theoretical predictions as regards resonance conditions, beam collimation properties and frequency dependence. In order to compare the measured intensities of the scattered beams with the non-linear interaction theory, an independent assessment of the third-order elastic coefficients is required. Recently, the

author has evaluated all three third-order moduli for a sample of the polycrystalline magnesium used by Rollins, and these measurements will be described in Chapter 3. At the present time, these results are being correlated with Rollins' interaction experiments using a computer programme devised at Midwest Research Institute [77].

In all the work described up to this point, only small-amplitude elastic waves have been considered. It is reasonable, however, to expect that when waves of finite amplitude are propagated through a solid, the large strains should give rise to non-linear effects, and in such cases, the importance of the third-order elastic moduli is evident. A considerable number of investigations have been made recently into the propagation characteristics of finite-amplitude elastic waves in solids [78-81]. The primary effect is a tendency for the amplitude of the second harmonic to increase at the expense of the fundamental frequency component of the wave. Breazeale and Thompson [81] have expressed this quantitatively in the form:

$$A_2 = A_1^2 \frac{k^2}{4} \frac{K_3}{K_2} x \qquad (41)$$

where A_2, A_1 are the amplitudes of the second harmonic and fundamental

frequency components, k is the propagation constant, x is the propagation distance, and K_2, K_3 represent appropriate combinations of second- and third-order elastic coefficients, respectively. Equation (41) has been verified by experiment and it has been suggested that measurements of the quantity K_3 should yield information on certain combinations of the third-order moduli [81]. Seed has observed an interesting non-linearity in the frequency response of quartz resonators vibrating at high strain-amplitudes in 'thickness-shear' modes (AT- and BT-cuts [31]). As the strain-amplitude was increased, the response curves showed an increasing degree of instability in the form of a pronounced skew-distortion about the resonant frequency. A tentative explanation for the effect was based on a polynomial strain-energy function which included terms up to fourth-order. From the experimental results, Seed was able to estimate the magnitudes of two rather complicated mixed combinations of third- and fourth-order elastic coefficients.

A further non-linear problem which has received considerable attention recently is the phenomenon of acoustic amplification in piezo-electric semiconductors, first described by Hutson, McFee and White [84] and later explained by White et al. [85, 86]. It was found that an acoustic wave propagated along an appropriate direction in a piezo-

electric semi-conductor such as cadmium sulphide could be amplified or attenuated by applying a dc electric drift field. Amplification occurred when the electric field was large enough for the drift velocity of the charge carriers to exceed the velocity of the acoustic wave. Significant acoustic gain up to microwave frequencies has been reported by Quate et al. [87]. In some situations the gain may be so large that the elastic strains in the material must properly be considered as finite. Truell [88] has discussed this possibility and indicated how the theory should be modified by taking into account coupling terms involving third-order elastic coefficients.

One final example of the application of third-order elastic moduli in solid state problems is the case of thermal expansion, which as Ziman [26] has shown, is due to the anharmonicity of the interatomic forces. On the basis of a continuum model, Sheard [89] has calculated the thermal expansion from observed elastic anharmonicity of certain alkali halides and metals. The method involved calculation of the Gruneisen constant [90], γ, from a detailed knowledge of the third-order elastic constants. Reasonable agreement was obtained between the Gruneisen constants computed by this technique and those calculated in the more usual way from thermal expansivities. Sharma and Joshi [91] have used the same model to determine the temperature dependence of the Gruneisen constants for copper and germanium with limited success.

CHAPTER 2

MEASURING EQUIPMENT AND EXPERIMENTAL TECHNIQUES

In this Chapter the design and principles of operation of a new type of pulsed ultrasonic interferometer are discussed. The relevant interference conditions are derived for several possible experimental arrangements and the measured parameters related to environmentally induced changes in the propagation velocity of ultrasonic waves. A standard method for the determination of absolute velocity is also described. In addition, the principal design features are outlined for special auxiliary equipment such as specimen holders, uniaxial stressing devices, and a jig for preparing very thin uniform coupling films between specimens and transducers.

2.1 CONDITIONS OF INTERFERENCE FOR PULSED ULTRASOUND

In any experiment where two or more wave motions are to be compared by interferometric techniques, whether the waves be mechanical, electrical or optical, the basic requirement must be met that the wave motions or 'signals' are coherent. All the interference

arrangements described here for ultrasonic waves have familiar optical analogues, but whereas the latter usually involve only continuous waves (cw), the former often include both pulsed and continuous waveforms.

In the simplest ultrasonic interference arrangements, only two waveforms are compared. One of these will be merely a reference signal, and the other will be derived from a specimen subjected to varying external constraints. The second signal will always be a short pulse or 'wave-packet' of finite duration, but the reference may be either a similar pulse from an identical comparison specimen, or part of a continuous waveform. However, in a few special situations, two separate ultrasonic signals propagated through the same specimen may be compared by interference and, in such cases, either pulse may properly be regarded as the reference waveform. At this stage, it is convenient to derive the detailed interference conditions for three general experimental arrangements only, since all others can be considered as special variations of these.

(i) Interference between ultrasonic pulse and c.w. signal

Consider the case where the electrical signals from multiple ultrasonic echoes are compared with a continuous electrical reference waveform. This technique has been used in several investigations of

small ultrasonic velocity changes [45, 92-95]. It is emphasised that the resulting interference pattern is purely electrical, and should be distinguished from true ultrasonic interference such as that described later in sub-section 2.1(iii). For a particular case where separate transmitting and receiving transducers are situated directly on the specimen, the interference conditions between the m^{th} received pulse-echo and the cw signal are shown schematically in Figure 1. It is assumed that the pulses are sufficiently long that the rise and fall transients do not influence the flat-topped central parts of the pulses, thereby justifying an infinite plane wave analysis.

The instantaneous electrical voltage from the m^{th} received pulse-echo may be written

$$U_1 = a \sin\left[\omega t - k(2m-1)L_o + 2(m-1)\gamma + \phi\right] \qquad (42)$$

and for the cw signal

$$U_2 = a \sin \omega t \qquad (43)$$

where a is the amplitude, adjusted to be equal for both signals, ω is the angular frequency, t the time, k the wave propagation constant, L_o the unstrained specimen thickness, γ is a phase shift produced on reflection at either transducer, and ϕ is some arbitrary phase angle. The wave propagation constant is defined here as

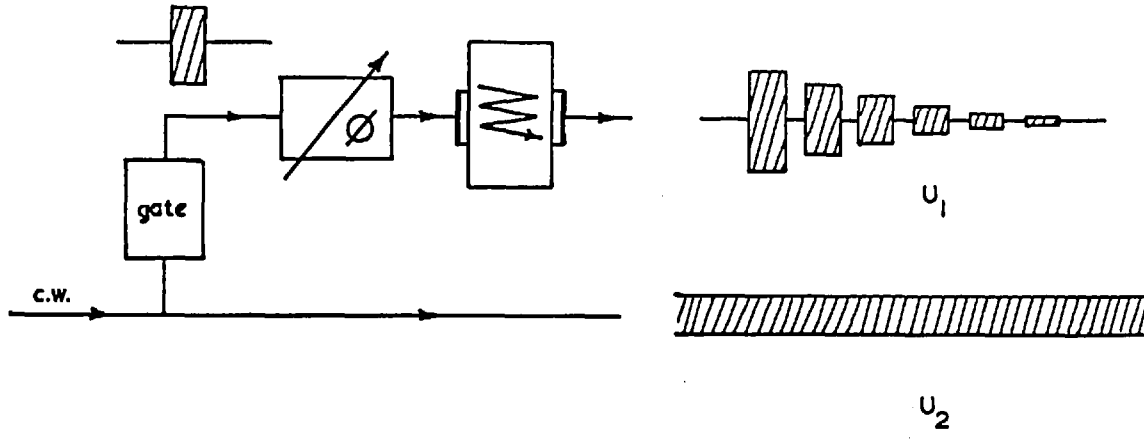

U_1 and U_2 are added algebraically and ϕ adjusted so that

$U_1+U_2 \rightarrow 0$ for m^{th} pulse

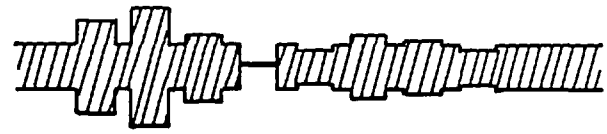

$U_1 + U_2$

FIGURE 1 SCHEMATIC REPRESENTATION OF INTERFERENCE CONDITIONS BETWEEN m^{th} PULSE-ECHO AND CW WAVEFORM

$$k = \frac{2\pi f}{W} \tag{44}$$

where f is the frequency and W is the 'natural velocity' of Thurston and Brugger's theory [40] (see equation 28 of Chapter 1). If the two signals are now added algebraically, the resulting sum is given by

$$U_1+U_2 = 2a \sin \frac{1}{2}\left[2\omega t - k(2m-1)L_o + 2(m-1)\gamma + \phi \right] \cos \frac{1}{2}\left[-k(2m-1)L_o+2(m-1)\gamma +\phi\right] \tag{45}$$

A condition of destructive interference results provided this sum is zero independently of time. For a given specimen this can be achieved either by varying the frequency or the phase shift, ϕ. In general, ϕ will not be frequency independent and it is preferable to vary the phase shift at constant frequency. The cosine term in equation 45 is identically zero whenever

$$\phi = \frac{2\pi f L_o(2m-1)}{W} + (2n+1)\pi - 2(m-1)\gamma \tag{46}$$

where n is an arbitrary integer. In a typical experiment the variation of W as a function of an external constraint such as applied stress will be so small that $W = W_o+\Delta W$ where $\Delta W/W_o \ll 1$ and W_o is the unstrained velocity, so that to a first approximation, equation 46 becomes

$$\phi = \frac{2\pi f L_o(2m-1)}{W_o}\left[1 - \frac{\Delta W}{W_o}\right] + (2n+1)\pi - 2(m-1)\gamma \qquad (47)$$

Assume now that the phase shifting device is a calibrated continuously variable electrical delay line with a linear characteristic delay of d seconds per scale division. The phase parameter may be written as the sum of two parts, one variable and the other a constant part representing parasitic phase shifts in the electronic apparatus. In terms of arbitrary delay line divisions, D,

$$\phi = 2\pi f d(D+D_o) \qquad (48)$$

where D_o is a constant at a particular frequency.

It is now possible to rewrite equation 47 in the very simple form

$$D = S\frac{\Delta W}{W_o} + C(f) \qquad (49)$$

where the quantity $S = \dfrac{-L_o(2m-1)}{W_o d}$ (50)

is independent of frequency. A change in frequency merely alters the starting position on the delay line. Since the primary concern is the determination of the slope, S, the measurement of the absolute value of the carrier frequency, f, proves unnecessary. It is sufficient simply that the frequency should remain constant during the experiment.

The relationship between $\Delta W/W_o$ and the first stress-derivatives appearing in the theory due to Thurston and Brugger [40] is readily derived from a Maclaurin expansion for W, retaining only the first order term. Then:

$$W = W_o + \Delta P \left[W'\right]_o = W_o + \Delta P \left[\frac{(\rho_o W^2)'}{2\rho_o W}\right]_o$$

Hence:

$$\frac{\Delta W}{W_o} = \frac{\Delta P}{2\rho_o W_o^2} \left(\rho_o W^2\right)'_o \qquad (51)$$

where ΔP is an applied macroscopic stress. In Table 3, the derivatives $(\rho_o W^2)'_o$ for an isotropic solid are given explicitly in terms of third-order elastic moduli. The experimental parameters of equations 49 and 50 are thereby directly linked to non-linear elastic theory by equation 51.

(ii) Interference between electrical signals from two similar pulsedultrasonic wavetrains

Consider now the case of electrical interference between signals derived from two separate but similar multiple ultrasonic echoes as shown schematically in Figure 2. In practice, there are two possible cases of interest. Either the ultrasonic echoes may be derived from two separate specimens, one of which is used merely for comparison [46, 96], or both sets of echoes may be established within the same specimen [20, 96].

The latter example is suitable only for shear wave interference, where the polarisation properties of the waves provide an essential distinction between the two otherwise identical sets of echoes.

The conditions of interference for the experimental arrangement of Figure 2 may be derived as follows. The instantaneous electrical voltages for the m^{th} received pulse-echoes in the two wavetrains are respectively:

$$U_1 = a \sin\left[\omega t - k_1 (2m-1)L_o + 2(m-1)\gamma_1 + \phi\right] \tag{52}$$

$$U_2 = a \sin\left[\omega t - k_2 (2m-1)L_o + 2(m-1)\gamma_2\right] \tag{53}$$

where it is assumed that $\gamma_1 \rightarrow \gamma_2$ and

$$\frac{k_1-k_2}{k_o} = \frac{\Delta k_{12}}{k_o} = \frac{\Delta W_{21}}{W_o} << 1 \tag{54}$$

Destructive interference occurs if the algebraic sum of U_1 and U_2 is identically zero, independent of time. By a procedure similar to that used in the previous sub-section it is easily verified that the phase shift ϕ must then satisfy the relation:

$$\phi = \frac{2\pi f L_o (2m-1)}{W_o} \left[-\frac{\Delta W_{12}}{W_o}\right] + (2n+1)\pi - 2(m-1)(\gamma_1-\gamma_2) \tag{55}$$

If the phase shifter is a linear calibrated electrical delay line then this last expression may be rewritten in terms of delay line divisions.

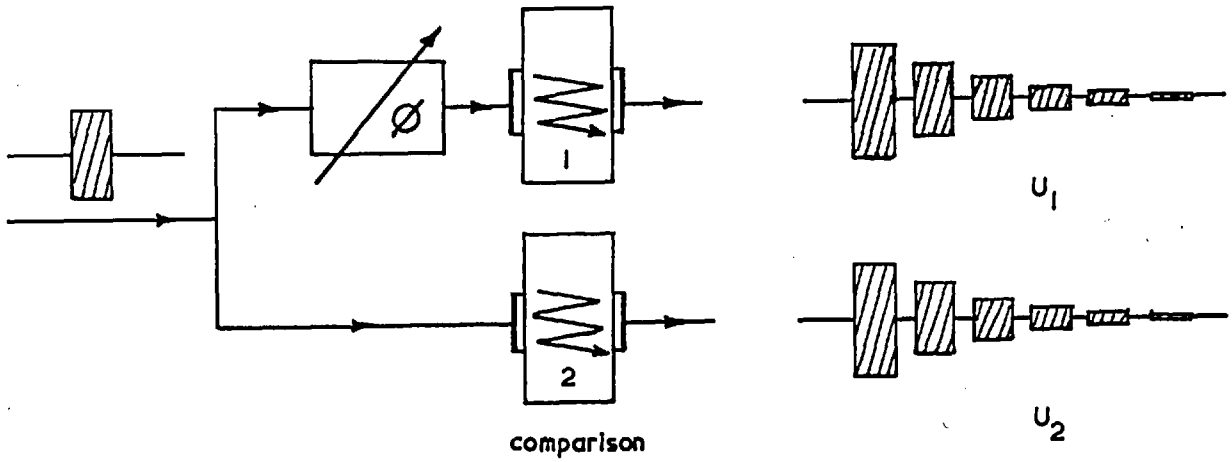

U_1 and U_2 are added algebraically and ϕ adjusted so that

$U_1 + U_2 \rightarrow 0$ for m^{th} pulse

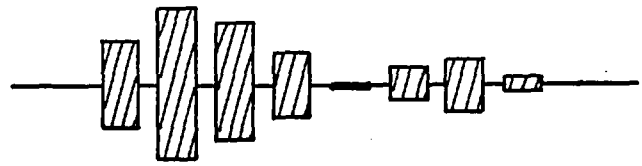

$U_1 + U_2$

FIGURE 2 DESTRUCTIVE INTERFERENCE BETWEEN TWO SIMILAR ULTRASONIC MULTIPLE ECHO PATTERNS

$$D = S \frac{\Delta W_{12}}{W_o} + A(f) \qquad (56)$$

where S is defined by equation 50. The relationship between the quantity $\Delta W_{12}/W_o$ and the first stress-derivatives $(\rho_o W^2)'_o$ of Thurston and Brugger may be derived from Maclaurin expansions for $(W_1 - W_2)$, retaining only first-order terms. There are two cases of interest. If a separate unstressed comparison specimen is used, then, W_2 remains constant, so that

$$\frac{\Delta W_{12}}{W_o} = \frac{\Delta P}{2\rho_o W_o^2} (\rho_o W_1^2)'_o + \left(\frac{\Delta W_{12}}{W_o}\right)_o \qquad (57)$$

In the special case where two ultrasonic shear waves, polarised parallel and perpendicular to an applied uniaxial stress direction, are propagated through the same specimen in a direction normal to this stress [20], then both W_1 and W_2 vary, and

$$\frac{\Delta W_{12}}{W_o} = \frac{\Delta P}{2\rho_o W_o^2} \left[(\rho_o W_1^2)' - (\rho_o W_2^2)'\right]_o + \left(\frac{\Delta W_{12}}{W_o}\right)_o \qquad (58)$$

(iii) Interference conditions for McSkimin phase-comparison technique

Either of the two methods outlined above are suitable for measuring small fractional changes in velocity, but in addition, it will often be necessary to evaluate the absolute velocity of ultrasonic

waves. The phase-comparison technique developed by McSkimin [51] is particularly convenient for absolute measurements. Figure 3 shows a typical experimental arrangement in which separate transmitting and receiving transducers are mounted directly on the specimen by means of a very thin film of a suitable coupling medium. If the transmitting pulse is lengthened until successive ultrasonic echoes overlap, interference effects are observed in the overlapped regions. The carrier frequency of the driving pulse may be varied to produce either destructive or constructive interference. In this phase comparison technique, the interference actually occurs within the specimen, in contrast to the electrical interference of methods (i) and (ii).

The instantaneous voltages of the signals derived from the m^{th} and $(m+1)^{th}$ pulse-echoes are respectively:

$$U_m = a \sin A \tag{59}$$

$$U_{m+1} = b \sin(A-2kL_o+2\gamma) \tag{60}$$

where $$A = \omega t - k(2m-1)L_o + 2(m-1)\gamma \tag{61}$$

Assume that the carrier frequency has been so adjusted that in the overlapped region, the resultant amplitude of the phase-added m^{th} and $(m+1)^{th}$ echoes is a minimum. It may be shown from equations 59 and 60 that this condition of destructive interference is satisfied whenever

$$k_n L_o - \gamma = (n+\tfrac{1}{2})\pi \tag{62}$$

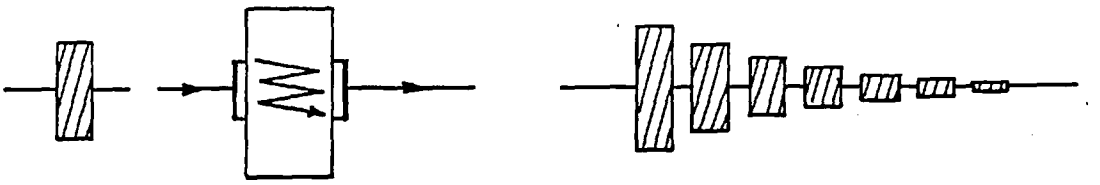

time-separated pulse-echoes

pulse length is increased and carrier frequency adjusted for

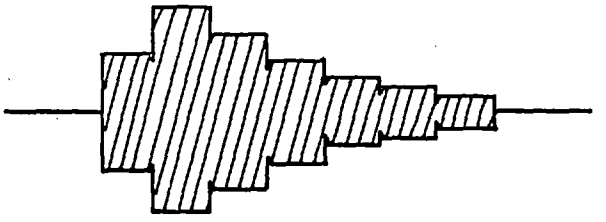

constructive interference

destructive interference

FIGURE 3 INTERFERENCE CONDITIONS IN McSKIMIN PHASE-COMPARISON TECHNIQUE

where n is a positive arbitrary integer. This result is independent of the pulse-echo number, m. (For constructive interference, the right hand side of equation 62 becomes $m\pi$). It is most important to know the frequency dependence of the reflection phase shift, γ. Williams and Lamb [52] have shown that if the coupling films are sufficiently thin and the damping is small, the phase shift near the resonant frequency of the transducer, f_o, is given sufficiently accurately by

$$\gamma = \left[1 - 2K(f - f_o)/f_o\right]\pi \tag{63}$$

where $K = Z_T/Z_S$ is the ratio of the characteristic mechanical impedances of transducer and specimen. If adjacent null frequencies (carrier frequencies at destructive interference condition) are denoted by f_n, f_{n+1}, then from equations 62 and 63,

$$2f_n\tau - 1 + 2K(f_n - f_o)/f_o = n + \frac{1}{2} \tag{64}$$

$$2f_{n+1}\tau - 1 + 2K(f_{n+1} - f_o)/f_o = n + \frac{3}{2}$$

where τ is the time delay for a single transit through the specimen, and is given by

$$\tau = \frac{L_o}{W_o} = \frac{L_o}{V_o} \tag{66}$$

Hence the frequency difference between adjacent nulls is

$$\Delta f = f_{n+1} - f_n = (2\tau+2K/f_o)^{-1} \tag{67}$$

If this relation is substituted back into equation 64, then

$$\frac{f_n}{\Delta f} - 2K = n+\frac{3}{2} \tag{68}$$

Provided the factor K is known approximately, the integer n may be calculated without ambiguity from the last equation, and it should then be possible to calculate τ from equation 64. However, the accuracy of this estimate would be limited by a lack of precise data for K. Williams and Lamb [52] have shown that this difficulty can be avoided by calculating the quantity τ' for a series of null frequencies on each side of the transducer resonant frequency, where τ' is given by

$$2f_n\tau' = n+\frac{3}{2} \tag{69}$$

The value of τ' at f_o is then computed from these results by interpolation, and it follows from equation 64 that at the resonant frequency of the transducer, $\tau = \tau'$. Hence the absolute velocity of the ultrasonic waves can be evaluated.

2.2 PRINCIPAL FEATURES OF ELECTRONIC MEASURING EQUIPMENT

A versatile ultrasonic interferometer, which can be operated in any of the basic interferometric arrangements outlined in the previous section, has been developed during the present work. At this stage it is convenient to present a short account of the principal design features and capabilities of the instrument, supplemented by simple block diagrams showing the appropriate interconnection schemes for particular measuring applications. A full description of the electronic details will be given in Appendix 1.

Of the two methods described in Section 2.1 for measuring fractional changes in ultrasonic velocity, the first one, which relies on interference between a received pulse-echo wavetrain and a continuous reference signal, is undoubtedly the more convenient and economical. The alternative method, using a comparison specimen, requires twice the number of transducers (and specimens). The design of a transmitter suitable for the former type of measurement is particularly simple, since it is sufficient merely to gate the output from a continuous oscillator and provide a calibrated variable delay between the cw reference and the gated output. However, since the gating action does not occur at any particular part of the rf cycle (unless special phase-locking arrangements are included [45]), the oscilloscope display of the carrier wave within the pulse-echo

envelope is incoherent from one sweep to the next, although the envelope is itself stationary. On the other hand, if the oscillator is pulsed, rather than operated continuously, a completely stable display is obtained, since the pulsing action is synchronised to the sweep of the oscilloscope time base. In this latter case, however, there is no possibility of interference between the received pulse-echoes and the transmitter pulse, since if the echoes are to be time-separated, they must arrive at the receiver after the termination of the transmitter pulse.

In order to obtain maximum precision in adjusting the delay line for an interference 'null', it is most desirable that the oscilloscope display for both carrier wave and pulse envelope should be completely stationary with time. The two apparently conflicting requirements of a stable display (pulsed oscillator), and interference between the pulse-echoes and a continuous reference waveform (gated cw oscillator) have been reconciled in the present apparatus by a novel combination.

The solution may be summarised as follows: the oscillator is switched on at a particular instant and the rf output quickly reaches a steady state, after which a short selected portion of the carrier wave is gated out and used to drive an ultrasonic transducer;

the carrier wave is maintained at a constant level for a further time until the ultrasonic echoes are substantially attenuated, and then the oscillator is switched off. The foregoing technique retains the desirable feature of a stable oscilloscope display by using a pulse-modulated oscillator, but also allows the possibility of controlled interference between the pulse-echoes and the latter part of the carrier wave, which continues after the short gating action. The sequence of operations is represented in Figure 4, which shows a block diagram of the electronic pulse generator and transmitter.

A typical cycle of events is initiated in the pulse generator by a blocking oscillator, which either may be synchronised by an external source, or alternatively may 'free-run' at a basic repetition rate variable from about 10 to 600 c/s. The blocking oscillator provides simultaneous positive and negative trigger pulses, the former of which is used to trigger a Tektronix 545A oscilloscope, while the latter triggers a pair of multivibrators, one directly and the other via a short variable delay as shown in Figure 4. The directly triggered multivibrator generates a long negative timing waveform (about 150 s), which is subsequently inverted and reshaped to yield a positive voltage rectangle. By a similar process, the second multivibrator, inverter and shaper provide a shorter, delayed gating waveform, variable in length from about 0 to 35μs.

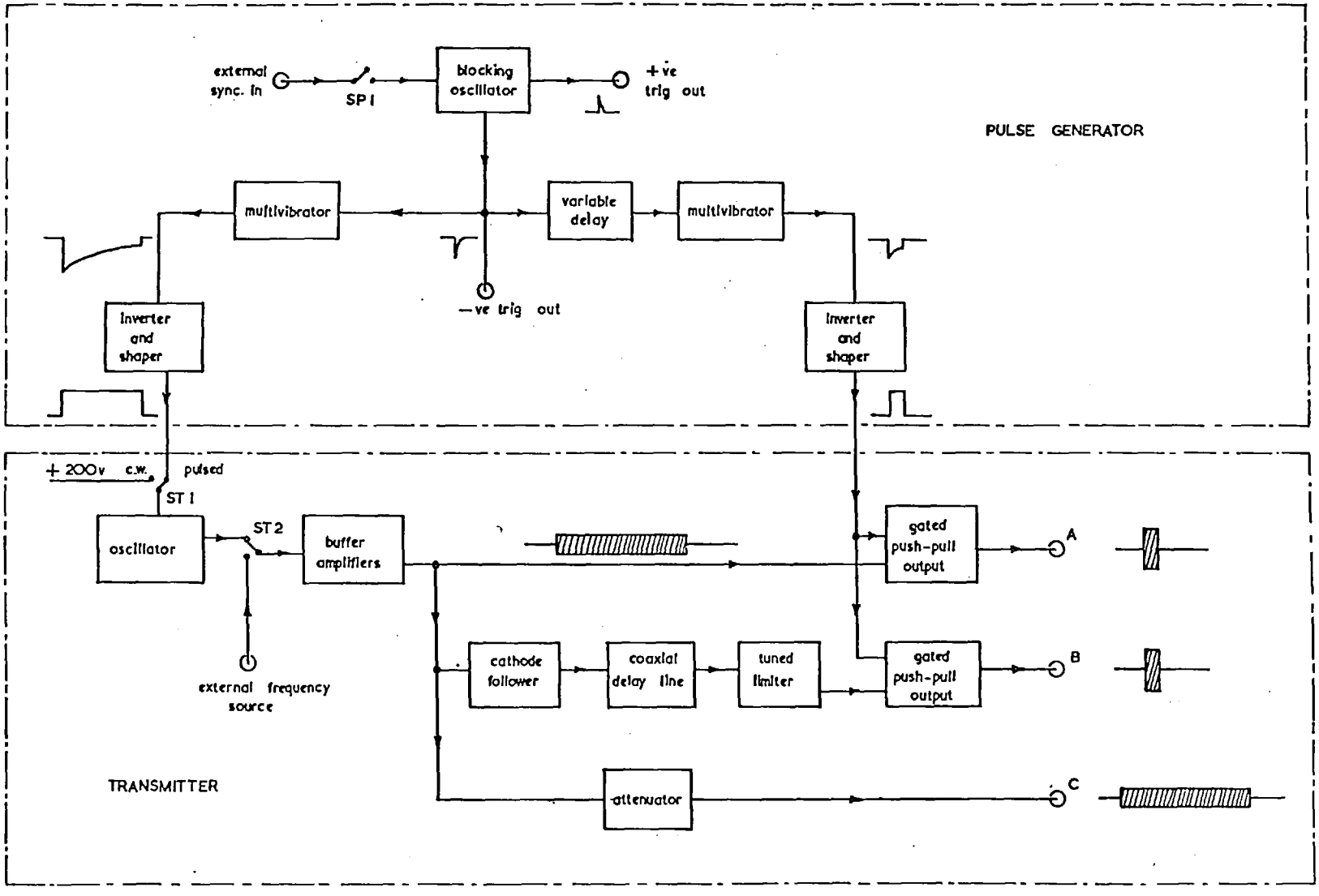

FIGURE 4 BLOCK DIAGRAM OF PULSE GENERATOR AND TRANSMITTER

The longer (150μs) positive voltage rectangle is used to switch on a tuned oscillator in the transmitter, and the resulting 5 Mc/s rf output is amplified in buffer stages before being split into three separate channels. In the first of these the long pulse of carrier wave is fed directly into a push-pull output stage, where a short selected portion is gated out by the delayed gating waveform from the pulse generator (output A). In the second channel, which is isolated from the other two by a cathode follower stage, the long rf pulse is fed into a coaxial delay line (Cossor 1048), which is the most important unit in the entire electronic equipment. The delay line is linear and continuously variable from 0 to almost 0.4μs, which allows a total possible phase shift of more than 3π radians at a frequency of 5 Mc/s. If any small distortions of the carrier wave are introduced in the delay line, they are removed by a tuned limiter before the phase-shifted signal is fed into a gated push-pull output stage identical to that in the first channel (output B). In the third channel, the long transmitter pulse is attenuated and then fed directly to output C.

All of the interferometric applications discussed in the previous section may be realised in practice by using suitable combinations of the three transmitter outputs, A, B and C.

(i) Practical arrangement for observing electrical interference between received pulse-echoes and extended transmitter pulse

As mentioned above, very small changes in the propagation velocity of small-amplitude ultrasonic waves can be measured very conveniently by a technique based on interference between received pulse-echoes and an extended transmitter pulse. The theory developed in Section 2.1(i) is valid for this case, and most of the measurements reported in Chapter 3 have been obtained using this method, which is equally applicable to both longitudinal and transverse ultrasonic waves. A practical arrangement suitable for these measurements is shown in Figure 5.

The scheme shown is based on the pulse generator and transmitter described above. A quartz transducer, attached to the specimen under investigation, is driven by the variable-phase, gated, rf pulse from transmitter output B. The multiple ultrasonic echoes are received by a similar transducer, and the resulting electrical signals are amplified and fed into one input of a dual channel preamplifier (type CA) of a Tektronix 545A oscilloscope. The long pulse of reference carrier wave from transmitter output C is attenuated and fed into the second input channel of the oscilloscope preamplifier. Photographs of some typical oscilloscope displays obtained with this arrangement are shown in Figure 6.

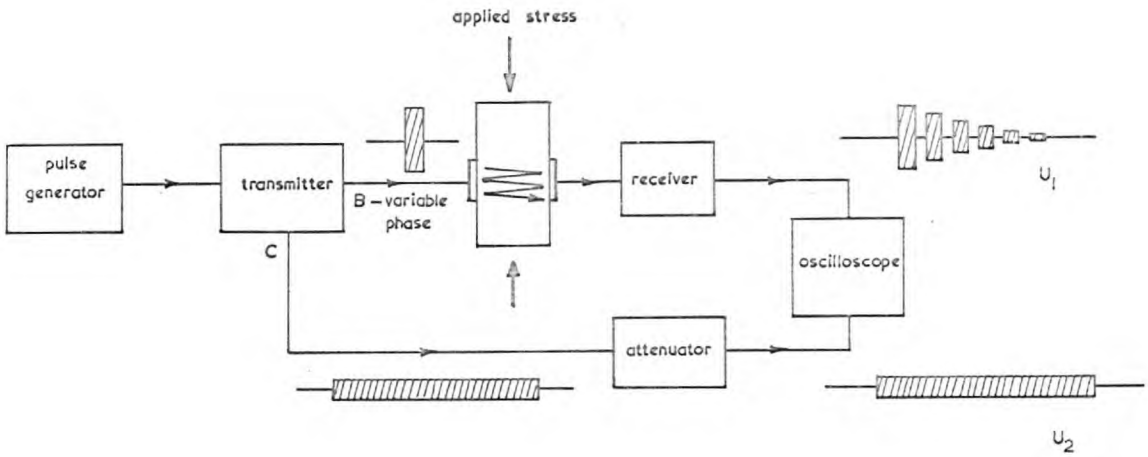

FIGURE 5 ELECTRICAL LAYOUT FOR INTERFERENCE BETWEEN RECEIVED PULSE-ECHOES AND EXTENDED TRANSMITTER PULSE

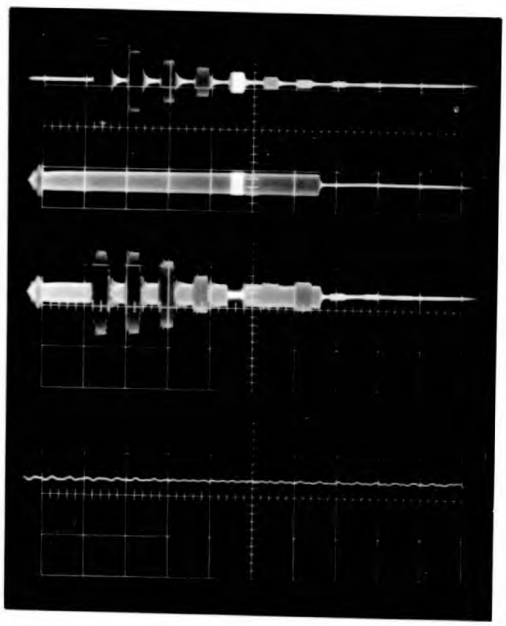

FIGURE 6 TYPICAL OSCILLOSCOPE DISPLAYS OBTAINED WITH ARRANGEMENT SHOWN IN FIGURE 5

(i) Individual signals, U_1 and U_2.
(ii) Phase-added signals, $U_1 + U_2$.
(iii) Bright portion of trace (ii) expanded.

The top pair of traces represent the received pulse-echoes and the extended transmitter pulse, respectively. If these two signals are algebraically summed in the preamplifier, and the delay line in the transmitter is critically adjusted, then interference effects are observed, such as shown in the middle trace of Figure 6. In this particular case, the system has been adjusted for destructive interference between the 5^{th} pulse-echo and the extended reference pulse (brightened portion of middle trace). The lowest display shows the brightened portion of the middle trace expanded at a faster sweep rate.

During a measurement, the delay line is adjusted to maintain the 'null' condition as a function, say, of the load applied to the specimen. It will be noticed that even in the 'null' condition, the expanded trace is not a degenerate straight line, but shows some second harmonic content. This second harmonic is due to a slight skew distortion, introduced intentionally into the long transmitter pulse, but filtered out in the shorter, gated transmitter pulse. There is a perfectly good reason for this unusual procedure. It was found by experience that small departures from the destructive interference null could be detected by an initial asymmetry of the 'harmonic' trace more easily than corresponding departures from the degenerate straight

line trace obtained with pure sinusoidal waveforms.

The sensitivity of the technique may be illustrated by the following example. Each division on the calibrated delay line corresponds to a time interval of slightly less than 0.4 ns. With practice, the interference null can be set reproducibly to better than half a scale division. The sensitivity of detecting small changes in the transit time (or velocity) of an ultrasonic pulse is directly proportional to the transit time itself. In a typical case, the pulse will have travelled a distance in the specimen corresponding to about 100μs, so that the sensitivity would be of the order of 1 or 2 parts in 10^6. For investigations of the stress-dependence of ultrasonic velocity in polycrystalline solids, this sensitivity is more than adequate, though for single crystals the full sensitivity might well be required.

(ii) Practical arrangement for observing electrical interference between two similar received pulse-echo wavetrains

An alternative method of measuring small changes in ultrasonic velocity relies on electrical interference effects between two similar pulse-echo wavetrains. The necessary theory for the interference conditions was derived in sub-section 2.1(ii). Figure 7 shows an experimental

arrangement which is suitable for this particular interferometric technique. In the case illustrated, the relevant transmitter outputs are the two short, gated, rf pulses (labelled A, B in Figure 4) which are used to drive quartz transducers attached to two identical specimens. The multiple ultrasonic echoes are received by separate transducers, amplified, and fed into the dual trace preamplifier of the Tektronix 545A oscilloscope.

The phase relationship between the two sets of received echoes may be altered by means of the variable delay line situated in channel B in the transmitter. If the two echo wavetrains are algebraically summed in the oscilloscope preamplifier, interference effects are observed as shown in the middle photograph of Figure 8. The delay line has been adjusted for destructive interference between the 5^{th} pulse-echoes in the two channels. In the lowest photograph, the brightened portion of the middle trace is shown expanded at a faster sweep rate, and again, it will be noticed that a small amount of second harmonic remains unbalanced in the null condition. The second harmonic occurs only in the channel A echoes, since any harmonic content in channel B is filtered out in the tuned limiter stage following the delay line in the transmitter (see Figure 4). The sensitivity of the apparatus is comparable with that discussed in the preceding sub-section.

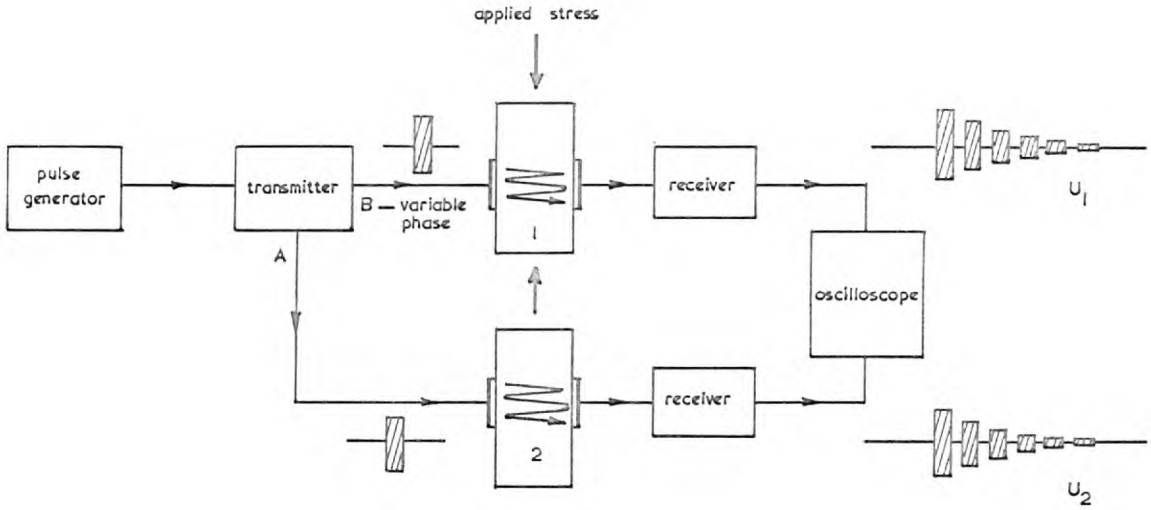

FIGURE 7 ELECTRICAL LAYOUT FOR INTERFERENCE BETWEEN TWO SIMILAR PULSE-ECHO WAVEFORMS

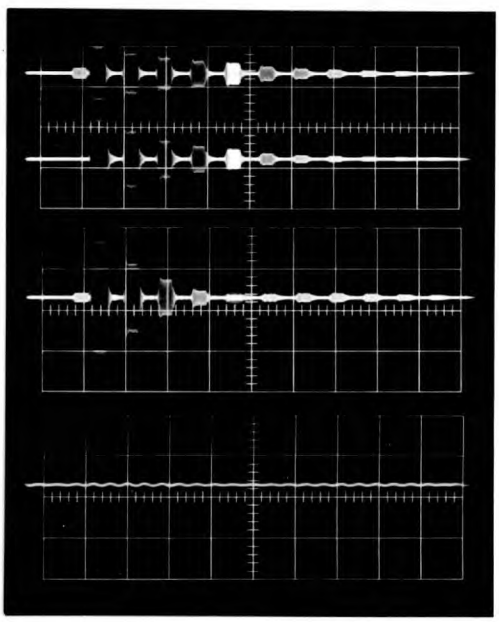

FIGURE 8 TYPICAL OSCILLOSCOPE DISPLAYS OBTAINED WITH ARRANGEMENT SHOWN IN FIGURE 7

(i) Individual signals, U_1 and U_2.
(ii) Phase-added signals, $U_1 + U_2$.
(iii) Bright portion of trace (ii), expanded.

If a comparison specimen is used, as in the case illustrated in Figure 7, this technique is applicable to both longitudinal and shear wave measurements. There is one other interesting case where the two sets of ultrasonic echoes are established within the same specimen. This latter arrangement is possible only for pure shear waves, polarised parallel andnormal, respectively, to a principal axis of the specimen. In the case of an isotropic material loaded uniaxially, the principal axis is along the direction of the applied stress. If two shear waves, polarised as above, are propagated through the specimen in a direction normal to this principal axis, the very small difference between their phase velocities can be measured using the foregoing technique [20]. However, the more economical method using interference between the pulse-echoes and an extended transmitter pulse is generally preferable in all other investigations of small velocity changes.

(iii) McSkimin phase-comparison method for measurement of absolute velocity

In Section 2.1(iii), the theoretical conditions of ultrasonic interference were drived for the special case known as McSkimin's phase-comparison method of absolute velocity measurement [51]. No further explanation is required here other than to show how the pulse generator and transmitter of Figure 4 can be used for this particular measurement.

Referring back to Figure 4, it should be mentioned that the internal oscillator in the transmitter can be continually tuned over a bandwidth of about 1 Mc/s centred at 5 Mc/s. The internal oscillator can be switched by switch ST1 so as to operate continuously, and the carrier frequency measured directly by a Hewlett-Packard, model 524C, digital electronic counter, connected to transmitter output C. If the length of the gated transmitter pulse is increased so that successive ultrasonic echoes overlap in the specimen, interference effects are observed in the received signals. The carrier frequency may be tuned through a range on either side of the resonant frequency of the identical transmitting and receiving transducers, and the 'null' frequencies measured for the destructive interference positions, using the electronic counter.

Alternatively, the internal oscillator may be switched off altogether and replaced by an external frequency synthesiser (Schomandl, type ND5, with associated equipment), as shown in Figures 4 and 9. In this case there is no need for the electronic counter, as the synthesised frequency may be read off directly, in digital form, from the Schomandl setting dials. The experimental arrangement using this external frequency source is shown in Figure 9. Either of the two short gated pulses from transmitter outputs A or B may be used to drive the quartz transmitting transducer. In Figure 10, typical oscilloscope displays are shown for time-separated pulses, overlapped pulses in constructive interference, and finally, overlapped pulses in destructive interference.

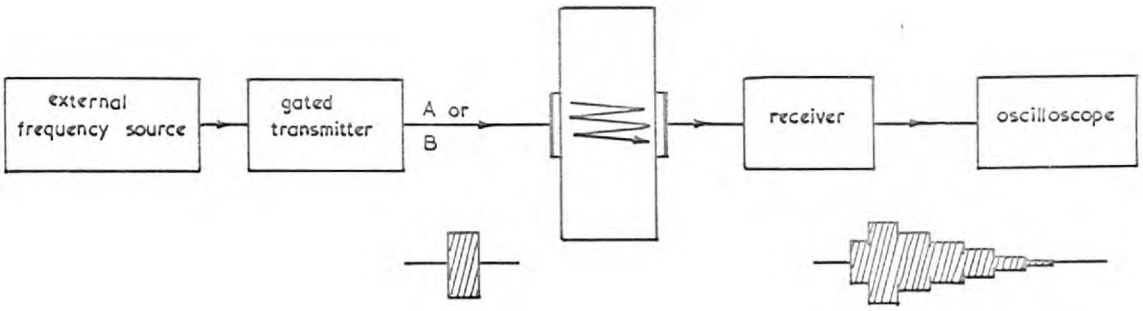

FIGURE 9 ELECTRICAL LAYOUT FOR McSKIMIN PHASE-COMPARISON TECHNIQUE

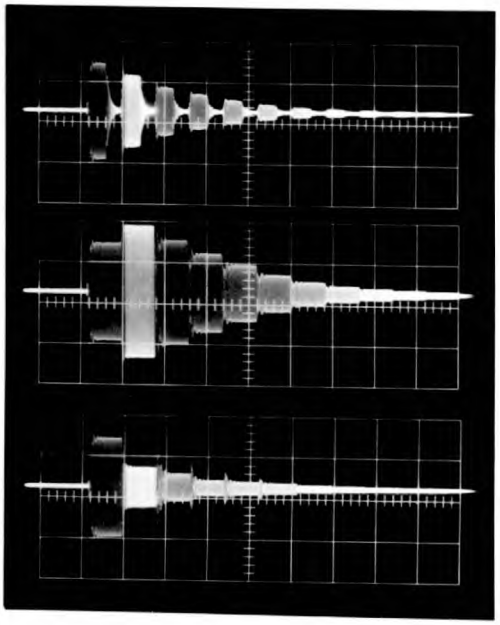

FIGURE 10 TYPICAL OSCILLOSCOPE DISPLAYS OBTAINED WITH ARRANGEMENT SHOWN IN FIGURE 9

(i) Time-separated pulses
(ii) Pulse length increased; frequency adjusted for constructive interference, and
(iii) destructive interference

2.3 SPECIMEN HOLDER

In order to evaluate all three third-order elastic constants for 'quasi-isotropic' polycrystalline metals, it is only necessary to investigate the velocity changes of ultrasonic waves, both longitudinal and transverse, propagated through the specimens in a direction perpendicular to a uniform applied uniaxial stress. Specimens in the shape of rectangular parallelepipeds are particularly suitable for this experimental configuration, since the requirement of a uniform uniaxial stress is satisfied by applying a uniform static compressive thrust between any opposite pair of parallel faces. Furthermore, ultrasonic waves can be propagated in a direction perpendicular to this stress by means of transducers attached directly to either of the two remaining pairs of parallel faces.

The specimen holder (Figure 11), consists of two parts machined from aluminium alloy and bolted together to form a rectangular block approximately 2" x 2" x 2¼". In the larger part, a central rectangular slot was milled parallel to one of the principal axes of the block. In addition, a circular hole, 1¼" in diameter was bored through the centre of the block, but in a direction perpendicular to the axis of the slot. A typical specimen is held in the rectangular slot by means of two nylon screws as shown in the photograph.

FIGURE 11 SPECIMEN IN HOLDER SHOWING TRANSDUCER LOCATION

The primary function of the holder is the precise location and orientation of the ultrasonic transducers on the specimen faces. This is achieved with the help of perspex annular discs, which fit snugly into the circular hole in the main holder, and rest against the parallel-sided specimen. The circular quartz transducers may be 'wrung' on to the specimen, and aligned coaxially by means of the perspex discs, since the central holes in the latter are only very slightly larger in diameter than the transducers themselves. (See Figure 11). In the case of longitudinal wave transducers no further orientation is required. However, for shear wave transducers, the vibration directions of the transmitting and receiving quartz crystals must be precisely aligned not only with each other, but also with the principal axes of the specimen. The necessary orientation can be controlled by direct visual observation through the transparent perspex locating discs while the transducers are rotated and their vibration directions (see Appendix 3) compared with the principal axes marked on the specimen.

The back electrodes of the transducers consist of very thin gold films evaporated on to the quartz under vacuum. Electrical contact to these back electrodes is made via very light phosphor-bronze springs, which are soft-soldered to the centre conductors of

conventional uhf plugs (Amphenol 83-1R) as shown in Figure 11. The metallic specimens, which themselves act as front electrodes for the transducers, are electrically grounded by direct mechanical contact with the aluminium specimen holder.

2.4 UNIAXIAL STRESSING DEVICES

Although it would be useful to investigate ultrasonic velocity changes in solids both under conditions of uniaxial compression and also under uniaxial tension, the present experimental work has been confined, from considerations of simplicity of specimen geometry, to compressive loading. In this case, sufficiently uniform stress distributions can be produced by compressing the specimens along a principal axis by means of some simple hydraulic mechanism. Accordingly, two hydraulic systems were designed to develop maximum thrusts of twenty-five tons and two tons, respectively, the former for use with polycrystalline metals and the latter with single crystals.

The 25-ton hydraulic system consists of a commercial hydraulic jack (Tangye, model 625, 'Hydralite') supported on the lower of two circular steel plates, $1\frac{1}{4}$" thick, held rigidly apart and parallel to each other by three $1\frac{1}{4}$" diameter steel rods, as shown in Figure 12. Specimens are compressed between the machined top surface of the ram of

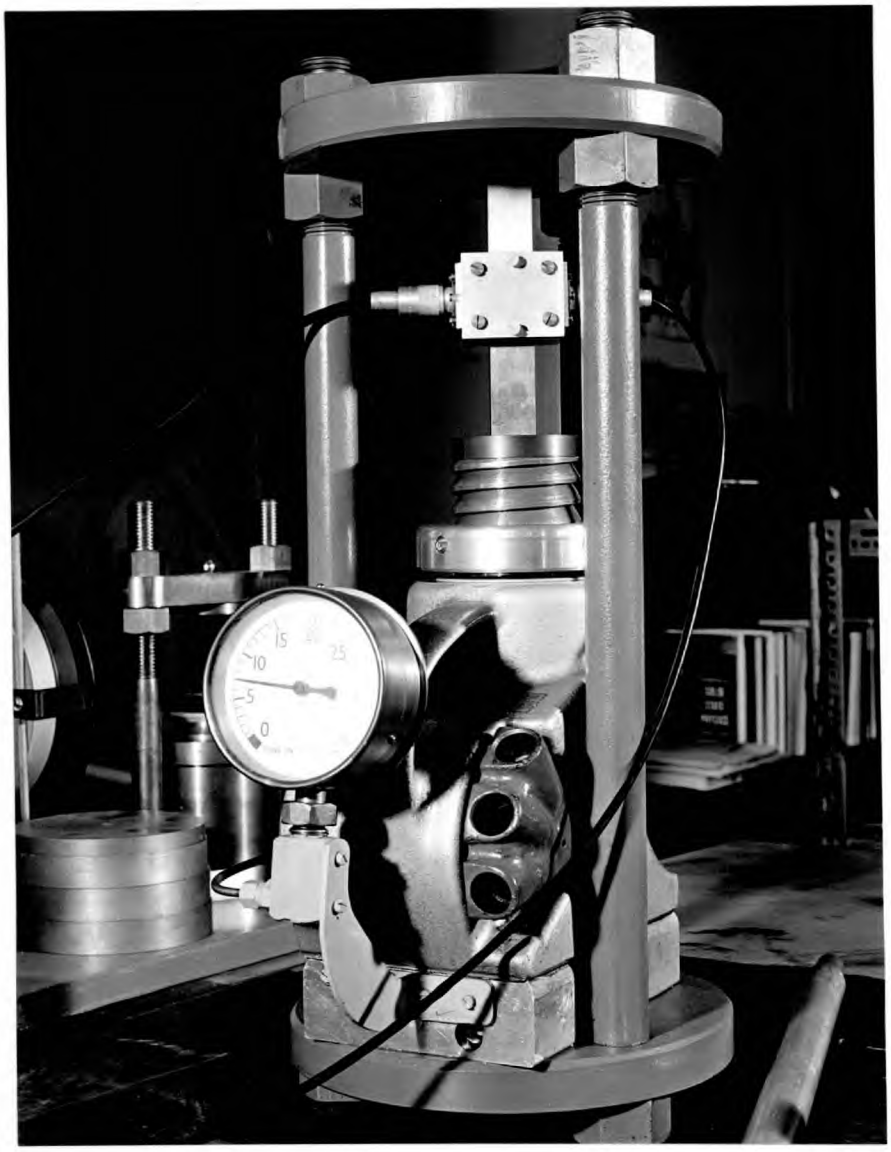

FIGURE 12 25-TON HYDRAULIC UNIT WITH STEEL SPECIMEN IN POSITION

the hydraulic jack and the machined lower surface of the upper steel plate. These two surfaces may be approximately aligned for parallelism by suitable adjustment of the locating nuts which hold the upper plate in position on the vertical steel rods. Any small deviations from parallelism may be counteracted by inserting a very thin aluminium plate between the specimen and the upper steel plate. Since aluminium extrudes quite readily under the pressures used in typical experiments on polycrystalline metals, this ensures a uniform distribution of the load over the end faces of the specimen. The compressive thrust can be estimated to within $\frac{1}{4}$-ton weight by a Bourdon-type gauge calibrated to read directly in tons weight for the particular hydraulic jack used. Figure 12 shows a 6" x 1" x 1" steel specimen compressed uniaxially in the above device. The quartz transducers (not visible in the photograph) are located on the lateral surfaces of the specimen by means of the special holder described in the previous section.

The 2-ton hydraulic system, which was designed for use with single crystals, is considerably more sophisticated than the 30 ton device. For example, special precautions were taken to ensure very uniform loading conditions, and furthermore, an auxiliary hydraulic 'dead-weight' unit was connected in parallel with the main specimen unit to regulate

the oil pressure. The 'plumbing' scheme is shown in Figure 13 and requires no further explanation here. In Figure 14, a specimen is shown in position in the main unit. (For clarity, the specimen holder is not shown). It should be noticed that the pressure is applied through a 5/8" diameter steel ball which also acts as a universal coupling joint, ensuring that the specimen is loaded evenly over its end faces, provided these faces and the corresponding contact surfaces on the hydraulic unit are perfectly flat. The latter surfaces were hand-lapped for this purpose. Figure 15 shows the 'dead-weight' hydraulic unit, which fulfills two functions. Firstly, it can be used in conjunction with standard weights to calibrate the pressure gauge, and secondly, it acts as a maximum thrust regulator for the main hydraulic unit. Thus, if because of over-vigorous hand pumping, the oil pressure exceeds the downward pressure exerted by the 'dead-weight' piston and the standard weights, then the piston simply moves upwards, and the oil pressure is reduced. In order to avoid bending this piston (which is only 3/8" in diameter) by asymmetrical loading, the standard weights are located on the weight table by means of a central rod, coaxial with the piston itself.

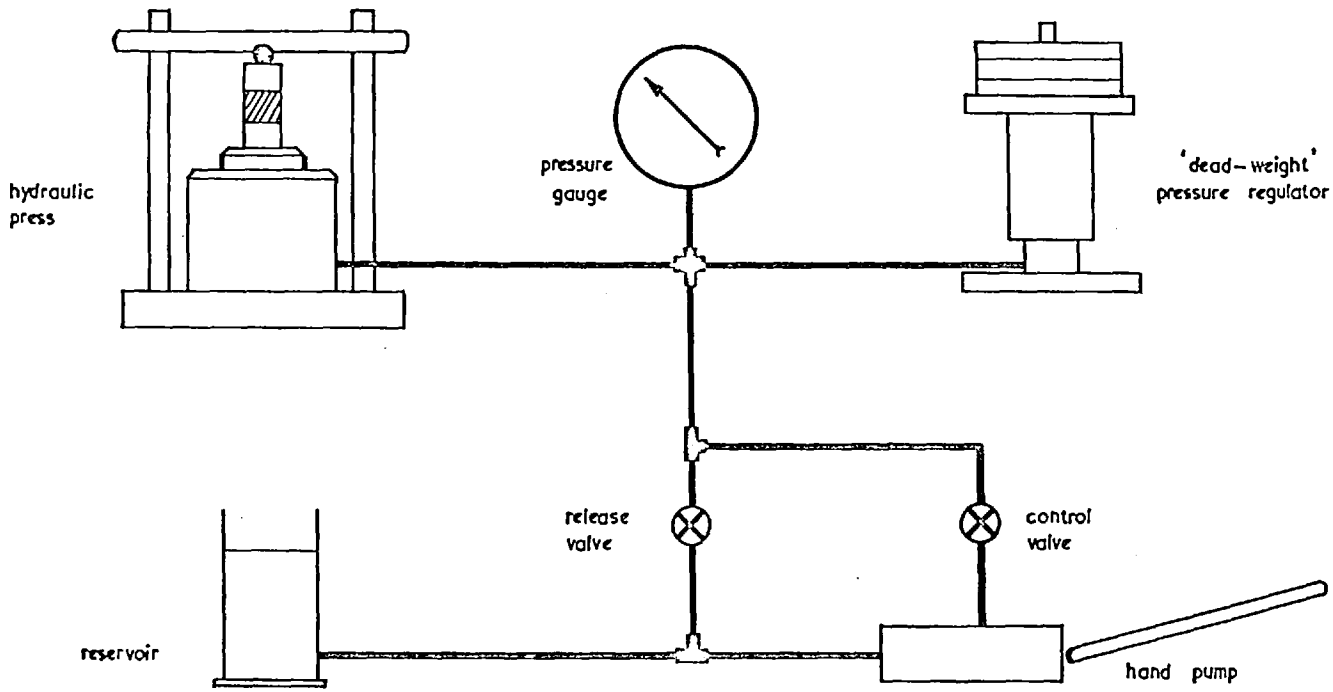

FIGURE 13 PLUMBING ARRANGEMENT FOR 2-TON HYDRAULIC SYSTEM

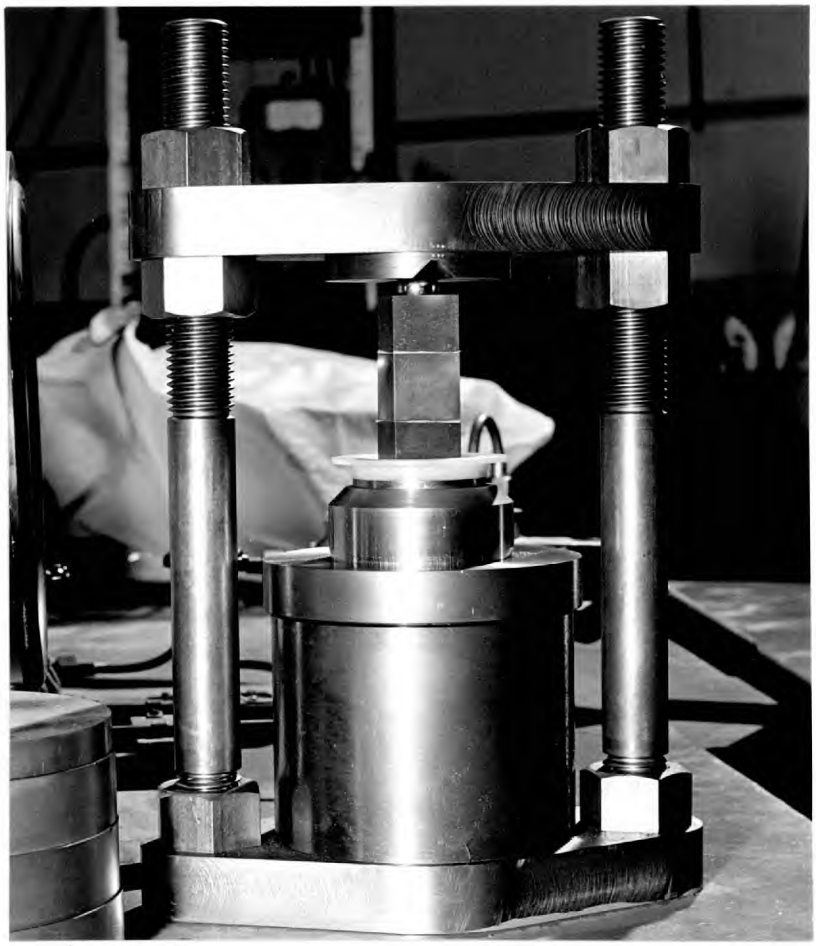

FIGURE 14 MAIN UNIT FOR 2-TON HYDRAULIC SYSTEM

FIGURE 15 DEAD-WEIGHT UNIT FOR 2-TON HYDRAULIC SYSTEM

The calibrated gauge has a maximum scale deflection of 1000 p.s.i. and can be read to about 5 p.s.i., the actual thrust on the specimen being calculated from the gauge pressure and the known area of the piston in the main hydraulic unit.

2.5 PREPARATION OF THIN COUPLING FILMS FOR SHEAR WAVES

There are no particular difficulties associated with coupling longitudinal waves into solids. In the case of shear waves, however, most liquid coupling materials are ruled out, since they cannot sustain shear vibrations unless they possess a very high shear viscosity. Nevertheless, a few materials remain, such as 'Nonac' stopcock grease*, 'salol' (phenyl salicylate) and one or two viscous resins, which are commonly used for coupling shear waves into solids. One such viscous resin (Dow 276-V9+) was found to be especially useful for the present measurements, since not only did it have excellent thin-film transmission characteristics, but also it was non-setting at normal room temperatures. Hence the transducers could be aligned and subsequently reorientated on the specimen without either removing or damaging them.

---

* Fisher Scientific Co.

\+ Dow Chemical Co.

In order to obtain good shear wave transmission over a reasonably wide bandwidth centred on the resonance frequency of the transducer, it is absolutely essential to prepare very thin, uniform coupling films. McSkimin found that extremely thin films of Dow resin 276-V9 (poly-α-methylstyrene) could be obtained by heating the material at 60°C under a moderate surface pressure of about 25 p.s.i. [97] At this temperature, the resin flows quite readily, and under the applied pressure, most of the excess 'liquid' is squeezed out from between transducer and specimen. Provided the contacting surfaces of the latter are sufficiently flat (fine-ground finish), uniform coupling films can be obtained which are typically less than 0.001 in. thick.

A simple assembly jig, which proved most satisfactory for preparing thin films of Dow resin, is shown schematically in Figure 16. Using only very small drops of resin, an identical pair of shear wave transducers (Y-cut quartz) are first 'wrung-on' by hand pressure to opposite sides of the specimen, which is mounted in the holder previously described in Section 2.3. The entire specimen-holder unit is then supported symmetrically on one of these transducers (the lower one shown in the diagram), which rests on an aluminium rod projecting vertically into the central hole bored through the specimen holder. A light pressure is applied to both transducers through a second

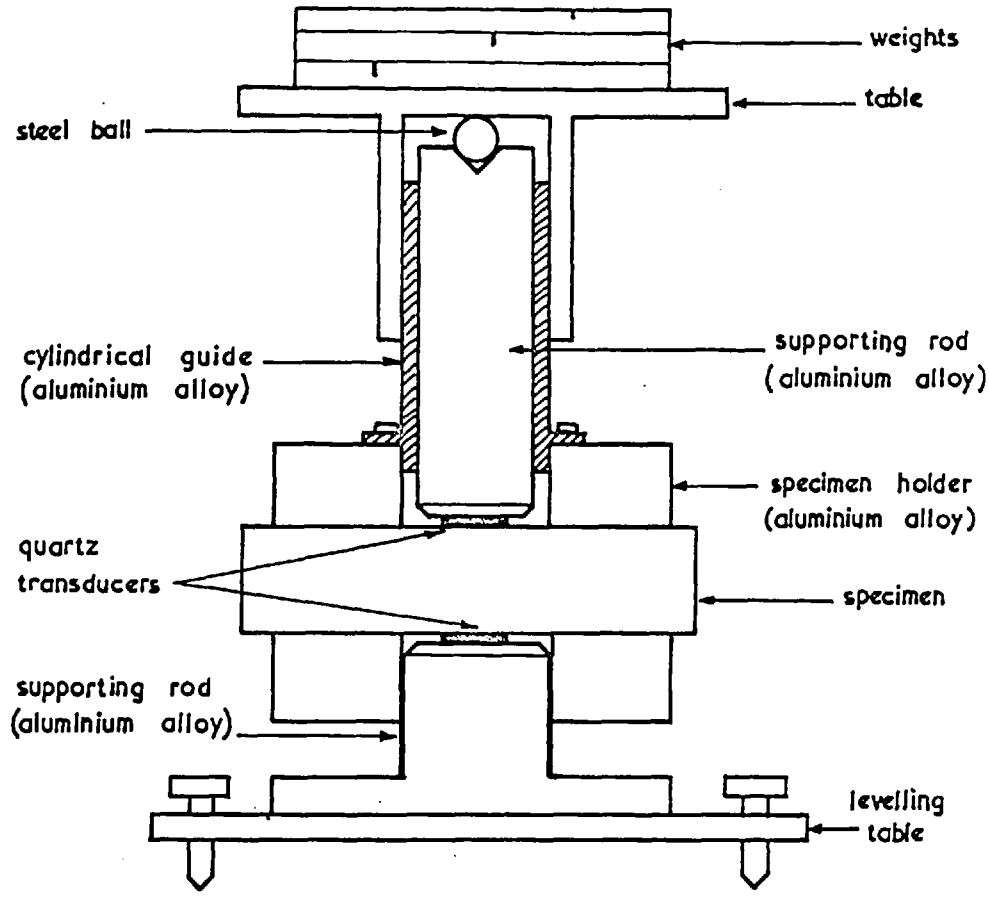

FIGURE 16 TRANSDUCER-SPECIMEN ASSEMBLY JIG FOR PREPARING UNIFORMLY THIN COUPLING FILMS FOR SHEAR WAVES

aluminium rod which supports a weight table and appropriate weights on a 3/8" diameter steel ball. The upper rod and the weight table are both located by a cylindrical guide, bolted to the specimen holder. Those surfaces of the aluminium rods which are in direct contact with the transducers are hand-lapped to ensure a uniform pressure distribution. After assembly, the whole unit is heated in an oven for about an hour at 60°C, so that the excess 'liquid' resin is squeezed out, leaving very thin, uniform coupling films.

CHAPTER 3

EXPERIMENTAL MEASUREMENTS ON POLYCRYSTALLINE CRYSTALS

This chapter is principally concerned with the present experimental investigation of small, stress-induced, changes in the propagation velocity of ultrasonic waves in polycrystalline metal specimens. Details are presented of the specimens investigated, the experimental procedure, and the graphical results obtained, followed by a short section showing how the third-order elastic moduli are evaluated from the measurements. Finally, the calculated values of the third-order moduli are summarised, and the accuracy of measurement is briefly discussed.

3.1 THE SPECIMENS

Several polycrystalline metals were investigated, including six different steels, a magnesium alloy and sintered samples of tungsten and molybdenum. All of the specimens were machined into rectangular parallelepiped form, of nominal dimensions 6" x 1" x 1" for the steels, 2" x 1" x 1" for the magnesium and 2" x 3/4" x 3/4" for the tungsten and molybdenum. Detailed specifications are given for each of these samples in Table 4.

Material	Nominal Composition	Thickness* (cm)	Density ($gm.cm^{-3}$)	Source
Steel				
H1 Hecla 37	0.4% C	2.543	7.823	Hadfield's, Sheffield.
H2 Hecla 17	0.6% C	2.541	7.825	
H3 Galahad Special	13%Cr 1%Ni	2.541	7.711	
H4 Hecla ATV	36%Ni 10%Cr	2.541	8.065	
H5 Hecla 138A	2½%Ni; CrMo	2.541	7.843	
REX 535	Not known	2.541	7.836	Rolls-Royce, Derby.
Magnesium tooling plate	96%Mg 1%Zn 3%Al	2.539	1.776	Midwest Res. Inst., Kansas City
Tungsten (sintered)	99.99% W	1.901	14.16[a] 19.3[b]	L. Light and Co., Slough.
Molybdenum (sintered)	99.99% Mo	1.903	9.712[a] 10.3[b]	

* Thickness in propagation direction

a Observed density

b Theoretical density

TABLE 4 DETAILS OF POLYCRYSTALLINE METAL SPECIMENS

The allowed tolerances on the parallelism and flatness of the specimen surfaces are governed by the carrier frequency of the ultrasonic pulses, but the carrier frequency is itself limited by considerations of attenuation within the specimen. For polycrystalline metals, the main attenuation mechanism is the scattering of energy at the grain boundaries, which represent sudden discontinuities in acoustic impedance [98]. A carrier frequency of 5 Mc/s was chosen for the present measurements since this represents a reasonable compromise between the conflicting requirements of low attenuation (low frequency) and plane wave propagation (high frequency to avoid diffraction effects). Opposite faces of the specimens were machined parallel to within 5 minutes of arc, and provided with a fine-ground finish.

It is almost impossible to prepare samples of polycrystalline metals without introducing some preferential grain orientation. In such specimens, 'pure' shear waves can only be propagated along 'principal' directions, that is, either along or perpendicular to the grain flow. Since the present investigations also require the use of directional stresses, it is essential that the principal axes of stress and preferential grain alignment should coincide. Hence the polycrystalline metals investigated were all cut with their major axes along the direction of grain flow. The effects of preferential grain alignment on the experimental measurements will be discussed in the next chapter.

3.2 EXPERIMENTAL MEASUREMENTS AND RESULTS

For the purposes of the present investigation, the polycrystalline metal specimens have been considered as elastically isotropic, although 'quasi-isotropic' would be a more accurate description, since the presence of even a small amount of preferred orientation always leads to some directional properties. If ultrasonic shear waves are propagated through such solids, birefringent effects are observed, which could possibly lead to a quantitative method of measuring the amount of preferred orientation [98-100]. Nevertheless, provided the grain alignment is not excessive (see Chapter 4) and the samples are cut as described in the previous section, the assumption of elastic isotropy is not unreasonable.

All three third-order elastic moduli of an isotropic solid can be evaluated uniquely from the small changes in ultrasonic velocity, measured for one longitudinal and two transverse waves, as a function of a uniaxial stress applied perpendicular to the ultrasonic propagation direction. The transverse waves must be polarised either parallel or perpendicular to the direction of applied stress, as shown in Figure 17. For any other initial orientation, two 'principal' shear wave components are generated, which propagate with slightly different phase velocities and produce characteristic interference effects [20].

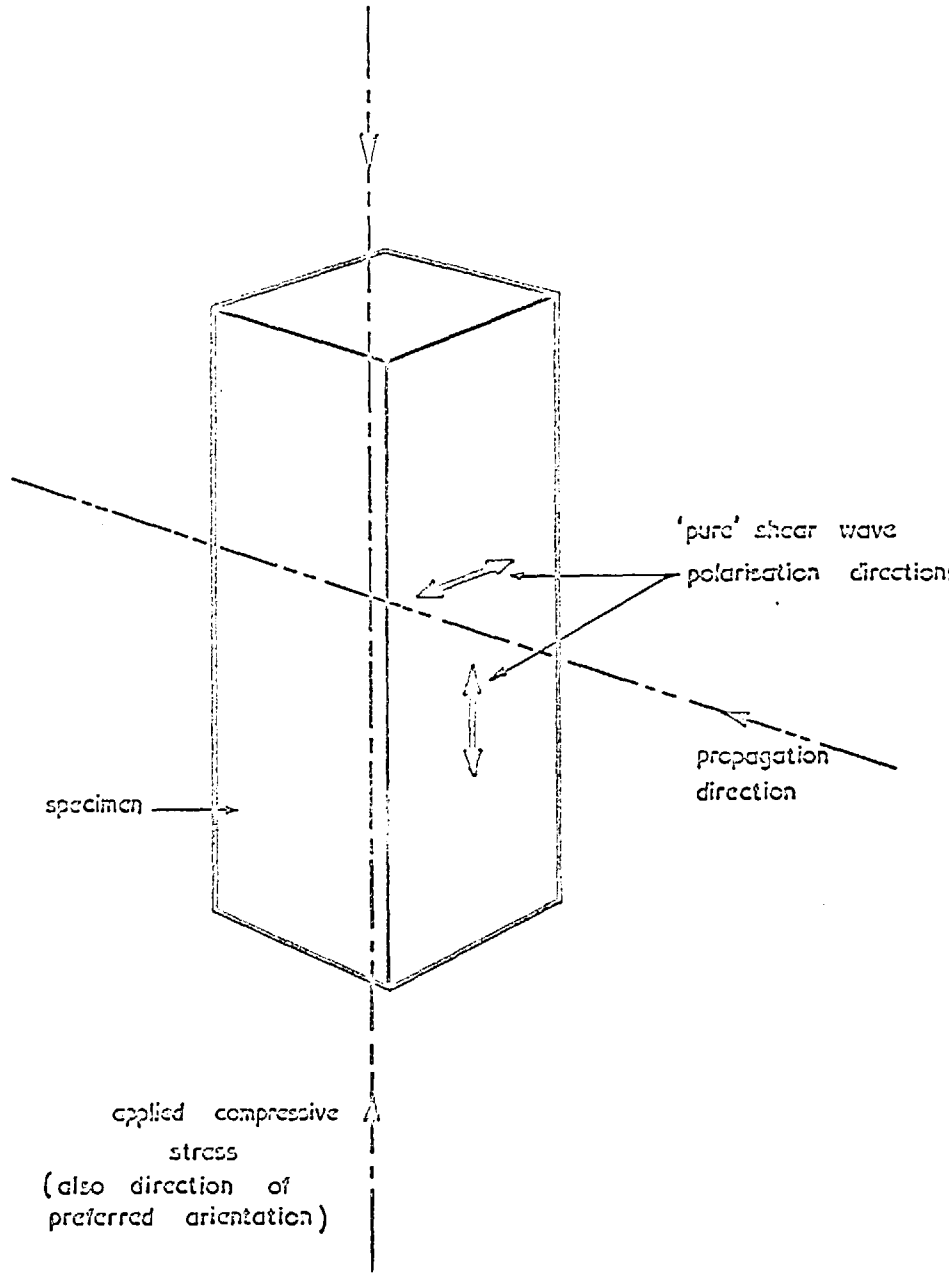

FIGURE 17 POLARISATION SCHEME FOR 'PURE' SHEAR WAVES

The velocity-stress dependence has been determined experimentally for both longitudinal and shear waves, polarised as above, for all the specimens listed in the previous section. In most cases, the technique used was based on electrical interference between the received pulse-echoes and an extended transmitter pulse, as described in Section 2.2(i). This method does not require a comparison specimen and is therefore more economical than the alternative method of Section 2.2(ii), which relies on interference between two similar sets of ultrasonic echoes. The latter method was used in two cases, however, namely for the magnesium and the tungsten samples.

For the shear wave measurements, Dow-resin 276-V9, pre-heated under pressure as described in Section 2.5, was used as the transducer-specimen coupling film. The transducers themselves consisted of 1/2" diameter, 5 Mc/s Y-cut quartz discs with thin gold film electrodes evaporated on the back surfaces [101]. For coupling longitudinal waves into solids, a commercial lubricating oil (Electrolube No. 2A) available in an aerosol pack and normally used for electrical switchgear, was found to be particularly useful. To the author's knowledge, the application of this material as a coupling medium has not been mentioned previously in the literature. Excellent bonds were obtained simply by squirting a very small quantity of oil from the aerosol on to one face of the

transducer, wiping off the excess liquid, and then 'wringing-on' the transducer by finger pressure. The longitudinal wave transducers consisted of 1/2" diameter, 5 Mc/s X-cut quartz discs, with evaporated gold film electrodes as above.

The measured changes in the transit times of the m^{th} received ultrasonic pulses are plotted as a function of applied uniaxial compressive stress in Figures 18-26. Results are presented for all the samples listed in Table 4, and it may be seen that, except for the steel sample H3, there is a linear relationship between the applied stress and the pulse transit time. In all cases other than H3, the maximum applied stresses (about 200 bars for the magnesium, 1500 bars for the steels and 3000 bars for the tungsten and molybdenum) were low enough for the resulting strains to remain well within the respective elastic limits. There is definite evidence of 'elastic hysteresis' in the case of the steel H3, however, and typical limits for the transit time changes observed during loading and unloading are indicated by the vertical lines drawn through the data points of Figure 20. The sense of the loading and unloading sequence is represented by the partial arrowheads.

In all cases investigated, the greatest velocity changes were observed for shear waves polarised parallel to the applied stress direction. Smaller changes, usually of opposite sign, were found for

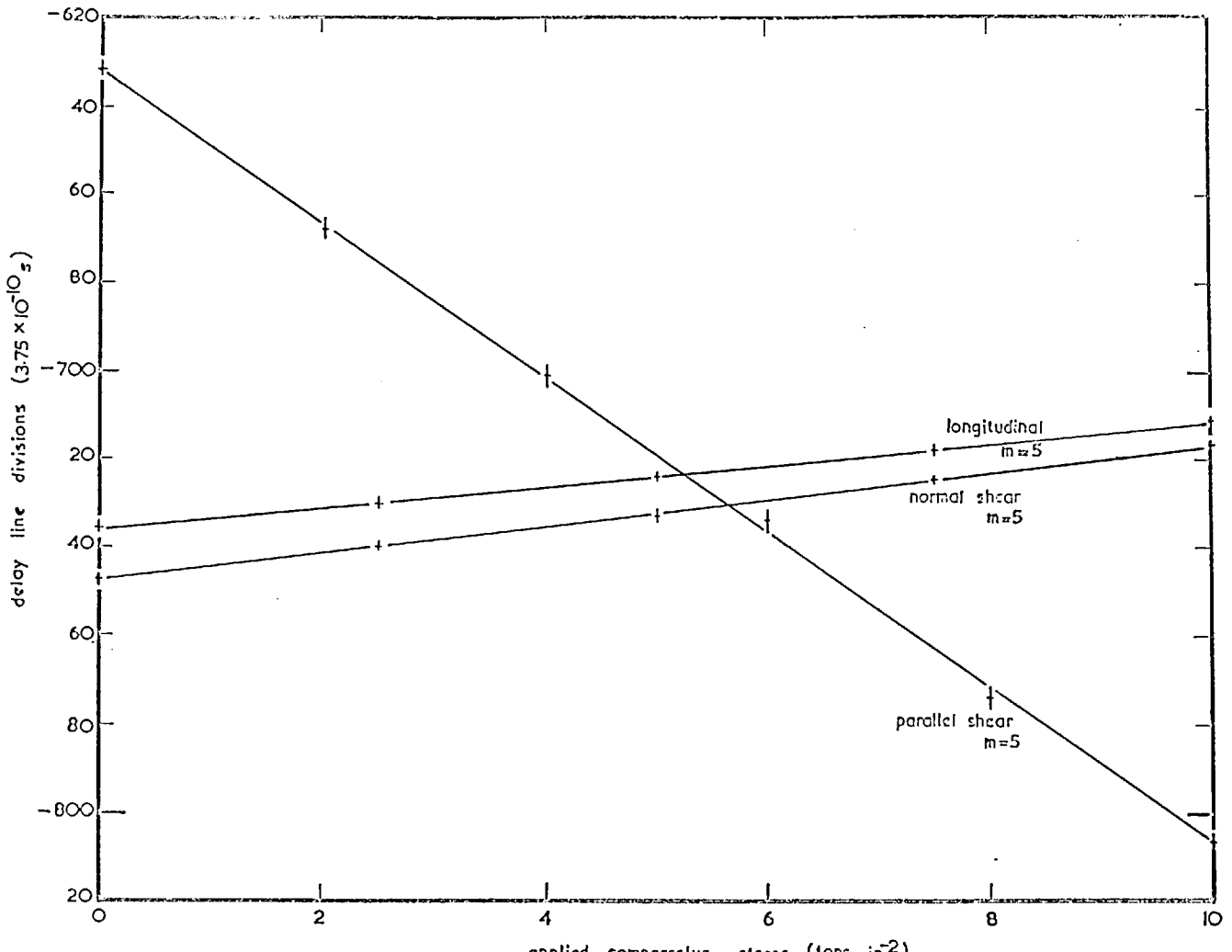

FIGURE 18 TRANSIT TIME CHANGES FOR m^{th} RECEIVED PULSE VERSUS APPLIED COMPRESSIVE STRESS. STEEL H_1.

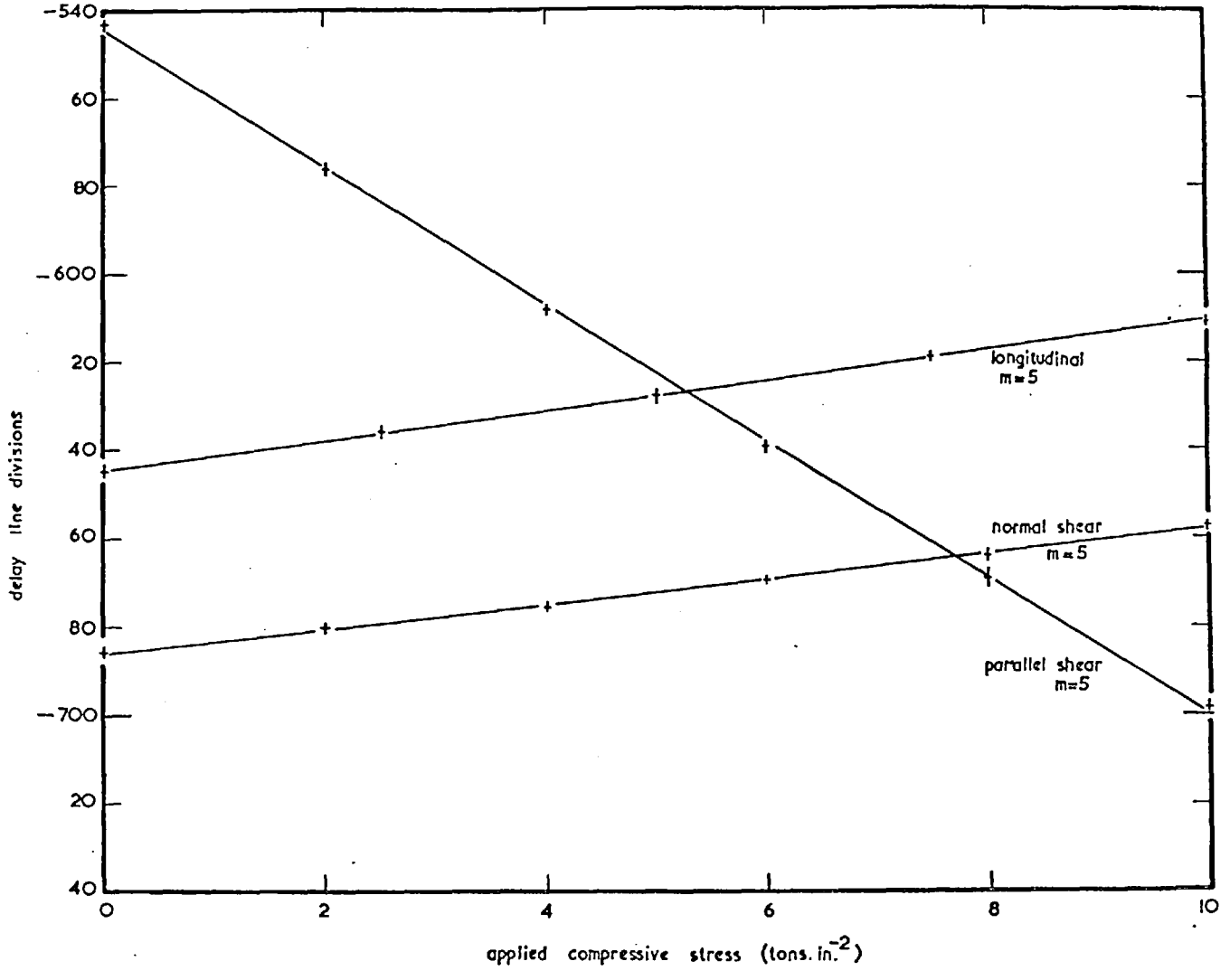

FIGURE 19 TRANSIT TIME CHANGES FOR m^{th} RECEIVED PULSE VERSUS APPLIED COMPRESSIVE STRESS. STEEL H_2.

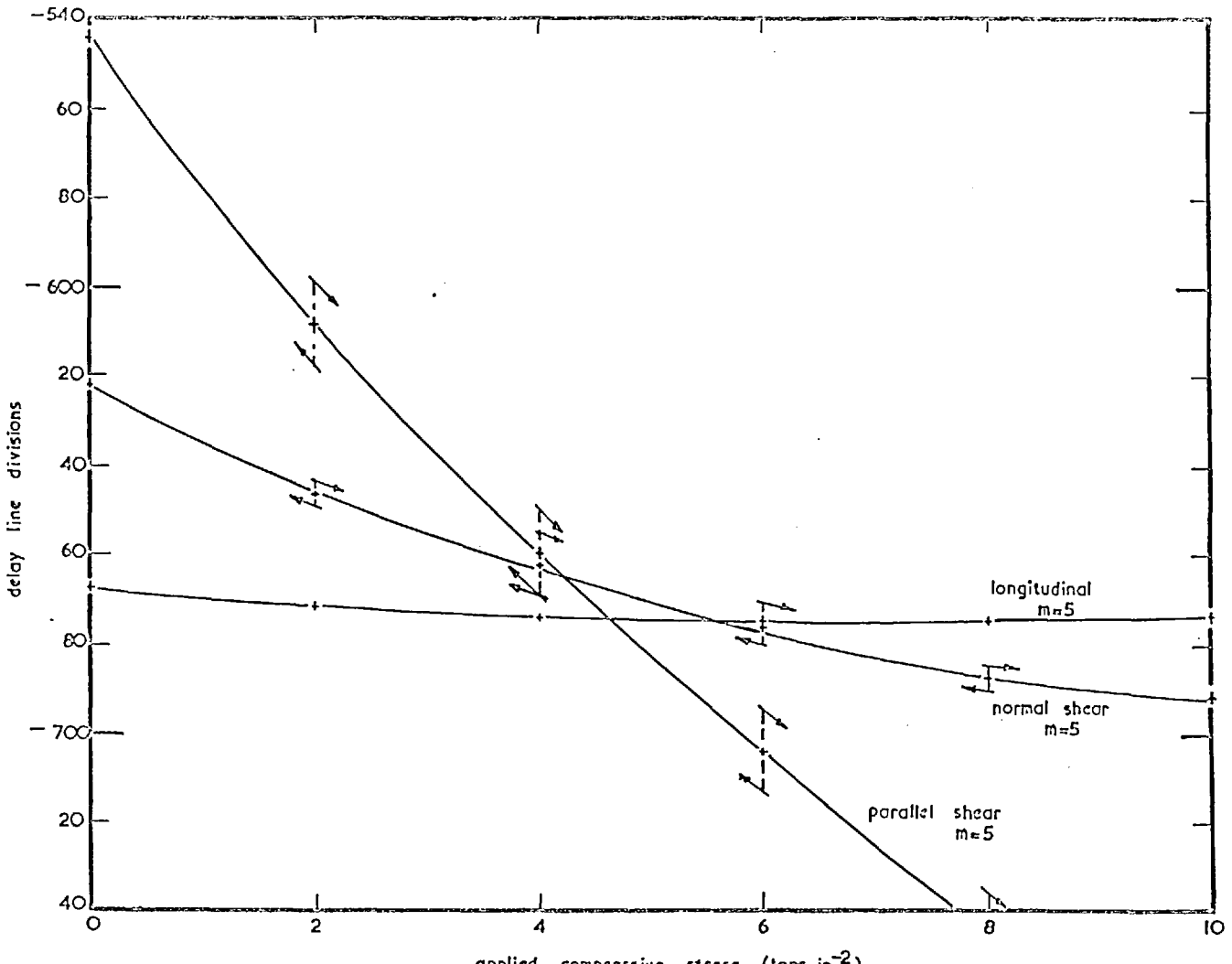

FIGURE 20 TRANSIT TIME CHANGES FOR m^{th} RECEIVED PULSE VERSUS APPLIED COMPRESSIVE STRESS. STEEL H_3.

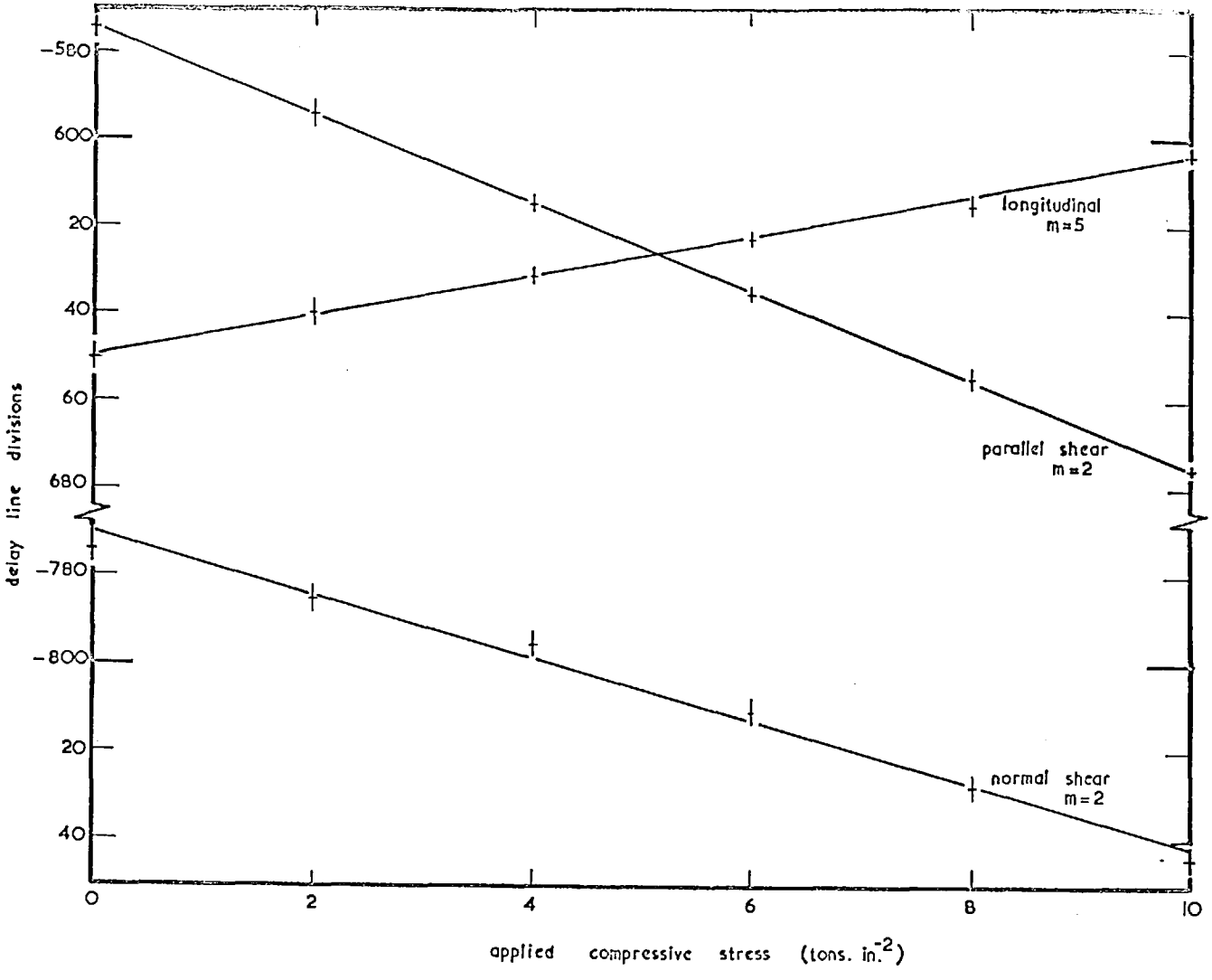

FIGURE 21 TRANSIT TIME CHANGES FOR m^{th} RECEIVED PULSE VERSUS APPLIED COMPRESSIVE STRESS. STEEL H_4.

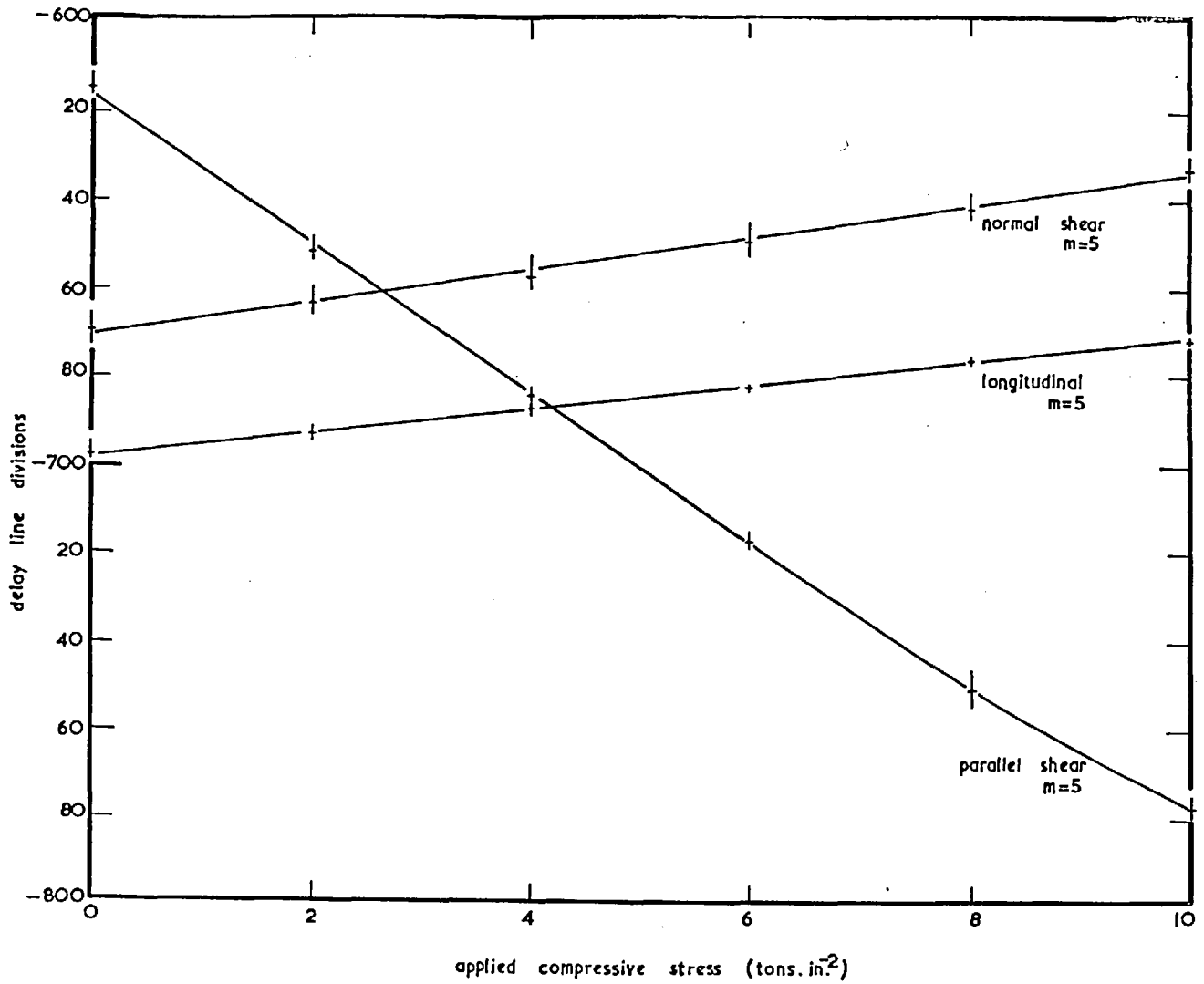

FIGURE 22 TRANSIT TIME CHANGES FOR m^{th} RECEIVED PULSE VERSUS APPLIED COMPRESSIVE STRESS. STEEL H_5.

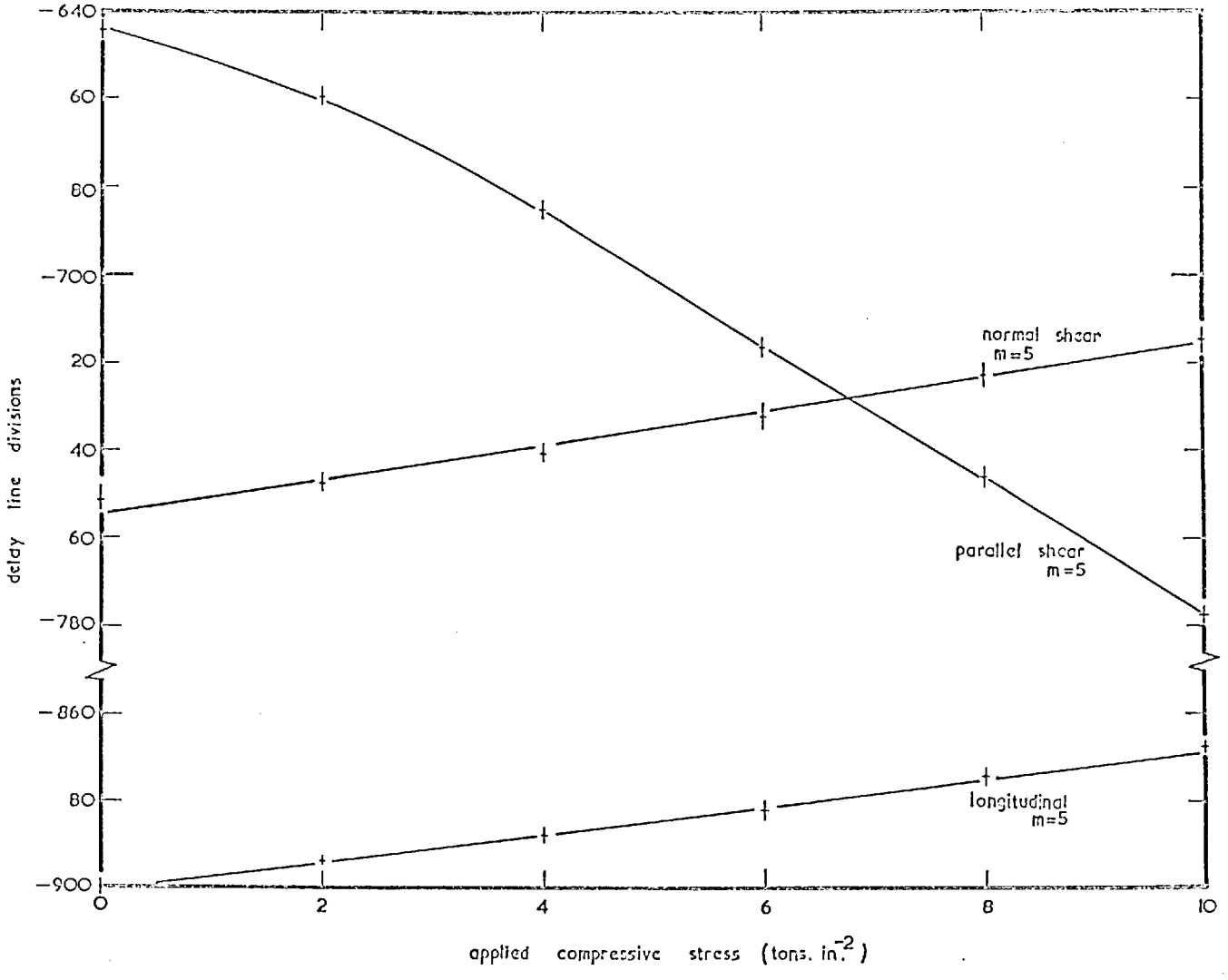

FIGURE 23 TRANSIT TIME CHANGES FOR m^{th} RECEIVED PULSE VERSUS APPLIED COMPRESSIVE STRESS. STEEL REX 535

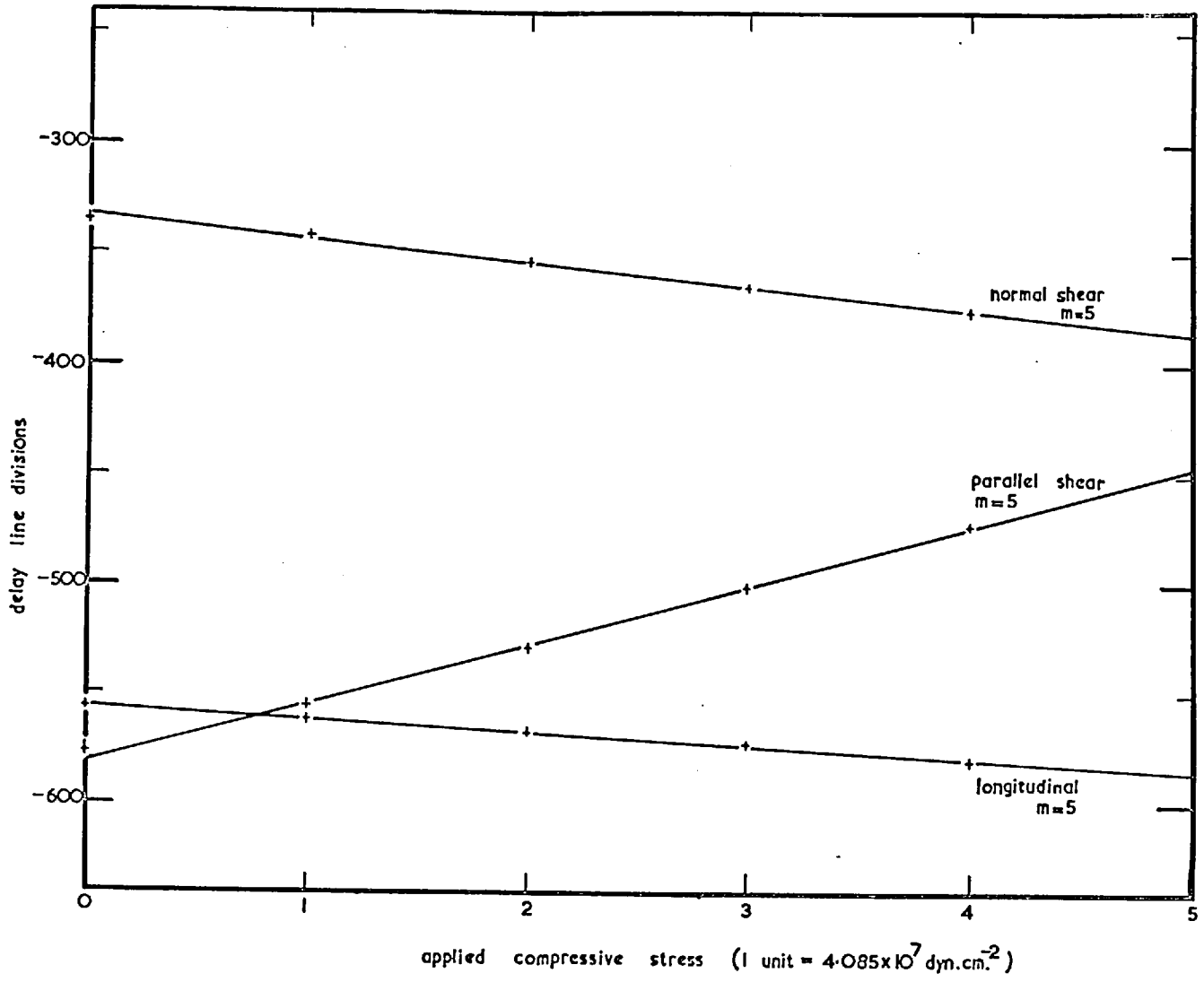

FIGURE 24 TRANSIT TIME CHANGES FOR m^{th} RECEIVED PULSE VERSUS APPLIED COMPRESSIVE STRESS. MAGNESIUM TOOLING PLATE.

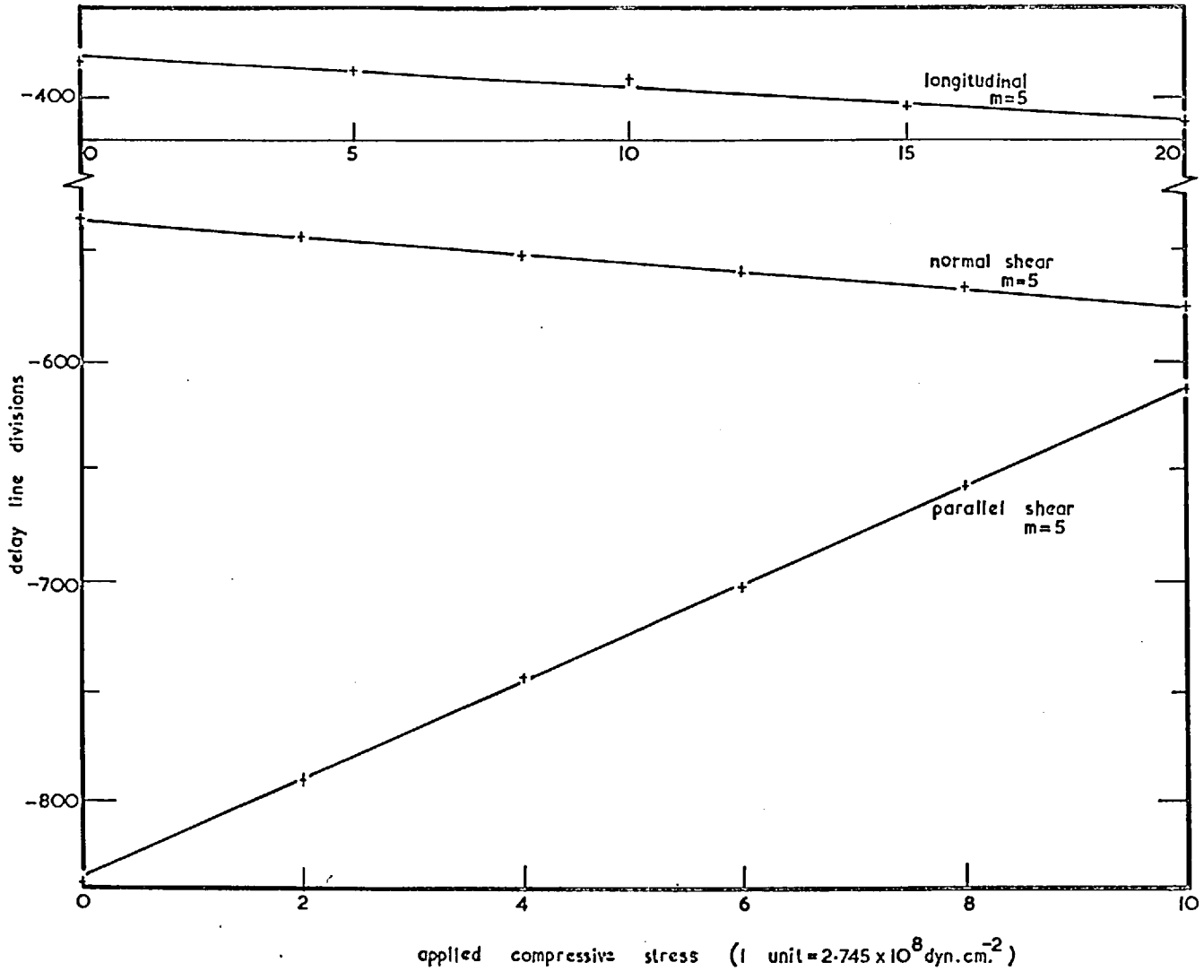

FIGURE 25 TRANSIT TIME CHANGES FOR m^{th} RECEIVED PULSE VERSUS APPLIED COMPRESSIVE STRESS. SINTERED TUNGSTEN.

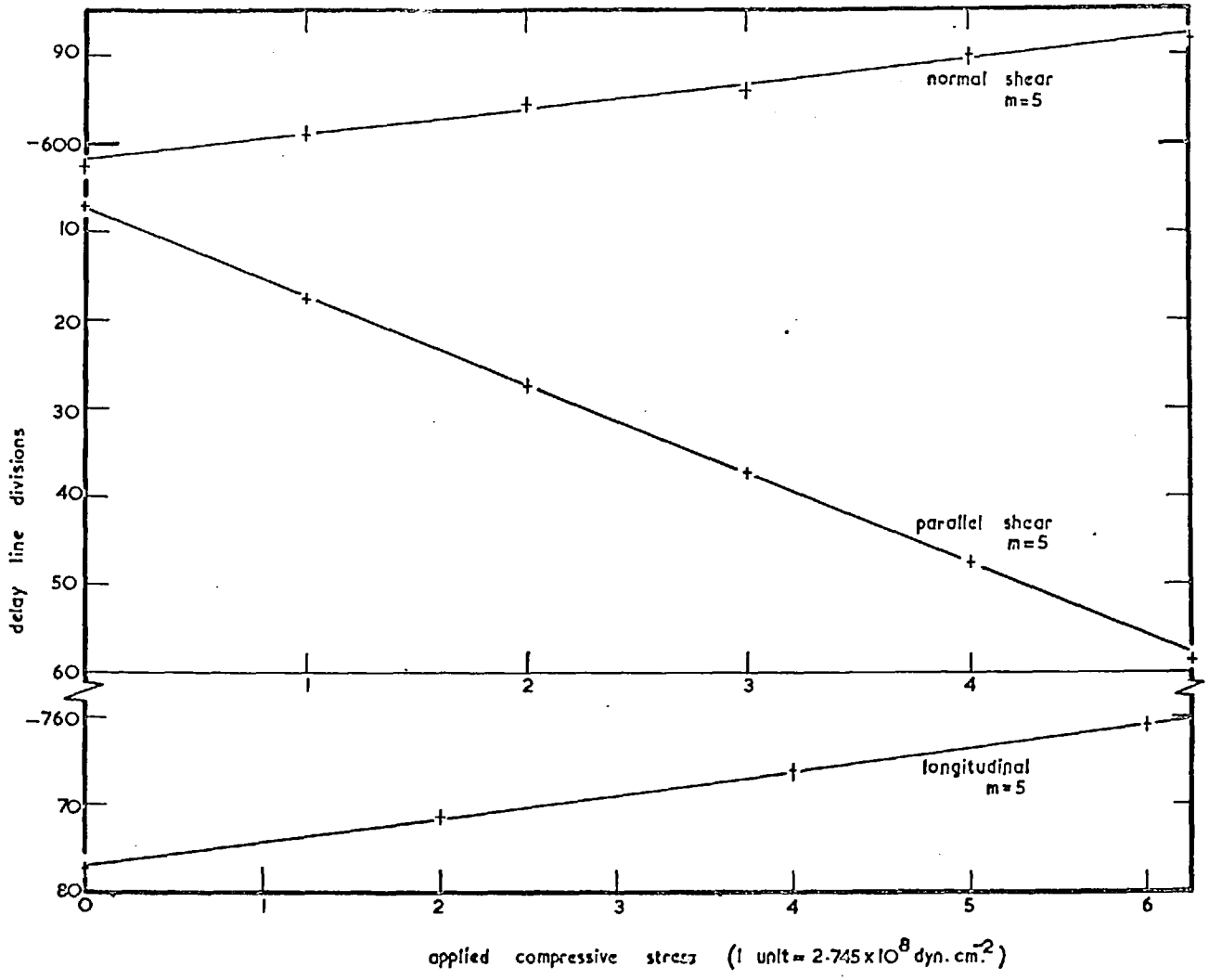

FIGURE 26 TRANSIT TIME CHANGES FOR m^{th} RECEIVED PULSE VERSUS APPLIED COMPRESSIVE STRESS. SINTERED MOLYBDENUM.

the other principal shear wave, polarised perpendicular to the stress direction, and for the longitudinal wave. It may be noted that the slopes of the experimental curves for the magnesium and tungsten samples are opposite in sign compared with the corresponding slopes for all the other specimens. The simple explanation is that the magnesium and tungsten were investigated by the interference technique described in Section 2.2(ii), but during these measurements, the transmitter outputs, A and B, shown in Figure 7, were interchanged.

The absolute velocity was determined for both longitudinal and shear waves for all specimens using McSkimin's phase-comparison technique, as described in Section 2.2(iii). A typical set of results is shown for the steel H4 in Figure 27, where the 'null' frequencies are plotted versus an arbitrary set of successive integers.

3.3 CALCULATION OF THIRD-ORDER ELASTIC MODULI FROM EXPERIMENTAL DATA

The conditions of destructive interference between the m^{th} received pulse-echo and the extended transmitter pulse were derived in Chapter 2. A general relationship between the delay line settings, D, for destructive interference, and the applied compressive stress, ΔP, is obtained by combining equations 49, 50 and 51. Thus:

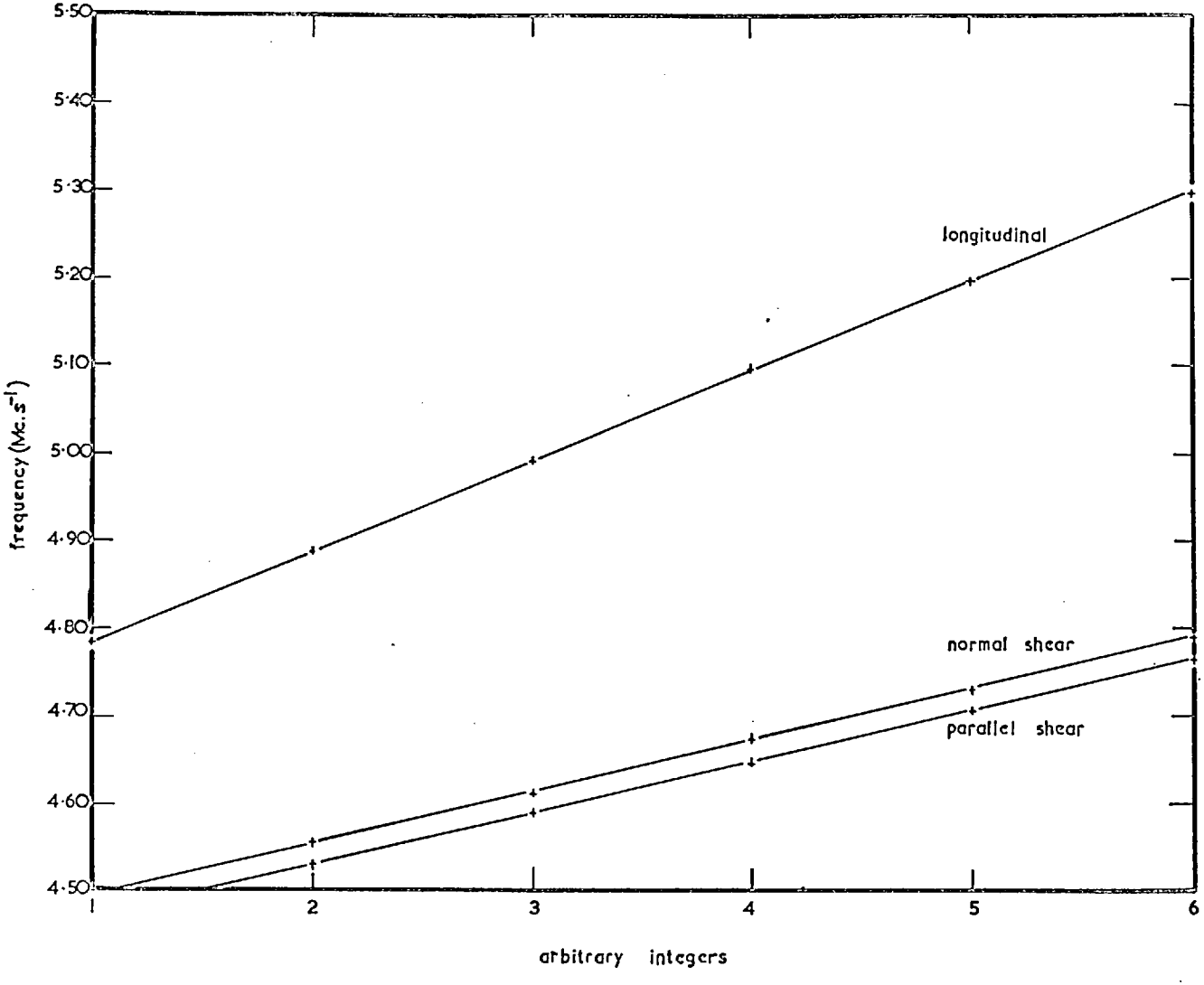

FIGURE 27 'NULL' FREQUENCIES FOR McSKIMIN PHASE-COMPARISON TECHNIQUE

Thus

$$D = Q\Delta P + C(f) \tag{70}$$

where

$$Q = \frac{-(2m-1)L_o}{2dW_o(\rho_o W^2)_o}\,(\rho_o W^2)'_o \tag{71}$$

Similarly, it is easily verified from equations 56 and 57 that the general relationships 70 and 71 are also valid for the case of interference between two similar sets of ultrasonic echoes, obtained respectively from a stressed and a comparison specimen. The quantities $(\rho_o W^2)$, and their first stress-derivatives $(\rho_o W^2)'$, both evaluated at zero stress, were listed for an isotropic solid in Table 3 of Chapter 1. Assume now that the relationship 70 has been determined experimentally for longitudinal waves and also for the two principal shear waves propagated perpendicular to the applied uniaxial stress direction. Then the initial slopes, Q, of the experimental curves may be related to the third-order elastic moduli, ν_1, by combining equation 71 with the last three entries appearing in Table 3.

$$Q_1 = \frac{R_1}{W_1 w_1 E}\left[2\sigma(w_1+4\nu_3) - \nu_1(1-2\sigma) + 2\nu_2(4\sigma-1)\right] \tag{72}$$

$$Q_2 = \frac{-R_2}{W_2 w_2 E}\left[2w_2 + \nu_2(1-2\sigma) + 2\nu_3(1-\sigma)\right] \tag{73}$$

$$Q_3 = \frac{R_3}{W_2 w_2 E}\left[2\sigma(w_2+2\nu_3) - \nu_2(1-2\sigma)\right] \tag{74}$$

In these equations

$$R_j = \frac{-(2m_j-1)L_o}{2d} \tag{75}$$

$$j = 1,\ 2 \text{ or } 3$$

and w was defined previously as

$$w = (\rho_o W^2)_o = (\rho_o V^2)_o \tag{35}$$

The subscripts on the Q's, W's, w's and R's are defined as follows.

1 = longitudinal wave

2 = shear wave polarised parallel to uniaxial stress

3 = shear wave polarised perpendicular to uniaxial stress.

The quantities E and σ are, respectively, Young's modulus and Poisson's ratio, defined by

$$E = \frac{(3\lambda+2\mu)}{(\lambda+\mu)} \tag{76}$$

and

$$\sigma = \frac{\lambda}{2(\lambda+\mu)} \tag{77}$$

where λ, μ are the familiar Lamé second-order elastic constants. The constant μ may also be identified as the 'rigidity' modulus. For an isotropic solid, the velocities for longitudinal and shear waves are given respectively by

$$w_1 = \rho_o W_1^2 = \lambda + 2\mu \tag{78}$$

$$w_2 = w_3 = \rho_o W_2^2 = \mu \tag{79}$$

In equations 72 to 79 it should be understood that the quantities Q, W, w, E, σ, λ and μ are all evaluated at zero stress, though the subscript, o, has been omitted for simplicity.

The third-order moduli, ν_1, ν_2, ν_3, can be evaluated uniquely from equations 72 to 74, but the computational errors will be different in each case. The velocity changes for the longitudinal wave are usually smaller than for the two principal shear waves, the changes for the shear wave polarised parallel to the stress being the largest of all. Hence the experimentally determined Q's may be arranged in order of decreasing precision: Q_2, Q_3, Q_1. Either of the third-order moduli ν_3 or ν_2 can be evaluated uniquely by eliminating the other between equations 73 and 74. However, the constant ν_1, can only be calculated from equation 72 after substituting for the previously determined values of ν_3 and ν_2. In practice, the moduli ν_3, ν_2, and ν_1 are computed (in

that order) from the following equations, which are derived from equations 72 to 74.

$$\nu_3 = -\left[\frac{W_2 w_2 E}{2(1+\sigma)}\left(\frac{Q_2}{R_2} - \frac{Q_3}{R_3}\right) + w_2\right] \tag{80}$$

$$\nu_2 = \frac{-1}{(1-2\sigma)}\left[\frac{W_2 w_2 E}{R_2} \cdot Q_2 + 2w_2 + 2\nu_3(1-\sigma)\right] \tag{81}$$

$$\nu_1 = \frac{-1}{(1-2\sigma)}\left[\frac{W_1 w_1 E}{R_1} \cdot Q_1 - 2\sigma(w_1+4\nu_3) - 2\nu_2(4\sigma-1)\right] \tag{82}$$

Although alternative solutions could be found for the ν's, equations 80 to 82 represent the best arrangements with respect to minimising the cumulative computational errors which may arise from initial experimental inaccuracies in the Q's. The second-order elastic moduli, E, σ, and w, appearing in equations 80 to 82 may be calculated from the zero-stress absolute velocities, W_o, measured for both longitudinal and shear waves by McSkimin's phase-comparison technique.

3.4 SUMMARY OF RESULTS FOR THIRD-ORDER ELASTIC MODULI

The three third-order moduli have been calculated for all the polycrystalline specimens listed in Table 4 other than the steel H3 and the sintered tungsten and molybdenum. It did not seem worthwhile to

compute the third-order moduli for the steel H3 because of the pronounced elastic hysteresis observed. In the case of the sintered tungsten and molybdenum, the experimental curves shown in Figures 25 and 26 appeared quite satisfactory, since the changes in pulse transit time were linearly related to the applied stress. However, the absolute ultrasonic velocities, computed from the phase-comparison measurements at zero stress, were lower than the literature values by about 30 per cent for the tungsten and 5 per cent for the molybdenum. This serious discrepancy may be understood by referring to Table 4 which shows corresponding differences between the measured and the theoretical densities. Moreover, the final errors in the calculated second-order moduli are even greater than the above estimates, since the moduli are given by the product of the density and the square of the appropriate ultrasonic velocity. The 'third-order moduli', if computed for these sintered materials from equations 80 to 82, would have little real value, since the equations include several functions of the second-order moduli.

The tungsten and molybdenum were subsequently analysed, and it was verified that the dense matrix material consisted only of 4N (99.99%) pure metal. The low densities were entirely accounted for by the presence of finely dispersed pores containing, mainly, oxygen gas. During the measurements, no abnormal ultrasonic pulse distortions or

spurious internal reflections were observed, presumably because the pores were very small and evenly dispersed throughout the sintered specimens.

In Table 5, numerical results are presented for the second- and third-order moduli for all the polycrystalline specimens investigated, other than those already mentioned above. The author's results for the second-order elastic constants agree well with accepted values for magnesium and steel, and require no further comment here. On the other hand, the third-order data has not been published previously and will be discussed in some detail in the following chapter. At this stage, it seems sufficient merely to comment that the third-order moduli are, in general, negative, and slightly larger than the second-order moduli.

Of the two sets of data presented in Table 5 for the steel REX 535, one set has been calculated from the author's measurements, and the other from measurements reported recently by Crecraft [64]. Attention is drawn in particular to the serious disagreement between corresponding results for the second-order moduli. These differences are large enough for any quantitative comparison of the third-order data to be unrealistic. Crecraft's results for the second-order moduli are considerably lower than the corresponding values shown in Table 5 for the other steels (except for the unrepresentative steel H4, which is austenitic) and it is unlikely that they are correct.

Specimen	Second-order constants				Third-order constants		
	λ	μ	E	σ	ν_1	ν_2	ν_3
0.4% Carbon steel H1 (Hecla 37)	11.1 ±0.1	8.21 ±0.05	21.15 ±0.1	0.288 ±0.002	-35.8 ±7.0	-28.2 ±3.0	-17.7 ±0.8
0.6% Carbon steel H2 (Hecla 17)	11.05 ±0.1	8.20 ±0.05	21.1 ±0.1	0.287 ±0.002	-13.4 ±2.0	-26.1 ±2.0	-16.7 ±0.6
2.5% Ni.Cr.Mo steel H5 (Hecla 138A)	10.9 ±0.1	8.19 ±0.05	21.05 ±0.2	0.286 ±0.002	-32.3 ±5.0	-26.5 ±3.0	-17.7 ±1.0
Ni steel (REX 535)	10.9 ±0.05	8.18 ±0.05	21.0 ±0.1	0.286 ±0.002	-17.5 ±5.0	-24.0 ±5.0	-16.9 ±1.5
Ni steel (REX 535)(Crecraft[16])	9.09 ±0.1	7.80 ±0.1			+26 ±10	-22.5 ±4.0	-18.3 ±1.0
Austenitic steel H4 36%Ni 10%Cr (Hecla ATV)	8.7 ±0.2	7.16 ±0.3	18.3 ±0.3	0.274 ±0.005	+3.4 ±2.0	-55.2 ±8.0	-10.0 ±1.0
Magnesium tooling plate 96%Mg 1%Zn 3%Al	2.59 ±0.02	1.66 ±0.03	4.33 ±0.03	0.305 ±0.001	-6.54 ±0.1	-5.74 ±0.1	-4.21 ±0.04

All moduli in units of 10^{11} dyn.cm^{-2}

TABLE 5 NUMERICAL RESULTS FOR POLYCRYSTALLINE METALS

The author has consulted Crecraft on this point, and it would appear that the low values for the second-order moduli may be partly explained by the fact that Crecraft made no correction for the reflection phase shift inevitably produced at the transducers, which were bonded directly to the specimen. Furthermore, Crecraft used the 'sing-around' technique [47] for all his measurements. Now although this technique is ideally suited for detecting very small changes in ultrasonic velocity, it is not at all suitable for absolute velocity measurements, for the following reason. The 'sing-around' period is made up of two parts, namely, the ultrasonic pulse transit time, and parasitic time delays introduced in the electronic circuitry of the 'sing-around loop'. The reflection phase shift at the transducers and the parasitic electronic delays, if neglected, would both tend to lead to erroneously low results for the ultrasonic velocities and hence low calculated values for the second-order moduli.

One final point should be made concerning Crecraft's results. In computing the third-order moduli, Crecraft apparently used an uncertain literature value for Poisson's ratio for 'steel' (unspecified), rather than calculating it explicitly from the ultrasonic velocity data [102]. It is clear from equation 82 that the accuracy of the calculated third-order modulus, ν_1, is particularly strongly dependent on a correct value for Poisson's ratio because of the factor $(4\sigma-1)$.

From Table 5, comparison of the two sets of data for REX 535 shows that the greatest discrepancy does, in fact, occur for this same third-order modulus, ν_1.

5.3 ACCURACY OF EXPERIMENTAL MEASUREMENTS AND RESULTS

It may be seen from equations 80 to 82 that the final accuracy of the numerical results for the third-order moduli is primarily determined by two main sources of error. These are, firstly, inaccuracies in evaluating the slopes, Q, of the experimental curves of pulse transit-time versus applied stress, and secondly, errors in the Poisson's ratio values calculated from the absolute velocity measurements. Any additional errors arising from inaccuracies in the determination of Young's modulus, specimen length, delay line calibration (Appendix 2), etc., are relatively unimportant when compared with the above two factors, but they are included, of course, in the final estimate of the experiment error for a given specimen.

Velocity changes as small as one part in 10^6 can be detected by the interference techniques described in Chapter 2. This high sensitivity has been largely annulled, however, by uncertainties in determining the applied stress, since the pressure gauge on the 25-ton hydraulic unit was, at best, only accurate to within a few per cent.

This basic limitation on the stress measurements was partially counteracted by averaging the experimental data over at least five loading and unloading sequences. Nevertheless, the errors in determining the experimental slopes, Q, were occasionally as high as 10 per cent for longitudinal waves in the steel specimens. In the case of shear waves, especially those polarised parallel to the applied stress, the experimental inaccuracies in the Q's were much less significant. In all cases, the precision of the measurements would be improved considerably if a more accurate pressure gauge were available.

The third-order moduli ν_3 and ν_2 can both be evaluated more accurately than the modulus ν_1. Equation 82 shows that the latter depends not only on the relatively inaccurate quantity Q_1, but also on the quantity $(4\sigma-1)$, which may typically be in error by about 5 to 10 per cent, even though σ itself may be known to within 1 to 2 per cent. The experimental errors in the modulus ν_1 could be greatly reduced by measuring velocity changes for longitudinal ultrasonic waves propagated along the applied stress direction, since the changes are considerably larger in that case than in the present configuration. Additional complications would be introduced by the need to propagate the waves through the metal 'jaws' of the hydraulic press to avoid damage to the transducers, but Hughes and Kelly have shown how such an arrangement can be realised [39].

The second-order moduli can be determined with an accuracy of 1 per cent or better from the absolute velocity measurements, since any errors in the latter should be less than 0.1 per cent, provided the integer n in equation 68 can be found unambiguously.

CHAPTER 4

DISCUSSION OF EXPERIMENTAL RESULTS FOR POLYCRYSTALLINE METALS

In this chapter the significance of the experimental results is discussed, especially in relation to alternative data on non-linear elasticity. The early measurements of Bridgman on the compressibility of solids under high pressures are of particular interest in this context. The third-order moduli calculated in the previous chapter are compared with Bridgman's values using theoretical expressions derived by Hughes and Kelly. Finally, the influence of preferred orientation on the present measurements in polycrystalline metals is briefly considered.

4.1 THIRD-ORDER ELASTIC MODULI

(i) Steel Specimens

An examination of the data presented in Table 5 of the previous chapter shows that four of the five steel specimens listed have very similar second-order elastic properties. Among these four steels, namely H1, H2, H5 and REX 535, corresponding values of the second-order moduli differ by considerably less than 1 per cent in most instances,

although the nominal composition of the specimens varies quite widely. The remaining steel, H4, is austenitic, and its properties cannot reasonably be compared with the other four, since, apart from its special heat treatment, it contains about 46 per cent of metallic elements other than iron. The present discussion will therefore be restricted to the four steels first mentioned. Since the differences in the second-order moduli are so small, it seems reasonable to compare the third-order data and look for variations in the non-linear elastic properties.

From Table 5 it can be seen that in the case of the third-order moduli ν_2 and ν_3, little real significance can be attached to the small variations among the four specimens. Admittedly, the numerical differences are larger than in the case of the second-order moduli, but unfortunately, so also are the experimental errors. On the other hand, the third-order modulus ν_1 varies markedly among the four steels. It should be remembered that this same constant, ν_1, is the one which is most susceptible of the three to experimental error because of the experimental configuration used (see Section 3.5). Nevertheless, the observed differences are much too large to be accounted for by experimental error.

The author can offer no obvious explanation why ν_1 should show

large variations in contrast to the other constants ν_2 and ν_3, but it is interesting to note that variations do exist in the non-linear properties which were not apparent in the second-order data. Information on the third-order moduli of those polycrystalline metals often used as components in major engineering structures, could be useful in evaluating the elastic properties of these materials under typical working conditions of high strain.

(ii) Magnesium Specimen

In Chapter 1, Section 5, it was mentioned that resonant interactions had been detected between two intersecting, collimated ultrasonic beams in polycrystalline magnesium [75, 76]. The experiments were performed at Midwest Research Institute, Missouri, by F.R. Rollins, Jr., et al. The principal feature of the interactions was the generation of a third 'scattered' beam, provided the two primary beams satisfied certain selection rules as regards frequency, polarisation and propagation direction (i.e. angle between the intersecting beams). In order to compare the experimental data with theoretical expressions derived for the displacement amplitude of the scattered beam, an independent measurement of the third-order elastic moduli was required. During the present work, the third-order moduli were measured for a polycrystalline magnesium sample supplied by Rollins, and the results (shown in Table 5)

were sent to Midwest Research Institute as a private communication.

Using a quantum mechanical approach, Taylor and Rollins [103] have recently derived theoretical expressions for the displacement amplitudes of the scattered waves for several possible interaction cases (excluding collinear interactions). These expressions agree exactly with earlier work which was based on classical arguments [73]. In a further publication [104], Rollins et al. reported that all the theoretical interactions had been verified experimentally using low megacycle ultrasonic waves in a polycrystalline magnesium specimen. In the same paper, Rollins also reported that the displacement amplitudes of the scattered beams had been calculated for several possible experimental configurations from the theoretical expressions mentioned above [103], using the author's third-order elastic data for magnesium. The experimentally measured displacement amplitudes were always less than, but usually within an order of magnitude of the theoretical results. In these preliminary comparisons, no attempts were made to correct for dissipative effects, so that the experimentally measured amplitudes must necessarily have been lower than the true amplitudes. Under these circumstances, the agreement found between both the theory and experiments of Rollins and also the author's third-order modulus investigations may be regarded as very good.

4.2 COMPARISON WITH OTHER NON-LINEAR ELASTIC DATA

In the field of experimental measurements at high pressures the name of Professor P.W. Bridgman is pre-eminent. Bridgman investigated the dependence on pressure of many physical quantities and, in particular, his measurements of the compressibility of solids as a function of hydrostatic pressure are relevant in the present discussion. He expressed his experimental data in the form of an empirical relationship between the fractional change in volume, $\frac{\Delta v}{v_o}$, and the hydrostatic pressure, P, applied to the specimen.

$$-\frac{\Delta v}{v_o} = aP - bP^2 \tag{83}$$

The coefficients a and b describe, respectively, the linear elastic behaviour of the solid, and its deviation from linearity. The isothermal volume compressibility, β, which is equal to the reciprocal of the isothermal bulk modulus, B, may be defined as

$$\beta = \frac{1}{B} = \frac{-1}{v_o}\left(\frac{\partial v}{\partial P}\right) \tag{84}$$

Noting that $$\frac{\partial v}{\partial P} = \frac{\partial}{\partial P}(v_o+\Delta v) = \frac{\partial}{\partial P}(\Delta v) \tag{85}$$

it follows from equations 83 and 84 that

$$\frac{1}{B} = a - 2bP \tag{86}$$

Hence $$\frac{\partial B}{\partial P} = -B^2 \frac{\partial}{\partial P}\left(\frac{1}{B}\right) = \frac{2b}{(a-2bP)^2} \tag{87}$$

It can be seen from the last two equations that when the hydrostatic pressure is zero,

$$B_o = \frac{1}{a} \tag{88}$$

$$\left(\frac{\partial B}{\partial P}\right)_o = \frac{2b}{a^2} \tag{89}$$

Bridgman has evaluated the coefficients a and b for a large number of solid materials by measuring the fractional change in volume over a wide pressure range [105]. The isothermal bulk modulus and its first hydrostatic pressure derivative have been calculated from Bridgman's published data for pure iron and magnesium using equations 88 and 89, and the results are shown in Table 6.

Hughes and Kelly [39] showed that an initially isotropic solid remains isotropic under the action of hydrostatic pressure, and its elastic properties may be represented adequately by two 'effective' second-order elastic moduli (see Chapter 1, Section 2; also reference (35)). They derived expressions showing how the 'effective' isothermal bulk modulus, B, and rigidity modulus, μ, are related linearly to the

hydrostatic pressure. In these expressions, the coefficients of the pressure dependent terms were linear combinations of the (zero-pressure) second- and third-order elastic moduli. These coefficients, which may be identified as the pressure-derivatives of the isothermal bulk and rigidity moduli, may be written

$$\left(\frac{\partial B}{\partial P}\right)_o = \frac{-1}{B_o}\left(\nu_1 + 2\nu_2 + \frac{8}{9}\nu_3\right) \tag{90}$$

$$\left(\frac{\partial \mu}{\partial P}\right)_o = \frac{-1}{B_o}\left(\lambda + \mu + \nu_2 + \frac{4}{3}\nu_3\right) \tag{91}$$

Actually, Hughes and Kelly expressed their results in terms of the Murnaghan third-order constants, l, m, n, but equations 90 and 91, which include an alternative set of third-order constants, ν_1, ν_2, ν_3, have been derived from the results of Hughes and Kelly using the conversion scheme presented in Table 2, Chapter 1.

It should be noted that both the Bridgman expressions 88 and 89 and also the Hughes and Kelly derivatives 90 and 91 refer to the <u>isothermal</u> elastic moduli, whereas the moduli calculated from ultrasonic velocity measurements are <u>adiabatic</u>. However, the differences between the isothermal and the adiabatic moduli are very small for most solid

materials, and furthermore, the experimental errors on the adiabatic third-order moduli calculated in the previous chapter are almost certainly larger than these differences. Under these circumstances, it was not considered worthwhile to make the conversion from the adiabatic to the isothermal moduli. Hence the hydrostatic pressure derivatives have been computed from the experimental work by substituting the (adiabatic) third-order moduli, ν_1, ν_2, and ν_3, directly into equations 90 and 91. In Table 6, the results of these calculations for the polycrystalline magnesium and steel specimens described in the previous chapter are compared with the pressure derivatives determined for similar materials by Bridgman and other workers.

It can be seen from the second column of Table 6 that, in contrast to the present work, in which uniaxial stresses were used, all the other measurements (with the exception of Crecraft's measurements on the steel REX 535) were made under conditions of hydrostatic pressure. Nevertheless, the agreement between the present results and the alternative data shown in Table 6 is excellent. Apart from Crecraft's work [64], the author was unable to find any published data for the particular steel specimens investigated here, but the results for polycrystalline iron, obtained by Bridgman and others, are shown for comparison. Results are also presented for an unspecified 'drill rod' steel, investigated by Birch [108]. The austenitic steel, H4, cannot fairly be compared with the other steels

Material	Pressure Range (bars)*	B_o 10^{11}dyn.cm.$^{-2}$	$\left(\frac{\partial B}{\partial p}\right)_o$	μ_o 10^{11}dyn.cm.$^{-2}$	$\left(\frac{\partial \mu}{\partial p}\right)_o$	Source
Iron (polycrystal)	30,000 H	16.85	4.7			Bridgman[106]
	9,000 H	16.86	4.3	8.12	3.4	Hughes et al.[107]
	10,000 H	16.67	5.13	8.12	2.16	Voronov et al.[58]
Steels:						
Drill rod	4,000 H	16.5		8.11	1.95	Birch[108]
H1. Hecla 37 (0.4% C)	1,500 U	16.6±0.1	6.5 ±0.8	8.21±0.05	1.96±0.3	Author
H2. Hecla 17 (0.6% C)	1,500 U	16.5±0.2	4.87±0.3	8.20±0.05	1.77±0.2	Author
H5. Hecla 138A (2½% NiCrMo)	1,500 U	16.4±0.2	6.17±0.7	8.19±0.05	1.89±0.3	Author
REX 535 (Ni-steel)	1,500 U	16.4±0.1	4.92±1.0	8.18±0.05	1.68±0.5	Author
	1,500 U	14.3±0.2	2.47±0.7	7.80±0.1	2.10±0.3	Crecraft[64]
H4. Hecla ATV (austenitic)	1,500 U	13.5±0.3	8.6 ±1.0	7.16±0.1	3.9 ±0.7	Author
Magnesium (polycrystal)	12,000 H	3.32	6.08			Bridgman[109]
	10,000 H	3.599	4.18	1.657	1.53	Voronov et al.[58]
Mg tooling plate (96% Mg)	200 U	3.70±.03	5.88±.05	1.66±0.03	1.92±0.05	Author
Magnesium (single crystal)	6,500 H			c_{44}=1.64	$\frac{\partial c_{44}}{\partial p}$=1.58	Schmunk et al.[57]
	6,500 H			c' =1.68	$\frac{\partial c'}{\partial p}$ =1.36	Schmunk et al.[57]

* 1 bar = 10^6dyn.cm.$^{-2}$; H = hydrostatic pressure; U = uniaxial stress

$$c' = \tfrac{1}{2}(c_{11}-c_{12})$$

Note: All results other than Bridgman's[106,109] are derived from ultrasonic velocity measurements.

TABLE 6. COMPARISON OF SECOND-ORDER MODULI AND THEIR ZERO-PRESSURE DERIVATIVES.

or pure iron, for reasons given in the previous section.

The bulk and rigidity moduli of the remaining steels, H1, H2, H5 and REX 535 (author) are in good agreement with those of polycrystalline iron and the 'drill rod' steel. By contrast, Crecraft's results for the steel REX 535 are consistently low. The agreement between the pressure derivatives of the bulk and rigidity moduli of the various steel and iron specimens is at least as good as can be expected, bearing in mind the widely different compositions. (It was pointed out in Section 4.1 that differences could show up in the non-linear elastic properties, although none were apparent in the second-order elastic moduli.) In the case of the derivative of the bulk modulus, the author's results for the steel REX 535 agree much better with the polycrystalline iron data than do Crecraft's results. The derivatives of the rigidity modulus are in good agreement for all the steel and iron specimens other than the iron specimen investigated by Hughes et al.[107] and the austenitic steel, H4. However, the equipment used by Hughes et al. to measure small changes in ultrasonic velocity was not nearly so sensitive as that used in the present work. It is suggested that Hughes' data for $\left(\frac{\partial \mu}{\partial P}\right)_o$ may be in error.

In Table 6, the author's results for the polycrystalline magnesium tooling plate are compared with some incomplete data for pure magnesium, both in polycrystalline and single crystal form. The agreement is very good, considering that the magnesium tooling plate contains only 96 per cent magnesium. In the case of the magnesium single crystal, results are presented for the two shear moduli, c_{44} and $\frac{1}{2}(c_{11}-c_{12})$, and their zero-pressure derivatives. The agreement between the latter quantities and the corresponding data for the rigidity moduli of the polycrystalline specimens is quite good.

4.3 EFFECTS OF PREFERRED ORIENTATION

It has been pointed out previously that the elastic properties of a polycrystalline solid must become directional whenever some fraction of the individual grains is preferentially orientated. In a particular specimen, the magnitude of the anisotropy will depend not only on the amount of preferred orientation, but also on the inherent aeolotropy of the individual crystallites. A polycrystalline solid in which the grains are completely randomly orientated will be isotropic, regardless of the single crystal properties of the same material. On the other hand, the elastic properties of, say, a polycrystalline iron specimen, would be much more directional than those of a similar sample of aluminium possessing the same amount of preferred orientation. The difference in the properties

of the aggregates may be explained by comparing the relative aeolotropic characteristics of iron and aluminium in single crystal form.

The exact nature of the anisotropy in a polycrystalline material will depend strongly on the types of deformation which occur during fabrication, and on the crystal symmetry on the individual grains. For example, drawn aluminium wire possesses a radially symmetric grain orientation, and its elastic properties may be described as 'transversely isotropic', a condition which is equivalent to hexagonal symmetry. Hence, although single crystal aluminium has cubic symmetry and may be described by only three second-order elastic moduli, drawn aluminium wire requires five elastic moduli. For further details, and examples of textures and symmetries in polycrystalline materials, the reader is referred to publications by Bradfield [110, 111] and Papadakis [112]. It is emphasised that any polycrystalline solid will possess some degree of preferred orientation unless very special precautions are taken during the fabrication process.

By introducing directional characteristics, preferred orientation can radically affect the attenuation and velocity of ultrasonic waves propagated through a polycrystalline solid. In this discussion, the effect on the velocity, particularly of the shear waves, is of primary importance. The propagation velocity depends not only on the type of wave (longitudinal or transverse), but also on the directions of

propagation and polarisation relative to the preferred directions in the material [99, 100]. In practice, the departures from the appropriate isotropic velocity may vary between a few parts per million and several per cent [112].

In order that 'pure' waves may be propagated, it is essential that a polycrystalline specimen should be cut so that its faces are either parallel or normal to the principal directions (of preferred orientation). If such a specimen is loaded uniaxially between a pair of opposite faces, the principal stress and strain axes should coincide with the directions of preferred orientation, and the symmetry should remain unaltered. Under these conditions, a pure shear wave can only be propagated if the displacement vector is polarised either along or parallel to the principal directions. For any other polarisation, double refraction effects are observed [99, 100]. The foregoing requirements were satisfied in all the present experimental work.

In the previous chapter it was shown how the accuracy of the calculations for the third-order moduli depend strongly on the second-order moduli. Since the latter are computed directly from absolute velocity measurements, it is apparent that for a polycrystalline solid possessing preferred orientation, there are two possible values for the

rigidity modulus, neither of which is equal to the rigidity modulus of the isotropic material. The ambiguity lies in the small difference in the velocities of the two principal shear waves for the propagation direction in question. In principle, the exact 'isotropic' rigidity modulus could be calculated from the observed data using special techniques developed by Bradfield [111]. However, since the velocities of the two principal shear waves never differed by more than a small fraction of 1 per cent in the specimens investigated, it was considered sufficiently accurate to use the arithmetic mean of these velocities in the rigidity modulus calculation.

One further possible consequence of the effect of preferred orientation on the ultrasonic velocity should be mentioned here. It can be seen from equations 72 to 74 that the slopes of the experimental curves of pulse transit time versus applied stress depend on the absolute velocity of the appropriate ultrasonic wave at zero stress. On the other hand, the observed experimental errors associated with evaluating these slopes, are large enough to swamp the small systematic errors introduced by neglecting the effects of preferred orientation. It is considered that the errors quoted in Table 5 for the third-order moduli are large enough to include any departures from isotropy.

CHAPTER 5

THEORY OF SMALL-AMPLITUDE ELASTIC WAVE PROPAGATION IN STRAINED CRYSTALS OF TRIGONAL SYMMETRY

It was mentioned in Chapter 1 that the theory of small-amplitude elastic wave propagation in strained trigonal crystals has been developed by the author from a general theory of Thurston and Brugger [40]. The present chapter contains a summary of this analysis, which was stimulated in the first instance by an interest in the non-linear properties of crystalline quartz. Detailed schemes are presented for the second and third-order elastic moduli of the trigonal sub-groups C_{3v}, D_3, and D_{3d}, showing the conversion relationships between the full tensor notation used by Brugger [24] and the conventional reduced notation. Several features of elastic wave propagation in unstrained trigonal crystals are briefly described. The effects of applied macroscopic stresses are then considered in terms of a previously defined quantity $(\rho_o W^2)'_o$, for 28 particular experimental configurations. Solutions are presented for all these cases, of which only 23 are found to be independent. Finally, the results of the analysis are discussed in relation to experiments for evaluating the third-order elastic moduli.

5.1 RELATION BETWEEN ELASTIC MODULI IN TENSOR AND REDUCED NOTATION

The cartesian coordinate system used to describe trigonal crystals such as right-handed α-quartz [9, 27], is shown in Figure 28,

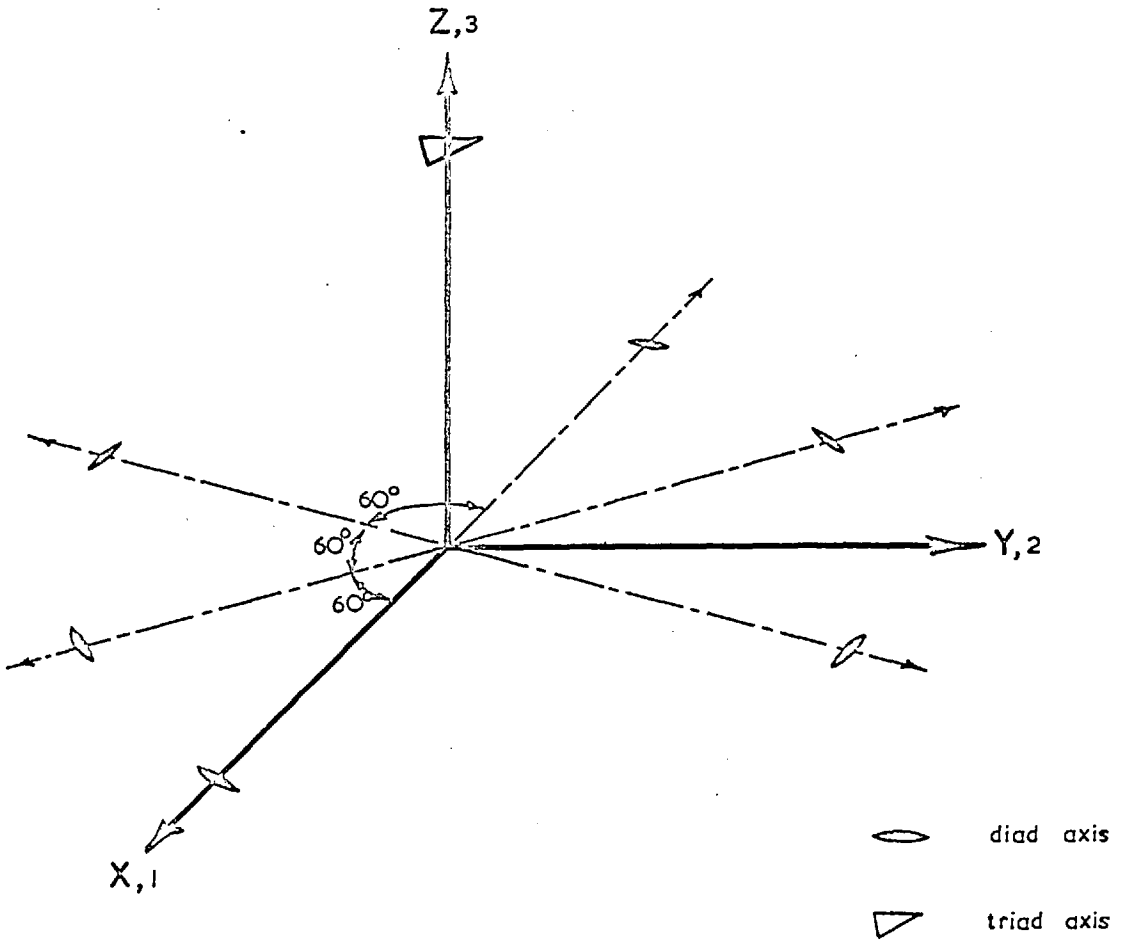

FIGURE 28 CARTESIAN COORDINATE SYSTEM FOR TRIGONAL CRYSTALS, SHOWING EQUIVALENT AXES IN THE X-Y PLANE

$$\begin{array}{cccccc} c_{11} & c_{12} & c_{13} & c_{14} & 0 & 0 \\ & c_{11} & c_{13} & -c_{14} & 0 & 0 \\ & & c_{33} & 0 & 0 & 0 \\ & & & c_{44} & 0 & 0 \\ & & & & c_{44} & c_{14} \\ & & & & & \tfrac{1}{2}(c_{11}-c_{12}) \end{array}$$

(i) 'Stiffness' moduli

$$\begin{array}{cccccc} s_{11} & s_{12} & s_{13} & s_{14} & 0 & 0 \\ & s_{11} & s_{13} & -s_{14} & 0 & 0 \\ & & s_{33} & 0 & 0 & 0 \\ & & & s_{44} & 0 & 0 \\ & & & & s_{44} & 2s_{14} \\ & & & & & 2(s_{11}-s_{12}) \end{array}$$

(ii) Compliance moduli

TABLE 7 SCHEMES OF NON-ZERO SECOND-ORDER ELASTIC AND COMPLIANCE MODULI FOR TRIGONAL SUB-GROUPS C_{3v}, D_3, D_{3d}.

while in tables 7(a) and (b), the complete schemes of non-zero second-order elastic and compliance moduli are presented in conventional reduced notation. (See, for example, Cady [113]). Only half of each table is shown since they are symmetrical about the diagonals. It should be noted that only 6 of the 12 non-zero elastic and compliance moduli are independent, and that the numerical coefficients of the dependent moduli, c_{56} and c_{66}, are different from the corresponding coefficients of the compliance moduli, s_{56} and s_{66}.

In Chapter 1, the n^{th}-order elastic moduli were defined in tensor notation, following Brugger [24], and general conversion relationships between corresponding moduli in the full tensor and reduced notations were derived. (Equations 17 and 18). From equation 17, it is apparent that for the stiffness moduli, the conversion is quite simple, and no numerical factors are involved. All that is required is to replace pairs of adjacent indices by a single index according to the scheme: $11 \rightarrow 1$; $22 \rightarrow 2$; $33 \rightarrow 3$; $23 \rightarrow 4$; $31 \rightarrow 5$; $12 \rightarrow 6$. From equation 18, however, it may be seen that for the compliance moduli, certain numerical factors occur in the conversion process. Thus:

$$\frac{s_{jkpq\ldots}}{s_{JP..}} = \tfrac{1}{2}(1+\delta_{jk})\tfrac{1}{2}(1+\delta_{pq}) \quad . \quad . \qquad (92)$$

In Table 8, the numerical ratios associated with reducing Brugger's tensor

Tensor compliance s_{jkpq}	Reduced compliance s_{JP}	Numerical ratio s_{jkpq}/s_{JP}
s_{1111}	s_{11}	1
s_{2222}	$s_{22} = s_{11}$	1
s_{3333}	s_{33}	1
s_{1122}	s_{12}	1
s_{1133}	s_{13}	1
s_{2233}	$s_{23} = s_{13}$	1
s_{1123}	s_{14}	$\frac{1}{2}$
s_{2223}	$s_{24} = -s_{14}$	$\frac{1}{2}$
s_{2323}	s_{44}	$\frac{1}{4}$
s_{1313}	$s_{55} = s_{44}$	$\frac{1}{4}$
s_{1312}	$s_{56} = 2s_{14}$	$\frac{1}{4}$
s_{1212}	$s_{66} = 2(s_{11}-s_{12})$	$\frac{1}{4}$

TABLE 8 REDUCTION OF SECOND-ORDER COMPLIANCES OF TRIGONAL CRYSTALS FROM BRUGGER TENSOR TO CONVENTIONAL FORM

coefficients to the conventional forms are shown for all the non-zero second-order compliances of trigonal crystals. The factor $\frac{1}{2}$, which occurs in the reduction of the tensor compliances s_{1123} and s_{2223}, should be noted, as these compliances appear frequently in the analysis described in Section 5.3.

The 'mixed' third-order stiffness moduli, C_{jkpqrs}, defined by Brugger, may be converted to the reduced form, C_{JPR}, without involving any numerical constants, as mentioned above. However, the reduced moduli thus obtained are not directly equal to corresponding reduced coefficients derived by other workers, notably Birch [21] and Hearmon [22]. The difference originates in the alternative definitions of the stored-energy function, as described in Chapter 1. Brugger [24] has shown that his reduced third-order moduli are related to Birch's reduced coefficients by the ratio

$$\frac{(C_{JPR})_{Birch}}{(C_{JPR})_{Brugger}} = \frac{1}{6} N(JPR) \qquad (93)$$

where N(JPR) is the number of ways in which C_{JPR} can be written with tensor indices. (For example, N(111) = 1, N(114) = 6 and N(456) = 48). For a trigonal crystal, there are 31 non-zero third-order elastic moduli in the reduced notation, and 14 of these are independent. The numerical ratio $\frac{1}{6}$ N(JPR) is listed for all 31 non-zero moduli in Table 9.

Independent Coefficients		Dependent Coefficients	
C_{JPR}	N(JPR)/6	C_{JPR}	N(JPR)/6
C_{111}	1/6	C_{122}	$\frac{1}{2}$
C_{222}	1/6	C_{156}	4
C_{333}	1/6	C_{166}	2
C_{444}	4/3	C_{223}	$\frac{1}{2}$
C_{112}	$\frac{1}{2}$	C_{224}	1
C_{113}	$\frac{1}{2}$	C_{233}	$\frac{1}{2}$
C_{114}	1	C_{234}	2
C_{123}	1	C_{244}	2
C_{124}	2	C_{255}	2
C_{133}	$\frac{1}{2}$	C_{256}	4
C_{134}	2	C_{266}	2
C_{144}	2	C_{355}	2
C_{155}	2	C_{356}	4
C_{344}	2	C_{366}	2
		C_{455}	4
		C_{456}	8
		C_{466}	4

TABLE 9 NUMERICAL RATIO OF BIRCH AND BRUGGER NON-ZERO THIRD-ORDER ELASTIC MODULI FOR TRIGONAL CRYSTALS

Hearmon [22] has derived complete schemes for all the Birch non-zero third-order moduli for each of the 32 crystallographic classes. Using Hearmon's results for the trigonal sub-groups C_{3v}, D_3, D_{3d}, in conjunction with the data shown in the final column of Table 9, the relationships between the dependent and independent third-order moduli can be derived for the Brugger system. In Table 10, these relationships are listed for all 17 independent third-order moduli in both the Birch and Brugger systems. It is apparent from the table that, in many cases, corresponding dependent relationships are not identical in the two systems. It is worth noting that the Brugger system of third-order moduli is exactly equivalent to a scheme derived by Fumi [33], using the so-called 'direct-inspection' technique [114]. In the analysis of elastic wave propagation in strained trigonal crystals, described in Section 5.3, the Brugger system has been used exclusively.

5.2 WAVE PROPAGATION IN UNSTRAINED TRIGONAL CRYSTALS

The basic theory of small-amplitude elastic wave propagation in a general unstrained aeolotropic crystal was summarised in Chapter 1. The general theory can be specialised for any given crystal symmetry and solved to yield the wave propagation conditions for a particular case. For a given propagation direction (wave-normal), three solutions to the equation of motion can be obtained, which represent three independent

Dependent modulus	Birch system equivalent		Brugger system equivalent
C_{122}	$3C_{111}+C_{112}-3C_{222}$	*	$C_{111}+C_{112}-C_{222}$
C_{156}	$2C_{114}+3C_{124}$	*	$\frac{1}{3}(C_{114}+3C_{124})$
C_{166}	$-6C_{111}-C_{112}+9C_{222}$	*	$\frac{1}{4}(-2C_{111}-C_{112}+3C_{222})$
C_{223}	C_{113}		C_{113}
C_{224}	$-C_{114}-C_{124}$	*	$-C_{114}-2C_{124}$
C_{233}	C_{133}		C_{133}
C_{234}	$-C_{134}$		$-C_{134}$
C_{244}	C_{155}		C_{155}
C_{255}	C_{144}		C_{144}
C_{256}	$2C_{114}-C_{124}$	*	$\frac{1}{2}(C_{114}-C_{124})$
C_{266}	$6C_{111}-C_{112}-3C_{222}$	*	$\frac{1}{4}(2C_{111}-C_{112}-C_{222})$
C_{355}	C_{344}		C_{344}
C_{356}	$2C_{134}$	*	C_{134}
C_{366}	$2C_{113}-C_{123}$	*	$\frac{1}{2}(C_{113}-C_{123})$
C_{455}	$-3C_{444}$	*	$-C_{444}$
C_{456}	$2C_{155}-2C_{144}$	*	$\frac{1}{2}(C_{155}-C_{144})$
C_{466}	$2C_{124}$	*	C_{124}

* signifies Birch and Brugger equivalents are not identical.

TABLE 10 RELATIONSHIPS BETWEEN DEPENDENT AND INDEPENDENT THIRD-ORDER MODULI FOR TRIGONAL SUB-GROUPS C_{3v}, D_3, D_{3d}

waves whose particle displacements form a real orthogonal set. However, the particle displacements will be orthogonal to the wave-normal in only a very few special cases, and even then the direction of energy flow will not necessarily lie along the wave-normal. For example, shear waves propagated along the Z-axis in quartz are polarised parallel to the X-Y plane, but the direction of energy flow deviates from the Z-axis by an angle of about 16 degrees.

In the present discussion of wave propagation in trigonal crystals (sub-groups C_{3v}, D_3, D_{3d}) only waves which are polarised either exactly parallel or perpendicular to the propagation direction (including cases such as the above example) will be considered. These waves are 'pure' in the sense of Borgnis [14], and in practice, all of them can be generated uniquely using appropriate transducers. The discussion will be further restricted to three propagation directions, namely, the X,Y and Z crystallographic axes. The X and Z-axes each support one 'pure' longitudinal and two 'pure' transverse waves. Hence it is possible to generate as many as seven 'pure' waves in a single specimen in the form of a rectangular parallelepiped, which is cut with its three pairs of opposite faces respectively parallel to the X, Y and Z-axes. In addition to these principal crystallographic axes, there exist other pure mode directions in crystals of trigonal symmetry. For example, pure shear waves may be propagated along the so-called AC and BC directions, which

lie in the Y-Z plane at angles of -59° and $+31^{\circ}$, respectively, to the Y-axis. For a detailed discussion of elastic wave propagation in trigonal crystals, the reader is referred to an excellent article by Farnell [9].

The seven 'pure' waves mentioned above for an X-Y-Z cut specimen have been analysed using the methods outlined in Chapter 1. The details of the analysis will not be presented here, since they are well known and have been fully treated elsewhere. (See, for example, references 9, 11, 12 and 115. References 9 and 115 deal exclusively with trigonal symmetry). In Table 11, the propagation characteristics of the seven waves are summarised, but the contents of the table and its footnotes may require some further explanation.

The entries shown in the final column of Table 11 are valid for ordinary trigonal crystals. However, α-quartz, which is of particular interest here, is not only trigonal, but also piezoelectric. McSkimin [115] has shown that if the strains produced by elastic waves travelling in a piezoelectric medium result in an electric field in the direction of propagation, the velocity of the waves is increased slightly over the 'zero-field' value. For α-quartz, two of the modes (1 and 4) listed in Table 11 are affected, but in both cases the formula for $(\rho_o W^2)_o$ may be corrected by the addition of a further term, $\frac{e_{11}^2}{\varepsilon_{11}}$, where e_{11} and ε_{11} are

TABLE 11 DESIGNATION AND PROPAGATION CHARACTERISTICS OF SEVEN PURE WAVES IN TRIGONAL CRYSTALS

Case	Type of Mode	Direction of Propagation	Direction of particle motion	Direction of maximum energy flow	Formula for $w = (\rho_o W^2)_o = (\rho_o V^2)_o$
1	L	X	X	X	c_{11} *
2	T	X	YZ plane[a]	X	$(c_{44}-w_2)(c_{66}-w_2)=c_{14}^2$
3	T	X	YZ plane[a]	X	$(c_{44}-w_3)(c_{66}-w_3)=c_{14}^2$
4	T	Y	X	YZ plane[b]	c_{66} *
5	L	Z	Z	Z	c_{33}
6	T	Z	X	YZ plane[c]	c_{44}
7	T	Z	Y	YZ plane[c]	c_{44}

L = longitudinal wave , T = transverse wave

* See text and reference 115

a See text. The transverse modes 2, 3 are polarised normal to each other in the YZ plane. The faster mode (eigenvalue w_2) has direction cosines (0,p,q) and the slower mode (w_3) has direction cosines (0,p',q'). (See equation 95)

b For complete specification, see McSkimin [115]. In α-quartz, the beam deviates by about 24° from +Y towards -Z.

c Energy flow for mode 6 deviates from +Z towards -Y; mode 7 deviates from +Z towards +Y by an equal amount [116]. In α-quartz, the angular deviations are about ±16°.

piezoelectric and zero-strain permittivity components, respectively.

The two transverse modes 2, 3 propagating along the X-axis are polarised in the Y-Z plane, and their particle displacements are assigned direction cosines (0,p,q) and (0,p',q'), respectively, as indicated in Table 11, footnote a. The direction of particle motion can be evaluated by standard methods outlined in Section 1.1, and described in detail by, for example, Farnell [9], Musgrave [11], or Hearmon [12]. It can be shown that the direction cosines of the faster transverse mode, 2, satisfy the following conditions.

$$p^2 = \frac{(w_2 - c_{44})^2}{(w_2 - c_{44})^2 + c_{14}^2}$$

$$q^2 = \frac{c_{14}^2}{(w_2 - c_{44})^2 + c_{14}^2} \qquad (94)$$

$$pq = \frac{c_{14}(w_2 - c_{44})}{(w_2 - c_{44})^2 + c_{14}^2}$$

Since the particle displacements of the two waves are orthogonal, their direction cosines are related to each other as follows.

$$p'^2 = q^2 \; ; \quad q'^2 = p^2 \; ; \; p'q' = -pq \qquad (95)$$

The definitions 94 and the dependent relationships 95 are used extensively in the discussion of wave propagation in strained trigonal crystals in the following section.

5.3 WAVE PROPAGATION IN STRAINED TRIGONAL CRYSTALS

Thurston and Brugger's general theory of elastic wave propagation in strained aeolotropic solids was outlined in Chapter 1, Section 3. The principal result of the theory was a completely general expression for the quantity $(\rho_o W^2)'_o$, which was defined previously, but is repeated here in full.

Thus

$$(\rho_o W^2)'_o = t'_{ab}(0)\left[N_a N_b + U^o_j U^o_k (2ws_{jkab} + N_r N_s s_{ipab} C_{jrksip})\right] \qquad (34)$$

where W is the 'natural' velocity of propagation, $\underline{N}$, $\underline{U}^o$ are, respectively, unit vectors along the propagation direction and particle displacement direction, and the tensor $t'_{ab}(0)$ is given by

$$t'_{ab}(0) = -\delta_{ab} \text{ for hydrostatic pressure} \qquad (37)$$

$$= -M_a M_b \text{ for uniaxial compression in direction of a unit vector } \underline{M} \qquad (38)$$

The compliances, s, are isothermal, but the superscript T has been omitted for simplicity. It should be remembered that the third-order

elastic moduli, C_{jrksip}, are 'mixed' coefficients, that is to say, they are neither truly isentropic nor isothermal (see Section 1.3). The general equation 34 may be rewritten in the form

$$-(\rho_o W^2)'_o = A + 2wF + G \tag{96}$$

where for hydrostatic pressure,

$$\begin{aligned} A &= 1 \\ F &= U^o_j U^o_k s_{jkaa} \\ G &= N_r N_s U^o_j U^o_k s_{ipaa} C_{jrksip} \end{aligned} \tag{97}$$

and for uniaxial compression in direction $\underline{M}$,

$$\begin{aligned} A &= 0 \text{ when } \underline{M} \text{ is perpendicular to } \underline{N}, \\ &= 1 \text{ when } \underline{M} \text{ is parallel to } \underline{N} \\ F &= M_a M_b U^o_j U^o_k s_{jkab} \\ G &= M_a M_b N_r N_s U^o_j U^o_k s_{ipab} C_{jrksip} \end{aligned} \tag{98}$$

The quantity w appearing in equations 34 and 96 may be identified as the relevant zero-strain eigenvalue, $(\rho_o W^2)_o = (\rho_o V^2)_o$.

The quantities F and G have been evaluated for all seven pure waves discussed in the previous section, and the results are presented in Table 12. In deriving the functions F and G, full use has been made of the detailed schemes for reducing the tensor moduli to the conventional forms (see Section 3.1). It will be noticed that both hydrostatic and uniaxial compressive stresses have been considered. In the latter case, three configurations may be distinguished, namely, stress applied parallel to the wave propagation direction, and stress applied perpendicular to the propagation direction (two orthogonal situations). In total, there exist twenty-eight possible combinations of the seven 'pure' wave modes and the four distinguishable stress configurations, but it is apparent from Table 12 that only twenty-three of these combinations are independent.

The second column in Table 12 has been labelled 'designation' and is to be understood as follows.

N_j denotes the direction of propagation of the wave, where the subscript j = 1,2,3 indicates the X, Y or Z axis, respectively.

M_j denotes the direction of applied stress, with j defined as above, except that j = 0 indicates hydrostatic pressure.

L, T denote longitudinal or transverse waves, respectively, and a subscript j indicates the direction of particle motion; single or double superscript dashes indicate, respectively, the

Case	Designation	F	G
1	$N_1M_oL_1$	$s_{11}+s_{12}+s_{13}$	$(s_{11}+s_{12}+s_{13})(C_{111}+C_{112}) + (2s_{13}+s_{33})C_{113}$
2	N_1M_oT'	$p^2(s_{11}+s_{12}+s_{13}) + q^2(2s_{13}+s_{33})$	$(s_{11}+s_{12}+s_{13})\left[\frac{1}{2}p^2(-C_{112}+C_{222}) + q^2(C_{144}+C_{155}) + 2pq(C_{114}+C_{124})\right] + (2s_{13}+s_{33})\left[\frac{1}{2}p^2(C_{113}-C_{123}) + q^2C_{344} + 2pqC_{134}\right]$
3	N_1M_oT''	$q^2(s_{11}+s_{12}+s_{13}) + p^2(2s_{13}+s_{33})$	$(s_{11}+s_{12}+s_{13})\left[\frac{1}{2}q^2(-C_{112}+C_{222}) + p^2(C_{144}+C_{155}) -2pq(C_{114}+C_{124})\right] + (2s_{13}+s_{33})\left[\frac{1}{2}q^2(C_{113}-C_{123}) + p^2C_{344} - 2pqC_{134}\right]$
4	$N_2M_oT_1$	$s_{11}+s_{12}+s_{13}$	$\frac{1}{2}(s_{11}+s_{12}+s_{13})(-C_{112}+C_{222}) + \frac{1}{2}(2s_{13}+s_{33})(C_{113}-C_{123})$
5	$N_3M_oL_3$	$(2s_{13}+s_{33})$	$2(s_{11}+s_{12}+s_{13})C_{133} + (2s_{13}+s_{33})C_{333}$
6 7	$N_3M_oT_1$ $N_3M_oT_2$	$s_{11}+s_{12}+s_{13}$	$(s_{11}+s_{12}+s_{13})(C_{144}+C_{155}) + (2s_{13}+s_{33})C_{344}$

TABLE 12 THE FUNCTIONS F and G FOR TRIGONAL SUB-GROUPS C_{3v}, D_3, D_{3d}

(i) Hydrostatic pressure

Case	Designation	F	G
8	$N_1M_1L_1$	s_{11}	$s_{11}C_{111}+s_{12}C_{112}+s_{13}C_{113}+s_{14}C_{114}$
9	N_1M_1T'	$(p^2s_{12}+q^2s_{13}+pqs_{14})$	$p^2(s_{11}C_{111}+s_{12}C_{112}+s_{13}C_{113}+s_{14}C_{114})$ $+ q^2\left[-\frac{1}{2}(s_{11}-s_{12})C_{111}-\frac{1}{4}(s_{11}+s_{12})C_{112}\right.$ $\left.+ \frac{1}{2}s_{13}(C_{113}-C_{123}) + s_{14}C_{124} + \frac{1}{4}(3s_{11}-s_{12})C_{222}\right]$ $+2pq\left[\frac{1}{2}(s_{11}+s_{12})C_{114} + \frac{1}{2}(3s_{11}-s_{12})C_{124}+s_{13}C_{134}\right.$ $\left.-\frac{1}{2}s_{14}(C_{144}-C_{155})\right]$
10	N_1M_1T''	$(q^2s_{12}+p^2s_{13}-pqs_{14})$	$q^2(s_{11}C_{111}+s_{12}C_{112}+s_{13}C_{113}+s_{14}C_{114})$ $+ p^2\left[-\frac{1}{2}(s_{11}-s_{12})C_{111}-\frac{1}{4}(s_{11}+s_{12})C_{112}\right.$ $\left.+ \frac{1}{2}s_{13}(C_{113}-C_{123}) + s_{14}C_{124} + \frac{1}{4}(3s_{11}-s_{12})C_{222}\right]$ $-2pq\left[\frac{1}{2}(s_{11}+s_{12})C_{114} + \frac{1}{2}(3s_{11}-s_{12})C_{124}+s_{13}C_{134}\right.$ $\left.-\frac{1}{2}s_{14}(C_{144}-C_{155})\right]$
11	$N_2M_2T_1$	s_{12}	$\frac{1}{2}(s_{11}-s_{12})C_{111}-\frac{1}{4}(s_{11}+s_{12})C_{112} + \frac{1}{2}s_{13}(C_{113}-C_{123})$ $-s_{14}C_{124} - \frac{1}{4}(s_{11}-3s_{12})C_{222}$
12	$N_3M_3L_3$	s_{33}	$2s_{13}C_{133}+s_{33}C_{333}$
13 14	$N_3M_3T_1$ $N_3M_3T_2$	s_{13}	$s_{13}(C_{144}+C_{155}) + s_{33}C_{344}$

TABLE 12 continued

(ii) Uniaxial compression parallel to propagation direction

Case	Designation	F	G
15	$N_1M_2L_1$	s_{12}	$s_{12}C_{111}+s_{11}C_{112}+s_{13}C_{113}-s_{14}C_{114}$
16	$N_1M_3L_1$	s_{13}	$s_{13}(C_{111}+C_{112}) + s_{33}C_{113}$
17	N_1M_2T'	$p^2s_{11}+q^2s_{13}-pqs_{14}$	$p^2\left[\frac{1}{2}(s_{11}-s_{12})C_{111}-\frac{1}{4}(s_{11}+s_{12})C_{112}+\frac{1}{2}s_{13}(C_{113}-C_{123})-s_{14}C_{124}-\frac{1}{4}(s_{11}-3s_{12})C_{222}\right]$ + $q^2(s_{11}C_{144}+s_{12}C_{155}+s_{13}C_{344}+s_{14}C_{444})$ + $pq\left[(s_{11}+s_{12})C_{114}-(s_{11}-3s_{12})C_{124}+2s_{13}C_{134}+s_{14}(C_{144}-C_{155})\right]$
18	N_1M_2T''	$q^2s_{11}+p^2s_{13}+pqs_{14}$	$q^2\left[\frac{1}{2}(s_{11}-s_{12})C_{111}-\frac{1}{4}(s_{11}+s_{12})C_{112}+\frac{1}{2}s_{13}(C_{113}-C_{123})-s_{14}C_{124}-\frac{1}{4}(s_{11}-3s_{12})C_{222}\right]$ + $p^2(s_{11}C_{144}+s_{12}C_{155}+s_{13}C_{344}+s_{14}C_{444})$ - $pq\left[(s_{11}+s_{12})C_{114}-(s_{11}-3s_{12})C_{124}+2s_{13}C_{134}+s_{14}(C_{144}-C_{155})\right]$
19	N_1M_3T'	$p^2s_{13}+q^2s_{33}$	$\frac{1}{2}p^2\left[s_{13}(-C_{112}+C_{222})+s_{33}(C_{113}-C_{123})\right]$ $+q^2\left[s_{13}(C_{144}+C_{155})+s_{33}C_{344}\right]$ + $2pq\left[s_{13}(C_{114}+C_{124})+s_{33}C_{134}\right]$
20	N_1M_3T''	$q^2s_{13}+p^2s_{33}$	$\frac{1}{2}q^2\left[s_{13}(-C_{112}+C_{222})+s_{33}(C_{113}-C_{123})\right]+p^2\left[s_{13}(C_{144}+C_{155})+s_{33}C_{344}\right]$ - $2pq\left[s_{13}(C_{114}+C_{124})+s_{33}C_{134}\right]$

TABLE 12 continued

(iii) Uniaxial compression perpendicular to propagation direction

Case	Designation	F	G
21	$N_2M_1T_1$	s_{11}	$-\frac{1}{2}(s_{11}-s_{12})C_{111}-\frac{1}{4}(s_{11}+s_{12})C_{112}+\frac{1}{2}s_{13}(C_{113}-C_{123})$ $+s_{14}C_{124}+\frac{1}{4}(3s_{11}-s_{12})C_{222}$
22	$N_2M_2T_1$	s_{13}	$\frac{1}{2}s_{13}(-C_{112}+C_{22})+\frac{1}{2}s_{33}(C_{113}-C_{123})$
23	$N_3M_1L_3$	s_{13}	$(s_{11}+s_{12})C_{133}+s_{13}C_{333}$
24	$N_3M_2L_3$		
25	$N_3M_1T_1$	s_{11}	$s_{12}C_{144}+s_{11}C_{155}+s_{13}C_{344}-s_{14}C_{444}$
26	$N_3M_2T_2$		
27	$N_3M_2T_1$	s_{12}	$s_{11}C_{144}+s_{12}C_{155}+s_{13}C_{344}+s_{14}C_{444}$
28	$N_3M_1T_2$		

TABLE 12 continued

(iii) Uniaxial compression perpendicular to propagation direction

faster and slower of the two transverse modes propagated along the X axis (modes 2 and 3 of Table 11).

5.4 EVALUATION OF THIRD-ORDER ELASTIC MODULI FROM ULTRASONIC VELOCITY MEASUREMENTS

In Chapters 2 and 3, it was shown how the quantities, $(\rho_o W^2)'_o$, may be determined from the initial variations in the 'natural' velocity of propagation of ultrasonic waves as a function of applied stress. From Table 12, it is apparent that, for materials belonging to the trigonal sub-groups C_{3v}, D_3, D_{3d}, all fourteen third-order elastic moduli can be evaluated uniquely. Several additional internal checks should be possible, since twenty-three of the relationships presented for $(\rho_o W^2)'_o$ are independent. The data of Table 12 has been summarised in Table 13, which shows how the fourteen third-order moduli occur in the various expressions for the function, G.

An examination of entries 5, 12 and 23 of Table 13 shows that the moduli C_{133} and C_{333} can be evaluated uniquely, with one additional check, by measuring the variation in velocity of longitudinal waves, propagated along the Z-axis, as a function of hydrostatic pressure and uniaxial stress (either along or perpendicular to the propagation direction). The moduli C_{144}, C_{155}, C_{344} and C_{444} can also be determined uniquely, but without any internal checks, by evaluating

Case	Designation	Third-order moduli													
		C_{111}	C_{222}	C_{333}	C_{444}	C_{112}	C_{113}	C_{114}	C_{123}	C_{124}	C_{133}	C_{134}	C_{144}	C_{155}	C_{344}
1	$N_1M_0L_1$	X				X	X								
2	N_1M_0T'		X			X	X	X	X	X		X	X	X	X
3	N_1M_0T''		X			X	X	X	X	X		X	X	X	X
4	$N_2M_0T_1$		X			X	X		X						
5	$N_3M_0L_3$			X							X				
6,7	$N_3M_0T_1, N_3M_0T_2$												X	X	X
8	$N_1M_1L_1$	X				X	X	X							
9	N_1M_1T'	X	X			X	X	X	X	X		X	X	X	
10	N_1M_1T''	X	X			X	X	X	X	X		X	X	X	
11	$N_2M_2T_1$	X	X			X	X		X	X					
12	$N_3M_3L_3$			X							X				
13,14	$N_3M_3T_1, N_3M_3T_2$												X	X	X
15	$N_1M_2L_1$	X				X	X	X							
16	$N_1M_3L_1$	X				X	X								
17	N_1M_2T'	X	X		X	X	X	X	X	X		X	X	X	X
18	N_1M_2T''	X	X		X	X	X	X	X	X		X	X	X	X
19	N_1M_3T'		X			X	X	X	X	X		X	X	X	X
20	N_1M_3T''		X			X	X	X	X	X		X	X	X	X
21	$N_2M_1T_1$	X	X			X	X		X	X					
22	$N_2M_3T_1$		X			X	X		X						
23,24	$N_3M_1L_3, N_3M_2L_3$			X							X				
25,26	$N_3M_1T_1, N_3M_2T_2$				X								X	X	X
27,28	$N_3M_2T_1, N_3M_1T_2$				X								X	X	X

TABLE 13. SUMMARY OF TABLE 12 SHOWING OCCURRENCE OF INDEPENDENT THIRD-ORDER ELASTIC MODULI.

the quantities F and G for the experimental configurations listed under entries 6, 13, 25 and 27 (or alternatively, 7, 14, 26 and 28) of Tables 12 and 13. Sixteen further relationships exist which may be used to evaluate the remaining eight moduli, C_{111}, C_{222}, C_{112}, C_{113}, C_{114}, C_{123}, C_{124} and C_{134}. Several internal checks should be possible.

Obviously, some of the experimental configurations are easier to realise in practice than others. For example, a particularly convenient arrangement occurs when the direction of propagation of the ultrasound is perpendicular to the direction of applied stress, whereas the problem becomes more complicated when the propagation direction and stress axis are coaxial. In the latter case, the transducers cannot be placed directly in contact with the specimen, but must be located on the back surface of a special 'buffer rod' or 'anvil' [39], through which the stress is applied. Hydrostatic pressure measurements, while requiring rather sophisticated equipment, have the advantage that higher strains may be produced in the specimen without risk of fracture or plastic deformation.

Deviation of the energy flow from the wave-normal should not affect the experimental measurements, provided reasonable precautions are taken to avoid complications due to reflections from the side

boundaries of the specimen [115]. It should be possible to eliminate such unwanted side reflections by suitably arranging the location of the transducers on the specimen.

SUGGESTIONS FOR FURTHER WORK

The main part of this thesis has been concerned with experimental determination of the third-order elastic moduli of quasi-isotropic polycrystalline metals, and in one case (magnesium), the measured data has been directly correlated with independent work on the interaction of ultrasonic beams. Although the observed agreement is most encouraging, it is felt that more useful and meaningful information would be obtained by investigating the non-linear elastic properties of single rather than poly-crystals. A programme of experimental work, similar to the present investigation, but directed towards the systematic evaluation of the third-order moduli of single crystals is therefore strongly recommended.

(1) Extension of experimental technique

The theory of elastic wave propagation in strained solids has been developed for both hydrostatic pressure and uniaxial stresses, applied either along or perpendicular to the propagation direction of the wave, whereas the present investigation has been limited to the latter configuration. The measurements should be extended to include hydrostatic pressure and also uniaxial stresses along the propagation direction. In addition, the uniaxial stresses should be applied in tension as well as compression.

(2) Polycrystalline specimens

The measurements on tungsten and molybdenum should be completed by comparing the non-linear properties of specimens having the correct density with the results obtained for the low-density sintered specimens described in Chapter 3. Several steels of different composition have already been investigated, but it would be interesting to see if the method of heat treatment affects their non-linear properties.

(3) Single crystal specimens

In Chapter 5, a sufficient number of experimental cases were analysed to allow a complete evaluation of the 14 third-order moduli of trigonal crystals. Measurements on α-quartz are particularly recommended, since information on the third-order moduli is required in connection with observations of phonon-phonon damping in this material (see Chapter 1, Section 5). Measurements should also be made on metal single crystals such as the refractory metals, tungsten and vanadium, which will withstand relatively large stresses without flow or fracture. (Tungsten is especially interesting since it is very nearly isotropic in single crystal form).

APPENDIX 1

ELECTRONIC EQUIPMENT

In Chapter 2, the principles of operation of the electronic equipment were discussed with the aid of simplified block diagrams. Since the basic units such as blocking oscillators, multivibrators, etc., are completely standard, they will not be elaborated here. Many of these units have been adapted from already existing circuits, and the reader is referred elsewhere for further details [117]. The complete circuit diagrams for the pulse generator, transmitter, and receivers are shown in Figures 29, 30 and 31, respectively, and a photograph of the entire equipment is shown in Figure 32.

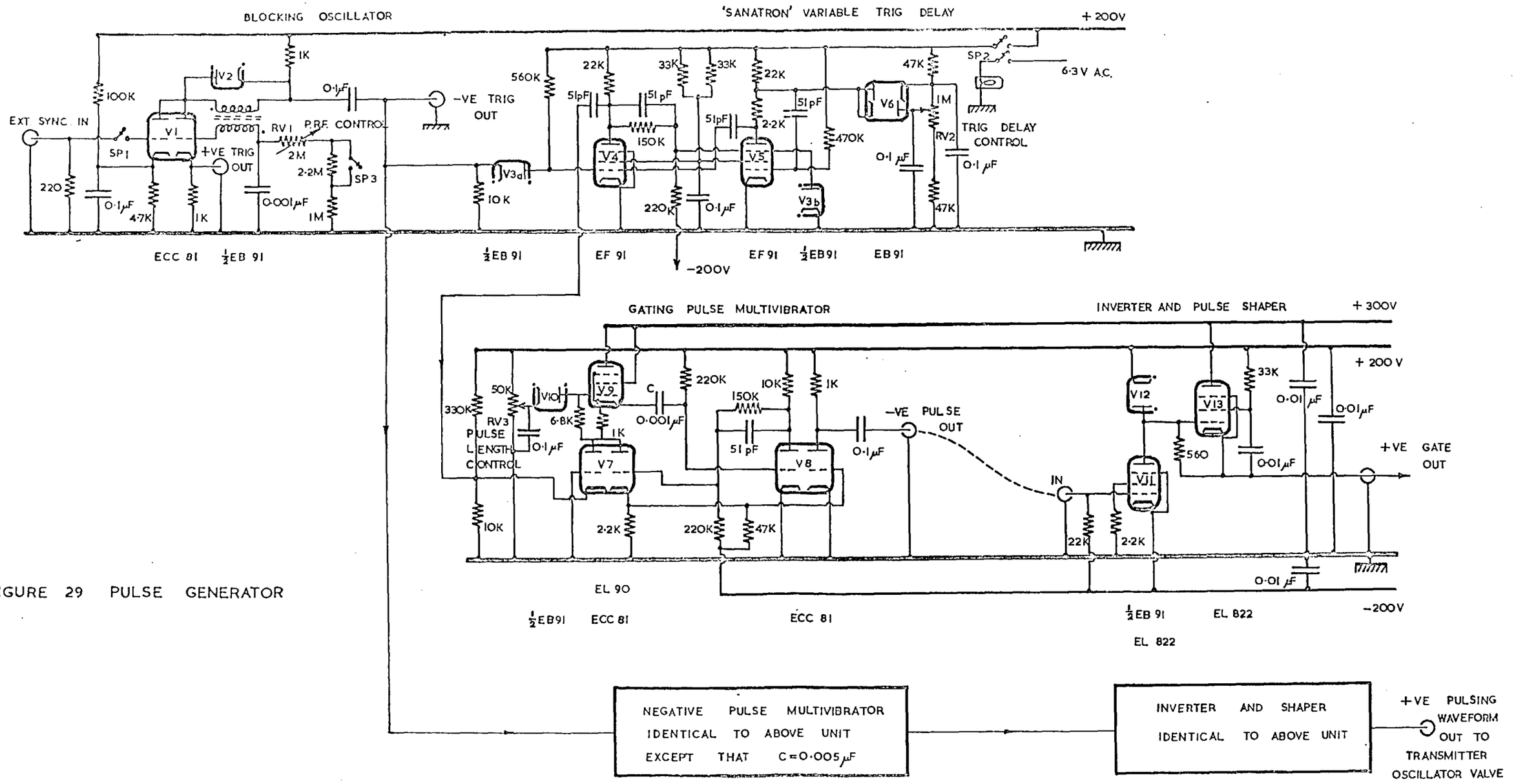

FIGURE 29 PULSE GENERATOR

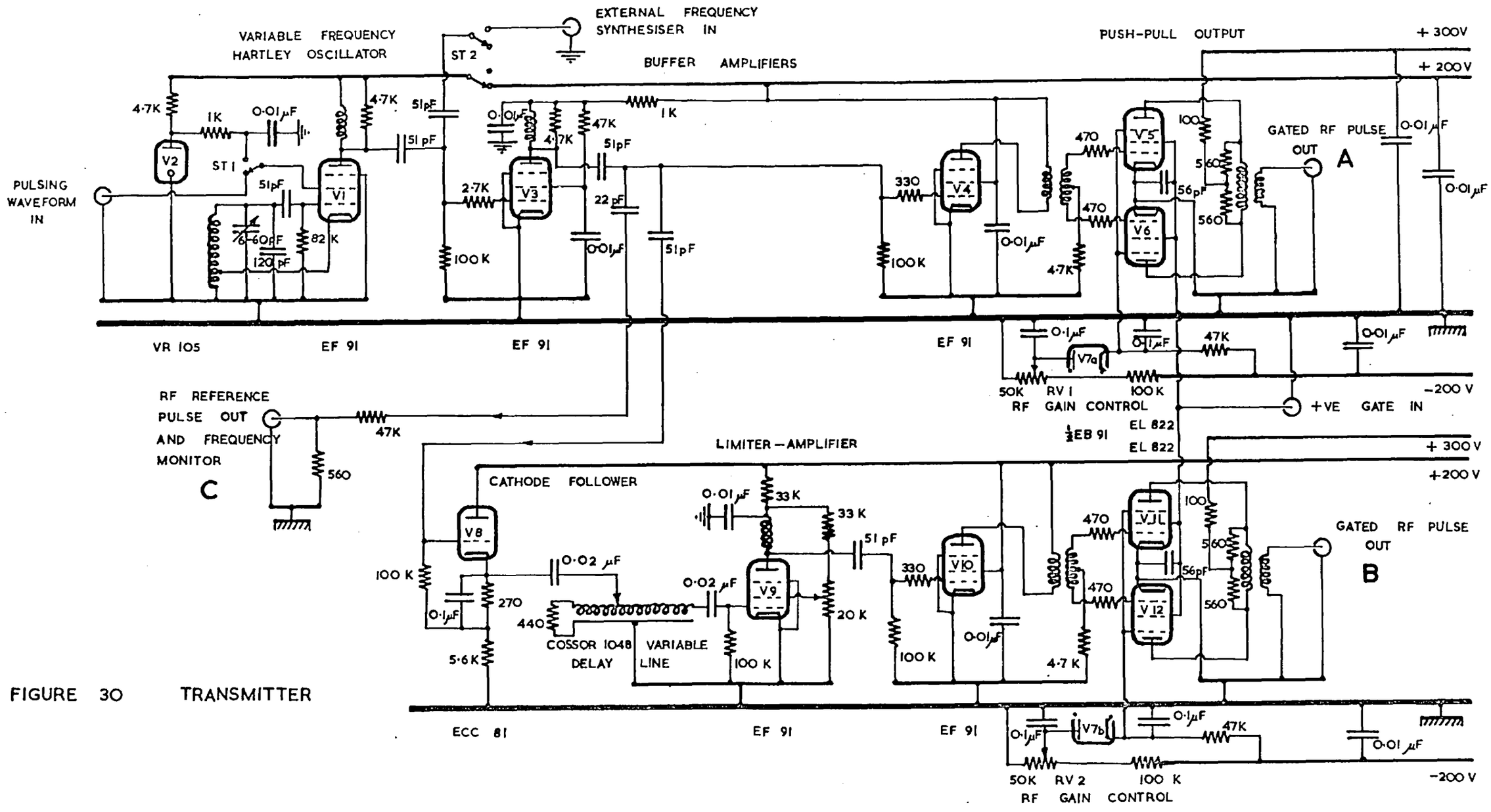

FIGURE 30 TRANSMITTER

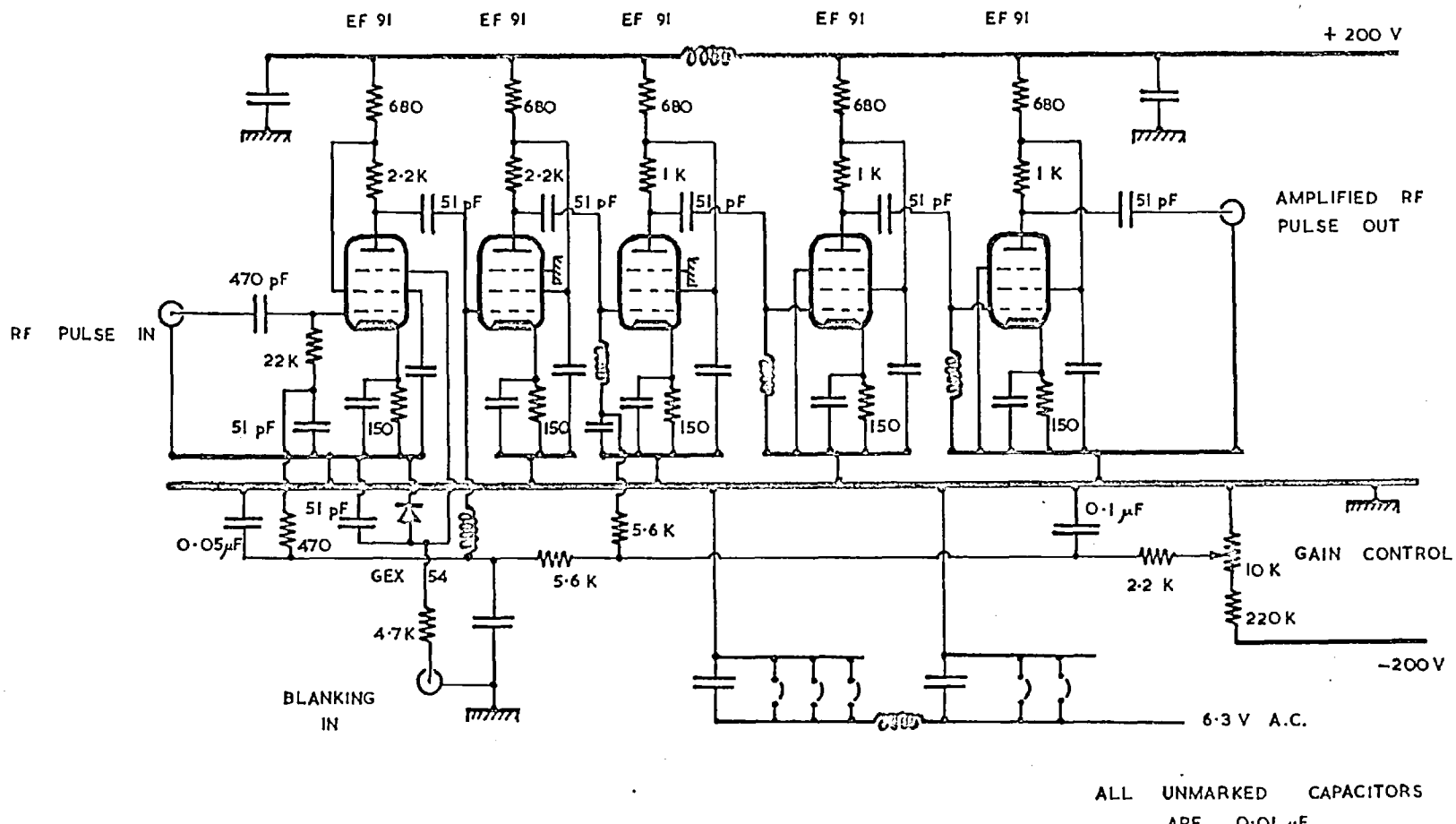

FIGURE 31 RECEIVER

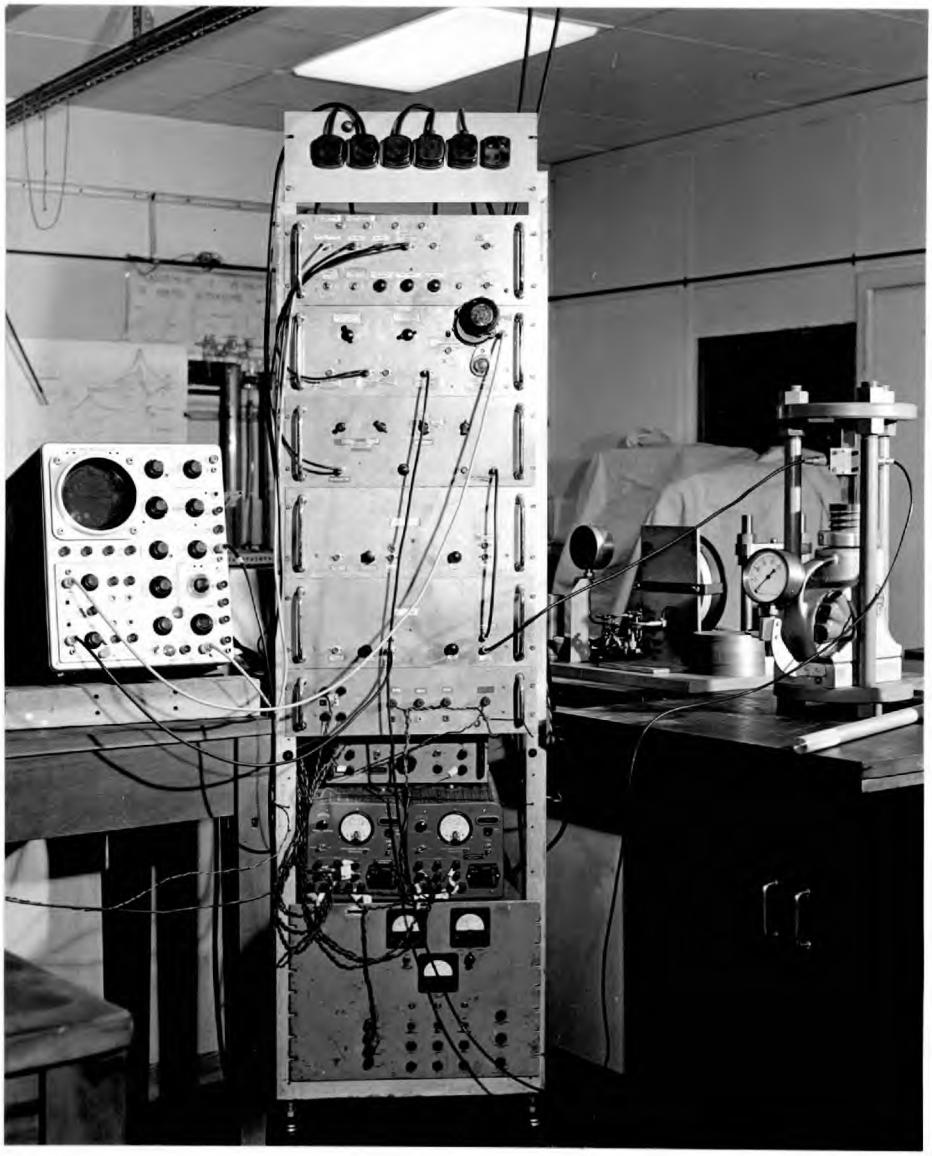

FIGURE 32 GENERAL VIEW OF ELECTRONIC EQUIPMENT

APPENDIX 2

CALIBRATION OF VARIABLE DELAY LINE

The calibration of the variable delay line (Cossor 1048) incorporated into the transmitter circuit was checked using an electrical interference method. A continuous rf signal from a Schomandl standard frequency source was fed into the transmitter which was operated in the gated-cw mode (see Figure 4, Chapter 2). The delayed, gated, rf signal from output B and the continuous signal from output C were added algebraically in the preamplifier of the Tektronix oscilloscope, and the delay line was adjusted to find several positions for which the two signals B and C were in phase opposition. This procedure was repeated for several standard frequencies at 50 Kc/s intervals in the range 4.850 to 5.150 Mc/s. The delay time, d, per scale division was computed from the simple relationship

$$d = \frac{1}{xf} \qquad (99)$$

where x is the number of scale divisions between two adjacent 'null' interference positions, and corresponds to a phase difference of 2π radians at the frequency f.

The mean value found for d over this frequency range was

$$d = (3.75 \pm 0.03) \times 10^{-10} \text{ s} \quad .$$

and was in reasonable agreement with the value 3.72×10^{-10} s quoted by the manufacturer.

APPENDIX 3

METHOD OF DETERMINING THE VIBRATION DIRECTION OF SHEAR WAVE TRANSDUCERS

The vibration direction of the Y-cut quartz transducers was determined by reference to a source of shear waves whose direction of particle motion was accurately known. The reference shear waves were generated by 'mode-conversion' of longitudinal waves incident obliquely on a solid/air interface in a specially designed 'shear wedge'. It is well known that for isotropic solids, a longitudinal wave incident obliquely at a solid/air interface will in general give rise to one reflected longitudinal and one reflected shear wave. Arenburg (118) has published comprehensive theoretical curves for isotropic solids showing the ratio of the amplitudes of the reflected and incident waves as a function of the angle of incidence and Poisson's ratio. For certain angles of incidence it is possible to convert a longitudinal wave almost completely into a reflected shear wave whose particle motion lies in the plane containing the incident wave and the normal to the interface.

A 'shear wedge', triangular in section, was machined from aluminium alloy (measured Poisson's ratio = 0.314), the angles of the wedge being determined from Arenburg's theoretical curves. The wedge is shown in section in Figure 33. A longitudinal wave generated at

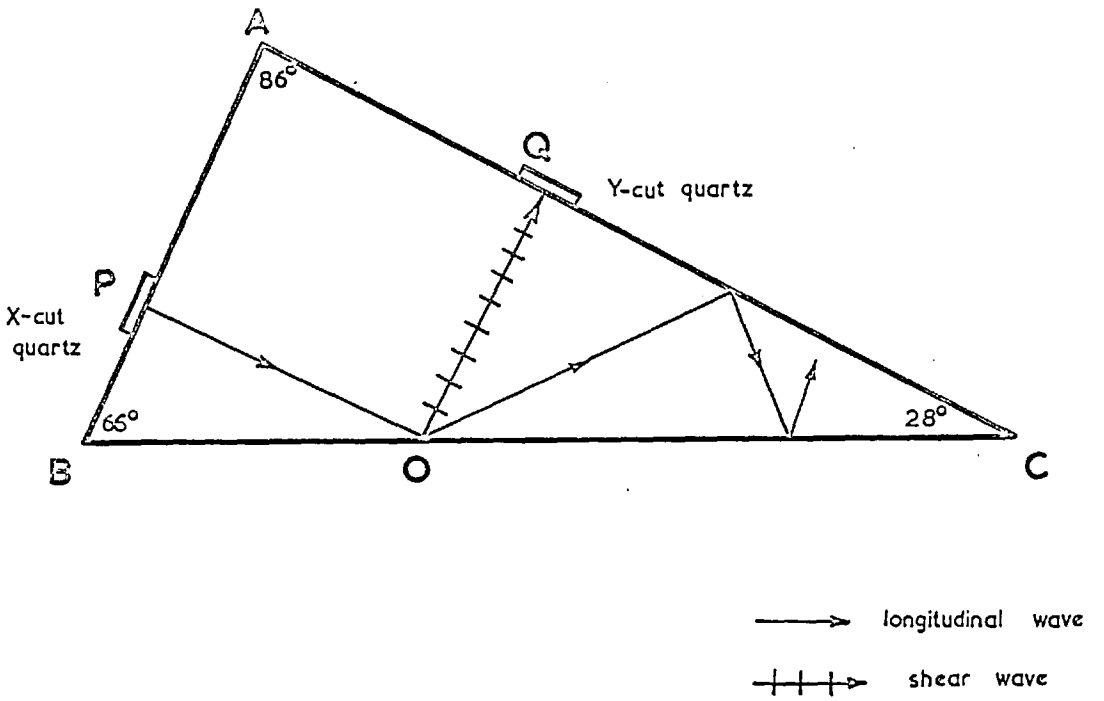

FIGURE 33 MODE-CONVERTER 'SHEAR WEDGE'

P by an X-cut quartz transducer is converted at O into a shear wave, which is received at normal incidence at Q by a Y-cut quartz transducer. The small amount of reflected longitudinal wave undergoes multiple reflections between the wedge faces AC and CB and does not influence the transducer at Q. The direction of particle motion of the shear wave lies along the direction AC, and if the signal received by the Y-cut transducer is monitored as the transducer is rotated about OQ, an orientation may be found such that the received signal is a minimum. In this condition, which can be critically adjusted, the shear wave transducer is polarised exactly perpendicular to the direction AC, and the direction of particle motion may be marked on the back electrode.

APPENDIX 4

RELATIONSHIP BETWEEN THE STRESS DERIVATIVES $(\rho_o W^2)'_o$ and $(\rho_o V^2)'_o$

FOR ISOTROPIC SOLIDS

The relationship between the quantities $(\rho_o W^2)'_o$ and $(\rho_o V^2)'_o$ may be rewritten from the results of Thurston and Brugger [40] (see equations 37 to 40, Chapter 1) in the form:

$$\left[(\rho_o V^2)' - (\rho_o W^2)'\right]_o = -2wN_k N_m s_{kmaa} \qquad \text{for hydrostatic pressure}$$

$$= -2wN_k N_m M_a M_b s_{kmab} \qquad \text{for uniaxial compression in direction of unit vector } \underline{M}$$

For an isotropic solid the above general relationships reduce to the following three cases only.

$$\left[(\rho_o V^2)' - (\rho_o W^2)'\right]_o = -2wE(1 - 2\sigma) \qquad \text{for hydrostatic pressure}$$

$$= -2w/E \qquad \text{for uniaxial compression parallel to propagation direction}$$

$$= +2w\sigma/E \qquad \text{for uniaxial compression perpendicular to propagation direction}$$

REFERENCES

(1) HAMILTON, Sir W.R. Collected papers (1832). Camb.Univ.Press; 1931.

(2) CAUCHY, A. Acad. Sci.; Paris, 2, 1836.

(3) GREEN, G. Trans. Camb. Phil. Soc.; 7, 121, 1842.

(4) CHRISTOFFEL, E.W. Ann.di Mat., Ser II; 8, 193, 1877.

(5) KELVIN, Lord Baltimore Lectures. Camb. Univ. Press; 1904.

(6) LOVE, A.E.H. A treatise on the mathematical theory of elasticity. 4th Edition; Camb. Univ. Press; 1927; also Dover, New York, 1944.

(7) MUSGRAVE, M.J.P. On the propagation of elastic waves in aeolotropic media. I General principles; Proc. Roy. Soc.; A226, 339, 1954
II Hexagonal symmetry; Ibid. A226, 356, 1954.

(8) MILLER, G.F. and MUSGRAVE, M.J.P. On the propagation of elastic waves in aeolotropic media. III Cubic symmetry; Proc. Roy. Soc.; A226, 352, 1956.

(9) FARNELL, G.W. Elastic waves in trigonal crystals. Can J. Phys. 39, 65, 1961.

(10) HUNTINGTON, H.B. The elastic constants of crystals. Solid State Physics. (Ed. Seitz and Turnbull); 7, 213, 1958.

(11) MUSGRAVE, M.J.P. Propagation of elastic waves in crystals and anistropic media. Rep. Prog. Phys. 22, 74, 1959.

(12) HEARMON, R.F.S. Introduction to applied anisotropic elasticity. Clarendon Press, Oxford, 1961.

(13) THURSTON, R.N. Wave propagation in fluids and normal solids. Physical Acoustics (Ed. Mason); 1A, 1, 1964. Academic Press.

(14) BORGNIS, F.E. Specific directions of longitudinal wave propagation in anisotropic media. Phys. Rev.; 98, 1000, 1955.

(15) SMITH, R.T. Propagation of elastic waves in anisotropic solid media. M.Sc. Dissertation, Univ. of London, June 1961.

(16) BRILLOUIN, L. On the 'tensions' of radiation. Ann. de Physique, 4, 528, 1925.

(17) BRILLOUIN, L. Les Tenseurs; Dover, New York, 1946.

(18) MURNAGHAN, F.D. Finite deformation of an elastic solid; Wiley, New York, 1951.

(19) TRUESDELL, C. Second-order theory of wave propagation in isotropic elastic materials. Intern. Symposium on 2nd order effects in Elasticity, Plasticity and Fluid Dynamics, Haifa, April 1962.

(20) SMITH, R.T. Stress-induced anisotropy in solids - the acousto-elastic effect; Ultrasonics, 1, 135, 1963.

(21) BIRCH, F. Finite elastic strain of cubic materials; Phys. Rev., 71, 809, 1947.

(22) HEARMON, R.F.S. Third-order elastic coefficients; Acta. Cryst., 6, 331, 1953.

(23) TOUPIN, R.A. and BERNSTEIN, B. Sound Waves in deformed perfectly elastic materials - Acousto-elastic effect; J.Acoust. Soc. Amer; 33, 216, 1961.

(24) BRUGGER, K. Thermodynamic definition of higher-order elastic coefficients; Phys. Rev., 133, A1611, 1964.

(25) VOIGT, W. Lehrbuch der Kristallphysik; Teubner, Leipzig, 1928.

(26) ZIMAN, J.M. Electrons and phonons; Chapter 3, Clarendon Press, Oxford, 1960.

(27) BRAINERD, J.G. et al. Standards on piezoelectric crystals; Proc. Inst. Radio Engrs., 37, 1378, 1949.

(28) KITTEL, C. Introduction to solid state physics; 2nd Edition p.19, Wiley, New York, 1958.

(29) KRISHNAMURTY, T.S.G. Fourth-order elastic coefficients in crystals; Acta. Cryst.; 16, 839, 1963.

(30) GHATE, P.B. Fourth-order elastic coefficients; J. Appl. Phys., 35, 337, 1964.

(31) MASON, W.P. Piezo-electric crystals and their application to ultrasonics; Van Nostrand, New York, 1950.

(32) FUMI, F.G. Third-order elastic coefficients of crystals; Phys. Rev., 83, 1274, 1951.

(33) FUMI, F.G. Third-order elastic coefficients in trigonal and hexagonal crystals; Phys. Rev., 86, 561, 1952.

(34) GOL'DBERG, Z.A. Interaction of plane longitudinal and transverse elastic waves; Soviet Physics - Acoustics, 6, 306, 1961.

(35) THURSTON, R.N. Effective elastic coefficients for wave propagation in strained elastic crystals; Private Communication, May 1964; to be published in J. Acoust. Soc. Amer., 1965.

(36) TRUESDELL, C. General and exact theory of waves in finite elastic strain; Archive. Rational Mech. and Analysis, 8, 263, 1961.

(37) GREEN, A.E. A note on wave propagation in initially deformed bodies; J. Mech. Phys. Solids, 11, 119, 1963.

(38) SEEGER, A. The application of second-order effects in elasticity to problems of crystal physics; Intern. Symp. 2nd-order effects in Elasticity, Plasticity, and Fluid Dynamics, Haifa, Israel, April 1962 (Pergamon).

(39) HUGHES, D.S. and KELLY, J.L. Second-order elastic deformation of solids; Phys. Rev., 92, 1145, 1953.

(40) THURSTON, R.N. and BRUGGER, K. Third-order elastic constants and the velocity of small-amplitude elastic waves in homogeneously stressed media. Phys. Rev.; 133, A1604, 1964.

(41) SEEGER, A. and BUCK, O. The experimental determination of higher-order elastic constants; Z. Naturforsch, 15a, 1056, 1960.

(42) BATEMAN, T.B., MASON, W.P., and McSKIMIN, H.J. Third-order elastic moduli of germanium; J. Appl. Phys., 32, 928, 1961.

(43) EINSPRUCH, N.G. and MANNING, R.J. Third-order elastic moduli of anisotropic solids. J. Appl. Phys. 35, 560, 1964.

(44) TRUESDELL, C. and TOUPIN, R. in Handbuch der Physik; Edit. Flugge, Vol. III, Pt. 1. p.226, - Springer-Verlag, Berlin, 1960.

(45) BLUME, R.J. Instrument for continuous high resolution measurement of changes in the velocity of ultrasound; Rev. Sci. Instrum., 34, 1400, 1963.

(46) ESPINOLA, R.P. and WATERMAN, P.C. An ultrasonic interferometer for measurement of velocity changes in solids; J. Appl. Phys., 29, 718, 1958.

(47) FORGACS, R.L. Improvements in the sing-around technique for ultrasonic velocity measurements; J. Acoust. Soc. Amer., 32, 1697, 1960.

(48) EROS, S. and REITZ, J.R. Elastic constants by the ultrasonic pulse-echo method. J. Appl. Phys., 29, 683, 1958.

(49) REDWOOD, M. Problems in the propagation of ultrasonic pulses in solids; Ultrasonics, 2, 174, 1964.

(50) MARKHAM, M.F. Measurement of elastic constants by the ultrasonic pulse method. Brit. J. Appl. Phys., Suppl. 6, 56, 1957.

(51) McSKIMIN, H.J. I.R.E. Trans. Ultrasonic Eng., UE 5, 25, 1957.

(52) WILLIAMS, J. and LAMB, J. On the measurement of ultrasonic velocity in solids. J. Acoust. Soc. Amer., 30, 308, 1958.

(53) McSKIMIN, H.J. Pulse superposition method for measuring ultrasonic wave velocities in solids., J. Acoust. Soc. Amer., 33, 12, 1961.

(54) LAZARUS, D. Variation of elastic constants of alkali halides at 10,000 bars. Phys. Rev., 76, 544, 1949.

(55) MURNAGHAN, F.D. Am. J. Math., 49, 235, 1937.

(56) DANIELS, W.B. and SMITH, C.S. Pressure-derivatives of the elastic constants of copper, silver and gold to 10,000 bars. Phys. Rev., 111, 713, 1958.

(57) SCHMUNK, R.E. and SMITH, C.S. Pressure-derivatives of the elastic constants of aluminium and magnesium. J. Phys. Chem. Solids., 9, 100, 1959.

(58) VORONOV, F.F. and VERESHCHAGIN, L.F. Influence of hydrostatic pressure on the elastic properties of metals. I Experimental data. Phys. Metals and Metallography, 11, 111, 1961.

(59) McSKIMIN, H.J. and ANDREATCH, P. Analysis of the pulse-superposition method for measuring ultrasonic wave velocities as a function of temperature and pressure. J. Acoust. Soc. Amer., 34, 609, 1962.

(60) McSKIMIN, H.J. and ANDREATCH, P. Elastic moduli of germanium versus hydrostatic pressure at 25°C and -195.8°C. J. Appl. Phys. 34, 651, 1963.

(61) McSKIMIN, H.J. Elastic moduli of germanium as a function of hydrostatic pressure. J. Acoust. Soc. Amer., 30, 314, 1958.

(62) ROLLINS, F.R., KOBETT, D.R. and JONES, J.L. Study of ultrasonic methods for non-destructive measurements of residual stress. WADD Technical Report 61-42, Part II, March 1962.

(63) PAUTHIER-CAMIER, S. Detection of the variation in elastic constants by means of transverse ultrasonic waves. Paper K32, 4th Intern. Congress Acoustics, Copenhagen, Aug. 1962.

(64) CRECRAFT, D.I. Ultrasonic wave velocities in stressed Ni-steel. Nature., 195, no. 4847, 1193, 1962.

(65) DRABBLE, J.R. and GLUYAS, M. Third-order elastic moduli of germanium and silicon. Intern. Conf. on Lattice Dynamics, Copenhagen, Aug. 1962, and Private Communication.

(66) BORN, M. and HUANG, K. Dynamical theory of crystal lattices. Clarendon Press, Oxford, 1954.

(67) ORBACH, R. Ph.D. Thesis, University of California, 1956.

(68) BOMMEL, H.E. and DRANSFIELD, K. Phys. Rev. 117, 1245, 1960.

(69) MARIS, H.J. Attenuation of ultra-high frequency acoustic waves in quartz at low temperatures. Nature; 198, no. 4883, 876, 1963. Also Ph.D. Thesis, University of London, 1963.

(70) KLEMENS, P.G. Effect of thermal and phonon processes on ultrasonic attenuation. Physical Acoustics, (Ed. W.P. Mason), Vol. 3, chap. 14, Academic Press, New York, to be published 1965.

(71) MASON, W.P. and BATEMAN, T.B. Ultrasonic wave propagation in pure silicon and germanium. J. Acoust. Soc. Amer., 36, 644, 1964.

(72) AKHIEZER, A. J. Phys. USSR. 1, 277, 1939.

(73) JONES, G.L. and KOBETT, D. Interaction of elastic waves in an isotropic solid. J. Acoust. Soc. Amer. 35, 5, 1963.

(74) CHILDRESS, J.D. and FRIED, Z. Bull. Am. Phys. Soc., Series II, 8, 16, 1963.

(75) ROLLINS, F.R. and WALDOW, P. Study of ultrasonic techniques for the non-destructive measurement of residual stress. WADD Technical Report 61-42, Pt.III, May 1963.

(76) ROLLINS, F.R. Interaction of ultrasonic waves in solid media. Appl. Phys. Lett., 2, 147, 1963.

(77) ROLLINS, F.R. Private Communication, August 1964.

(78) GEDROITS, A.A. and KRASIL'NIKOV, V.A. Finite-amplitude elastic waves in solids and deviations from Hooke's law. Soviet Physics, J.E.T.P., 16, 1122, 1963.

(79) GEDROITS, A.A., KRASIL'NIKOV, V.A. and ZAREMBO, L.K. Elastic waves of finite amplitude in solids and anharmonicity of the lattice. Acustica, 13, 108, 1963.

(80) GEDROITS, A.A., ZAREMBO, L.K. and KRASIL'NIKOV, V.A. Shear waves of finite amplitude in polycrystals and single crystals of metals. Soviet Physics, Doklady, 8, 478, 1963.

(81) BREASEALE, M.A. and THOMPSON, D.O. Finite-amplitude ultrasonic waves in aluminium, Appl. Phys. Lett., 3, 77, 1963.

(82) SEED, A. Damping in quartz at high strain amplitudes and high frequencies Ph.D. Thesis, University of London, 1962.

(83) SEED, A. Non-linear effect in quartz resonators. 4th Intern. Congress. Acoustic, Paper N54, Copenhagen, Aug. 1962.

(84) HUTSON, A.R., McFEE, J.H. and WHITE, D.L. Ultrasonic amplification in Cadmium Sulphide. Phys. Rev. Letters., 7, 237, 1961.

(85) HUTSON, A.R., and WHITE, D.L. Elastic wave propagation in piezoelectric semiconductors. J. Appl. Phys., 33, 40, 1962.

(86) WHITE, D.L. Amplification of ultrasonic waves in piezoelectric semi-conductors. J. Appl. Phys., 33, 2547, 1962.

(87) BLOTEKJAER, K. and QUATE, C.F. The coupled modes of acoustic waves and drifting carriers in piezoelectric crystals. Microwave Lab. Report 1057, Stanford University, California, July, 1963.

(88) TRUELL, R. Anharmonic effects and stress-wave propagation in Cadmium Sulphide. Symp. Sonic Investigation on Internal Damping in Solids, Imperial College, London, August 1964 (unpublished).

(89) SHEARD, F.W. Calculation of the thermal expansion of solids from the third-order elastic constants. Phil. Mag. 4, 1381, 1958.

(90) GRUNEISEN, E. Handbuch der Physik., 10, 1, 1926.

(91) SHARMA, K.C. and JOSHI, S.K. Thermal expansion of solids on the basis of anisotropic continuum dispersive model. Phil. Mag., 9, 507, 1964.

(92) CHASE, C.E. Propagation of ordinary sound in liquid helium near the λ point. Phys. Fluids, 1, 193, 1958.

(93) PERVUSHIN, I.I. and FILIPPOV, L.P. A method of measuring the velocity of ultrasound in solids and liquids. Soviet Physics - Acoustics, 7, 307, 1962.

(94) LEVY, M., RUDNICK, I. and STERN, R. Simple modification of attenuation equipment to measure velocity. J. Acoust. Soc. Amer. 34, 1788, 1962.

(95) BASTIEN, P. et al. Ultrasonic determination of the elastic and inelastic properties of solids. Appl. Mat. Res. 2, 170, 1963.

(96) ROLLINS, F.R. Study of methods for nondestructive measurement of residual stress. WADD Technical Report 59-561, December 1959.

(97) McSKIMIN, H.J. Properties of Dow-resin 276-V9. Private Communication, 1963.

(98) SMITH, R.T. Grain-boundary scattering of ultrasonic waves in polycrystalline solids. J. Appl. Mat. Res., 2, 200, 1963.

(99) SULLIVAN, P.F. and PAPADAKIS, E.P. Ultrasonic double-refraction in worked metals. J. Acoust. Soc. Amer., 33, 1622, 1961.

(100) SMITH, R.T. and STEPHENS, R.W.B. Effects of anisotropy on ultrasonic propagation in solids. Prog. Appl. Mat. Res., 5, 41, 1964.

(101) HOLLAND, L. Vacuum deposition of thin films. Chapman and Hall, 1956.

(102) CRECRAFT, D.I. Ph.D. Thesis. Electrical Engineering Department, University of Birmingham, 1964.

(103) TAYLOR, L.H. and ROLLINS, F.R. Ultrasonic study of three-phonon interactions. I Theory. Phys. Rev., 136, A591, 1964.

(104) ROLLINS, F.R., TAYLOR, L.H. and TODD, P.H. Ultrasonic study of three-phonon interactions. II Experimental results. Phys. Rev., 136, A597, 1964.

(105) BRIDGMAN, P.W. The physics of high pressure. 2nd Edition. G.Bell and Sons, 1949.

(106) BRIDGMAN, P.W. The linear compression of iron to 30,000 bars. Proc. Amer. Acad., 74, 11, 1940.

(107) HUGHES, D.S. and MAURETTE, C. Dynamic elastic moduli of iron, aluminium and fused quartz. J. Appl. Phys., 27, 1184, 1956.

(108) BIRCH, F. The effect of pressure on the modulus of rigidity of several metals and glasses. J. Appl. Phys., 8, 129, 1937.

(109) BIRCH, F. Handbook of physical constants. Geol. Soc. Amer., Special Paper 36, Table 4.2, 1942.

(110) BRADFIELD, G. The influence of texture and plastic deformation on the elasticity of polycrystalline metals. 4th Intern. Cong. Acoustics, Paper J54, Copenhagen, August 1962.

(111) BRADFIELD, G. Use in industry of elasticity measurements in metals with the help of mechanical vibrations. Nat. Phys. Lab. Note on Appl. Sci., no. 30, H.M. Stationery Office, London, 1964.

(112) PAPADAKIS, E.P. Ultrasonic study of simulated crystal symmetries in polycrystalline aggregates. IEEE Trans. Sonics and Ultrasonics Group, SU-11, 19, 1964.

(113) CADY, W.G. Piezoelectricity, Revised Edition, Dover, 1964.

(114) FUMI, F.G. Physical properties of crystals: the direct-inspection method. Acta Cryst., 5, 44, 1952.

(115) McSKIMIN, H.J. Measurement of the 25°C zerofield elastic moduli of quartz by high frequency plane wave propagation. J. Acoust. Soc. Amer., 34, 1271, 1962.

(116) McSKIMIN, H.J. A note on internal conical refraction of transverse mechanical waves in quartz. Private Communication, 1963.

(117) WILLIAMS, J.R. A precise electrical method for the measurement of velocity of stress waves in solids. Ph.D. Thesis, Univ. of London, 1959.

(118) ARENBURG, D.L. Ultrasonic solid delay lines. J.Acoust.Soc.Amer., 20, 1, 1948.